MITIGATION OF TSUNAMI DEBRIS IMPACT BY FENDER STRUCTURES FOR REINFORCED-CONCRETE BUILDINGS

Miss Zin Zin Tun

จุฬาลงกรณ์มหาวิทยาลัย
CHULALONGKORN UNIVERSITY

A Dissertation Submitted in Partial Fulfillment of the Requirements
for the Degree of Doctor of Philosophy in Civil Engineering
Department of Civil Engineering
FACULTY OF ENGINEERING
Chulalongkorn University
Academic Year 2020
Copyright of Chulalongkorn University

การลดผลของการกระแทกจากวัตถุที่มากับสึนามิด้วยโครงสร้างดูดซับพลังงานสำหรับอาคารคอนกรีตเสริมเหล็ก

น.ส.ซิน ซิน ตุล

Thesis Title   MITIGATION OF TSUNAMI DEBRIS IMPACT BY FENDER STRUCTURES FOR REINFORCED-CONCRETE BUILDINGS
By   Miss Zin Zin Tun
Field of Study   Civil Engineering
Thesis Advisor   Associate Professor Anat Ruangrassamee, Ph.D.

      Accepted by the FACULTY OF ENGINEERING, Chulalongkorn University in Partial Fulfillment of the Requirement for the Doctor of Philosophy

          .... Dean of the FACULTY OF ENGINEERING
          (Associate Professor SUPOT TEACHAVORASINSKUN, D.Eng.)

DISSERTATION COMMITTEE
          .... Chairman
          (Associate Professor TOSPOL PINKAEW, D.Eng.)
          .... Thesis Advisor
          (Associate Professor Anat Ruangrassamee, Ph.D.)
          .... Examiner
          (Assistant Professor CHATPAN CHINTANAPAKDEE, Ph.D.)
          .... Examiner
          (Assistant Professor PITCHA JONGVIVATSAKUL, Ph.D.)
          .... External Examiner
          (Assistant Professor Nuttawut Thanasisathit, Ph.D.)

จุฬาลงกรณ์มหาวิทยาลัย
CHULALONGKORN UNIVERSITY

ชิน ชิน ตุล : การลดผลของการกระแทกจากวัตถุที่มากับสึนามิด้วยโครงสร้างดูดซับพลังงานสำหรับอาคาร
คอนกรีตเสริมเหล็ก. (MITIGATION OF TSUNAMI DEBRIS IMPACT BY
FENDER STRUCTURES FOR REINFORCED-CONCRETE
BUILDINGS) อ.ที่ปรึกษาหลัก : อาณัติ เรืองรัศมี

-การกระแทกจากวัตถุขนาดใหญ่ที่ลอยมากับสึนามิ เช่น ตู้คอนเทนเนอร์ ส่งผลให้เกิดความเสียหายต่ออาคารในริม
ชายฝั่ง ในการศึกษานี้ได้พิจารณาอาคารที่มีการเชื่อมต่อกับโครงสร้างรับแรงกระแทกเพื่อให้สามารถลดผลจากการกระแทกได้
โดยได้ศึกษาประสิทธิภาพของอุปกรณ์รับแรงกระแทก ในการศึกษาได้ทำการวิเคราะห์โดยให้แรงผลักกับอาคารโดยวิธีควบคุม
แรงที่กระทำร่วมกับการควบคุมระยะการเสียรูป โดยพิจารณาการดูดซับพลังงาน, สัดส่วนการเคลื่อนตัวในแต่ละชั้นของอาคารที่
มีและไม่มีโครงสร้างรับแรงกระแทก จากผลการศึกษาพบว่าโครงสร้างรับแรงกระแทกสามารถดูดซับพลังงานได้อย่างมี
ประสิทธิภาพ การศึกษานี้ได้เสนอวิธีการออกแบบเพื่อเลือกอุปกรณ์รับแรงกระแทกที่เหมาะสมด้วย โดยแรงที่จุดครากเป็นตัว
แปรสำคัญต่อพฤติกรรมของอาคารหลัก จากนั้นได้ทำการวิเคราะห์อาคารแบบ 3 มิติ โดยพบว่าโครงสร้างรับแรงกระแทก
สามารถป้องกันการเสียหายต่ออาคารได้อย่างมีประสิทธิภาพ

จุฬาลงกรณ์มหาวิทยาลัย
CHULALONGKORN UNIVERSITY

สาขาวิชา	วิศวกรรมโยธา	ลายมือชื่อนิสิต ....
ปีการศึกษา	2563	ลายมือชื่อ อ.ที่ปรึกษาหลัก ....

5971494221 : MAJOR CIVIL ENGINEERING
KEYWORD: Tsunami force, Tsunami pushover methods, Energy absorption, Fender

Zin Zin Tun : MITIGATION OF TSUNAMI DEBRIS IMPACT BY FENDER STRUCTURES FOR REINFORCED-CONCRETE BUILDINGS. Advisor: Assoc. Prof. Anat Ruangrassamee, Ph.D.

The impact of large debris such as loaded shipping containers can cause significant damage to buildings at shorelines. In this study, the building and protection structures are connected with fenders to reduce the impact of large debris. The objective is to study the building with a fender structure that reduces the impact of the shipping container. For a fender structure, cone-shaped rubber fenders are used to absorb the impact energy. Various fender reactions are considered as a parameter to conduct the efficiency of the fender. Tsunami pushover analyses using the force-controlled and displacement-controlled methods are used to obtain the capacity of the building. The energy approach for shipping container impact is used to evaluate the resistance of the building. Capacity curves, energy absorptions, inter-story drift ratios of the buildings with and without fender structures are studied. The fender can effectively absorb the debris impact. A design recommendation is proposed for the building with a fender structure. It is found that fender yield forces in the fender structure is the key parameter for the performance of the main building. Then, a three-dimensional tsunami pushover analysis is conducted on the building with 6 fender units. It is found that building with fenders can effectively resist all types of shipping container impact cases.

จุฬาลงกรณ์มหาวิทยาลัย

CHULALONGKORN UNIVERSITY

Field of Study:	Civil Engineering	Student's Signature	....
Academic Year:	2020	Advisor's Signature	....

ACKNOWLEDGEMENTS

TABLE OF CONTENTS

LIST OF TABLES

LIST OF FIGURES

จุฬาลงกรณ์มหาวิทยาลัย

CHULALONGKORN UNIVERSITY

CHAPTER (1)
INTRODUCTION

1.1 Background

A tsunami is an intense and short period wave produced by undersea shallow-focus earthquakes, landslides, or volcanic activity and undersea crustal displacements (subduction of tectonic plates). The main cause of a tsunami is the earthquakes at the seabed. A tsunami can damage some structures several kilometers and over 15 meters above sea level. After a tsunami disaster, most non-engineer structures are damaged. However, most of the structures that learned from the surviving structure during the past tsunami are partially damaged. Facts such as tsunami flow velocity, inundation height, tsunami-prone area, resulting in flood loads obtained from the past tsunami are used as further evaluation and characteristic of the tsunami and structural response.

Before the Indian Ocean Tsunami in 2004, the design of the structure was considered for the tsunami with minor importance. Due to awareness of the Indian Ocean Tsunami, 2004 disaster, tsunami induced forces can lead to extensive damage or collapse of the structure as shown in Figure 1.1. Therefore, tsunami forces should be taken into consideration for the design of the building in the coastal region in seismic prone areas. Data collected after the December 2004 Indian Ocean Tsunami in Indonesia and Thailand showed that poorly detailed concrete structures experienced severe damage. Reinforce concrete structures have been observed to withstand tsunamis with acceptable low levels of damage. However, data collected from the 2004 Indian Ocean Tsunami observed that inundation depths of more than 5 m can damage concrete structures.

Tsunami loads can generally be divided into two parts: static and dynamic loads. Static loads include hydrostatic and buoyancy loads while dynamic loads involve hydrodynamic(drag), surge, and debris impact load. Three parameters are essential for defining the magnitude and application of these forces: (1) inundation depth, (2) flow velocity, and (3) flow direction. The parameters mainly depend on: (a) tsunami wave height and wave period (b) coast topography and (c) roughness of the coastal inland. Inundation depth at a specific location can be estimated using various

tsunami states involving varying magnitude and direction and various experiments. Nevertheless, the estimation of flow velocity and direction is generally more difficult.
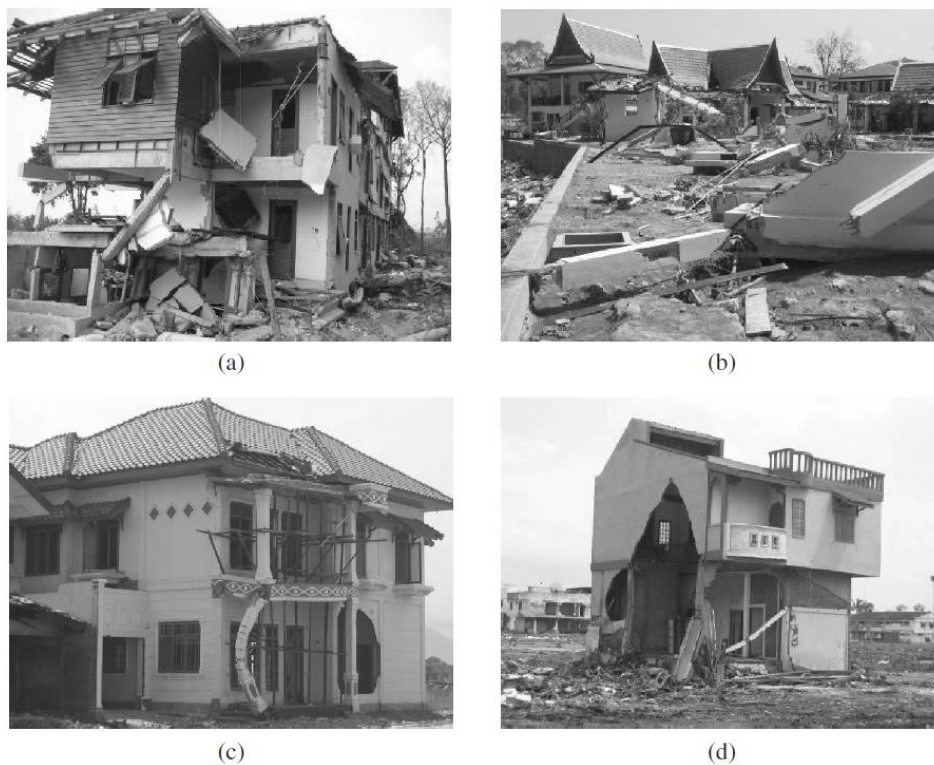
Figure 1.1 Tsunami damage in Thailand and Indonesia (Indian Ocean Tsunami, 2004): (a) structural damage in Thailand; (b) column failure of RC building in Phuket, Thailand; (c) column failure due to impact of debris in Indonesia; (d) punching failure of infill walls, Banda Aceh, Indonesia.

1.2 Motivation

A tsunami can cause huge damages to coastal and offshore structures. Flood waves can take entire buildings off their foundation and carry them inland. They can also damage the buildings through impact with debris such as containers, ships, and vessels from offshore and cause debris impact with an accumulation of such debris (See Figure 1.2).

Forces due to tsunami can be very large that it is uneconomical and impractical to design all structures to resist tsunami. The risk of large debris such as containers, fishing boats, and warships may be high in some regions. Therefore, tsunami resistant building such as building with fender system, shelters should be

considered to withstand these forces. The building with a fender structure is shown in Figure 1.3.

(a)   (b)

Figure 1.2 Examples of waterborne debris, (a) fishing boats debris 1993 Okushiri Tsunami (b) Shipping container debris in 2009 Samoa Tsunami [1]
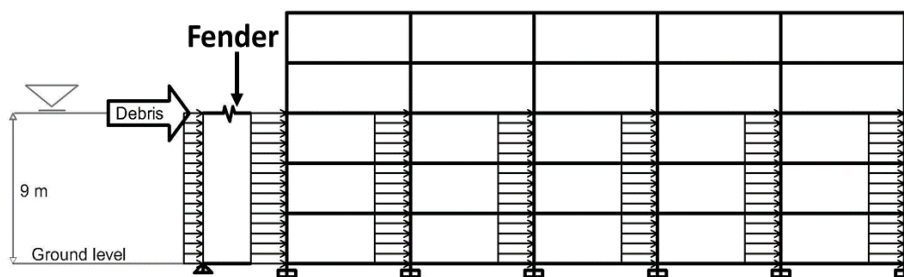
Figure 1.3 Building with fender structure under impact loading

1.3 Objective of the research

The objectives of the research are as follows:

1. To investigate the behavior of the buildings under tsunami loads.
2. To investigate the performance of the building with the fender system.
3. To study the efficiency of the fender
4. To recommend the suitable fender size based on the type of debris impact

1.4 Scope of the research

1. Two types of regular shaped, 5-story reinforced concrete building are considered.

2. Hydrodynamic, buoyance, and debris impact loads (such as shipping container impact) are considered as tsunami loads in this study.

3. Super cone fenders are used as energy absorbing devices.

4. The structures are evaluated using pushover analysis with the aid of SAP 2000 software.

1.5 Research methodology

To achieve the objectives mentioned above, the following procedures need to be conducted and can be seen in Figure 1.4.

1. Review the background of tsunami forces and mitigation effects to reduce tsunami forces including large debris impacts.

2. Review the background of various codes for estimating the tsunami forces.

3. Review the background of tsunami flow velocity that is important for the evaluation of tsunami forces.

4. Review the background of tsunami pushover methods for the capacity of the building.

5. Review the plastic hinge length equation for nonlinear modeling of the structural elements.

6. Choose the same area for two types of buildings.

7. Design the structural systems using tsunami load combinations.

8. Analyze the buildings using tsunami pushover analysis to conduct the capacity.

9. To investigate the detailed behavior of the building with a fender system, 2-dimensional of the building with a fender system is firstly conducted under tsunami pushover analysis.

10. Evaluate the response of the building with and without fender in the 2-dimensional analysis.

11. Based on the efficiency of 2-dimensional analysis, the building with fenders in the 3-dimensional analysis is conducted under tsunami pushover analysis.

12. Evaluate the response of the building with and without fender system in the 3-dimensional analysis.
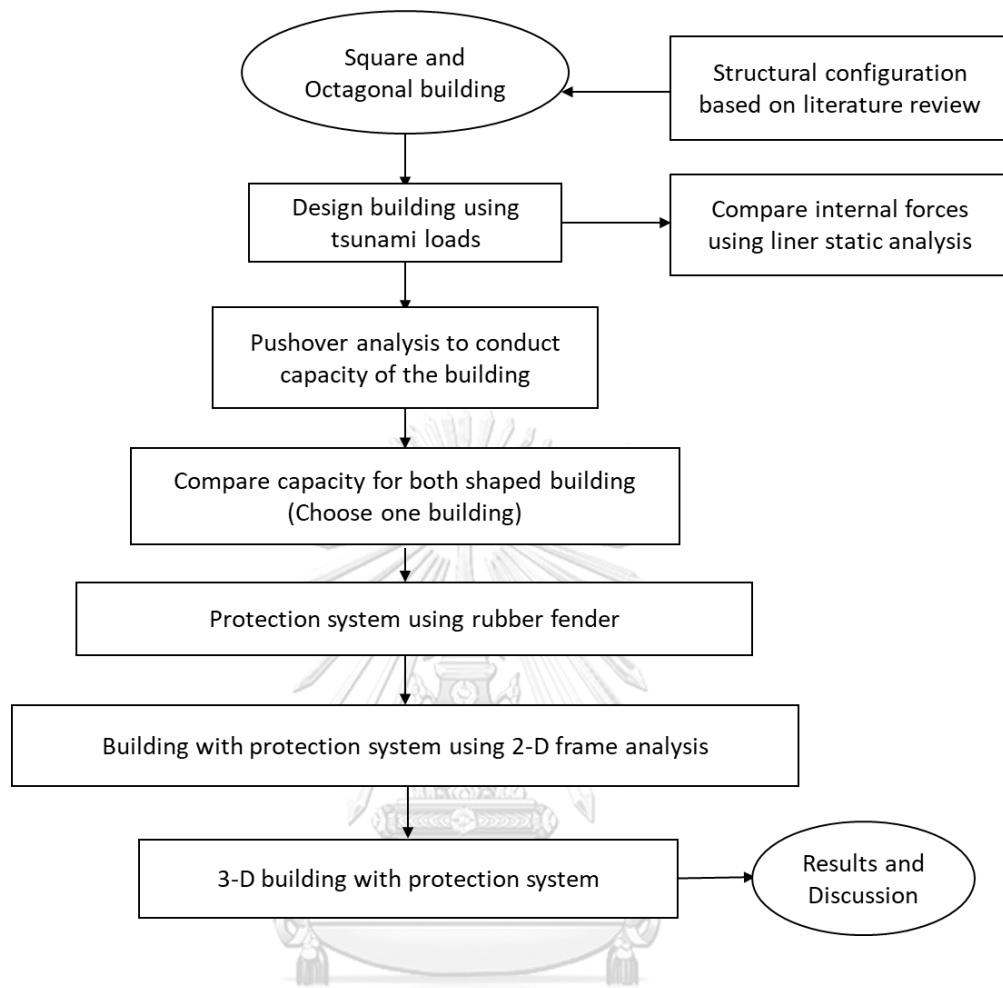
Figure 1.4 Flow chart of the research

1.6 Outline of the dissertation

This thesis is composed of five chapters which are briefly discussed as follows.

Chapter 1 includes the background of the importance of tsunami force on building in the tsunami-prone region. This chapter also includes the motivation, objectives, scopes of the study, and also research methodology.

Chapter 2 includes the literature review of tsunami forces, tsunami formula, mitigation concept of tsunami forces, tsunami velocity, fender system, tsunami pushover analysis, and plastic hinge length equations.

Chapter 3 provides the effects of tsunami forces on building using linear static and tsunami pushover analysis.

Chapter 4 presents the efficiency of the fender structure in the building.

Chapter 5 is the last chapter of this research which discusses and concludes the whole study results. Recommendations for the building with a fender system are also described in this chapter.

CHAPTER (2)
LITERATURE REVIEW

2.1 Introduction

In this chapter, tsunami forces on a structure under tsunami disaster are presented. Tsunami forces can cause the failure of the structure not only due to direct water but also due to water-borne debris. Parameters that are needed to evaluate tsunami forces are inundation depth, flow velocity, and flow direction. These parameters are mainly influenced by the tsunami wave period and wave height, the topography of the coastal area, and the roughness of the coastal region. The design manual, guidelines, and building codes advising for tsunami loads are available in ASCE/SEI Standard 7-16, the FEMAP-646 (Guidelines for Design of Structures for Vertical Evacuation from Tsunamis), FEMAP-55, and the City and County of Honolulu Building Code (CCH) and tsunami loads equations have also been presented by some researchers.

2.2 Impact forces due to tsunami
2.2.1 Hydrodynamic Load

Hydrodynamic force occurs when water flows around the structure. Due to a quasi-steady flow, hydrodynamic force is caused, and it is formed as a function of velocity, fluid density, and structure geometry. The design of the hydrodynamic force according to [2] and [1] can be computed by the following equation, Eq. (2.1). The position of hydrodynamic loading on a structural element is illustrated in Figure 2.1.

$$F_d = \frac{1}{2}\rho_s C_d B(hu^2)_{max} \qquad\qquad (2.1)$$

Where F_d =hydrodynamic or drag force acting in the flow direction

h = the flow depth at the considered structure when there is no structure

B= the width of the structure normal to the flow direction

ρ = density of the water

u = flow velocity at the location of the structure

C_d = 2.0 for square object and 1.2 for the cylindrical object (ASCE7/16)

The hydrodynamic force is directly based on the maximum momentum flux $(hu^2)_{max}$ occurring at the location at any time during flooding. To calculate the maximum value of (hu^2), [2] provides an equation (2.2) as a function of the ground elevation.

$$\frac{(hu^2)_{max}}{gR^2} = 0.125 - 0.235\frac{z}{R} + 0.11(\frac{z}{R})^2 \qquad (2.2)$$

Where hu^2 = momentum flux per unit width of the wall

R = the ground elevation at the maximum tsunami occur measured form the initial shoreline

z = the ground elevation of the structure that considered under a tsunami

The value of R and z can be achieved from the map of the tsunami inundation zone.
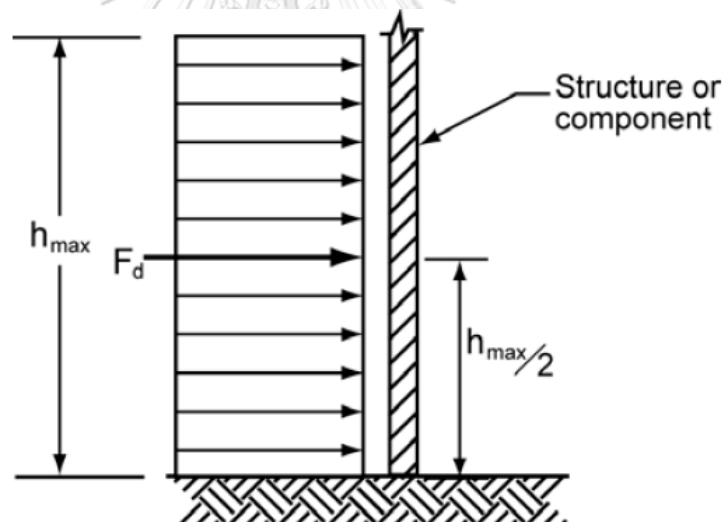
Figure 2.1 Distribution of hydrodynamic loading [1]

In some areas where is most often tsunami, the design for the structure is carefully investigated. In some of the existing codes such as [3] provide the tsunami-induced force for the design of the structure but this code is available for low rise building (less than three stories), one or two residential building in coastal areas The general formula for hydrodynamic force contributed in this code is as follows in Eq. (2.3) and [3] also provides the same formula with [4] for the hydrodynamic force but has a difference in a circular column for drag coefficient Cd.

$$F_d = \frac{pC_dAu^2}{2} \tag{2.3}$$

Where F_d = drag force acting in the flow direction

C_d = drag coefficient (2.0 for square column and 1.0 for a circular column, by [4] and 2 for square column and 1.2 for a circular column by [3]and 1.5 for w section)

ρ = density of the water

u = flow velocity

A = proposed area of the structure perpendicular to the direction of flow

[5] compared the experimental results and estimated results using FEMA P646. They demonstrated that the estimated hydrodynamic results are significantly lower than the test results. [6]are also studied to evaluate the hydrodynamic loads using a failure analysis in which results calculated from FEMA P646, 2008 are significantly underestimated. In 2009, [7] evaluated the drag forces using an experimental program and the test results are compared with FEMA 55 and CCH code in which results calculated from FEMA 55 got the overestimated values and CCH got underestimated values. The drag forces are not well predicted due to currently available formulations and inaccurate flow velocity.

2.2.2 Hydrostatic Force

When the flooding water slowly moves to the structural component or the structure, this flooding water creates hydrostatic forces. This force is due to the imbalance of water pressure on the other sides of the structure. This force is not consistent with a short width structure because the flooding water can easily be flow to the other sides. According to [1], hydrostatic forces can be used for an individual wall where the amount of water level on one side of the wall differ significantly to the other side and these forces are usually important for the structure with a long length such as dikes and sea walls Figure 2.2. [1] recommended that the hydrostatic force should be considered for individual walls and the equation used for this recommendation is as follows in Eq. (2.4):

$$F_h = p_c A_w = \frac{1}{2}\rho_s gbh^2{}_{max} \tag{2.4}$$

Where F_h = hydrostatic force

P_c = hydrostatic pressure

A_w = wetted area of the panel

ρ_s = density of the water (1200 kg/m^3)

g = acceleration due to gravity

b = width of the wall

h_{max} = maximum water height above the base of the wall at the structure that considered
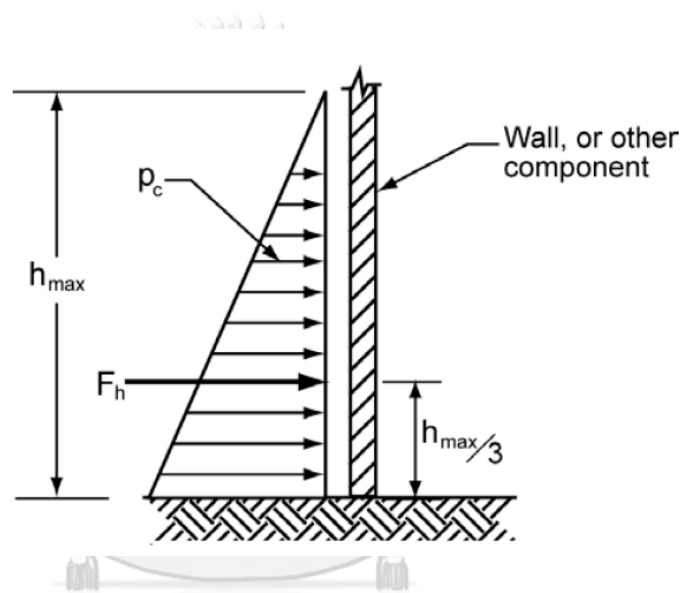
Figure 2.2 Hydrostatic force distribution and location of the resultant [1]

According to [4], the hydrostatic force per unit width can be computed although the [3] neglect the head of the velocity in their formulation. The hydrostatic force is significantly smaller than the drag and surge forces in case of a broken tsunami wave [8].

2.2.3 Buoyant Force

The buoyant force is caused due to the uplift pressure of flooding water and is applied vertically through the center of the mass of the inundated structure shown in Figure 2.3. The total buoyant force is equal to the weight of the water volume replaced by the inundated structure. In most code and provisions, the buoyant force equation is formulated with specific weight and volume of water (See Eq. (2.5)). In [1], buoyant force may concern with the structure that has less resistance to buoyancy:

for example- light wood frame buildings, empty tanks located above or below ground, basements, components designed considering only gravity loads, swimming pools.

$$F_b = \rho_s g V \tag{2.5}$$

Where

Fb = buoyant force (FEMA P-646 and CCH)

ρ_s = density of the water (1200 kg/m^3)

g = acceleration due to gravity

V = the volume of the water displaced by the submerged structure
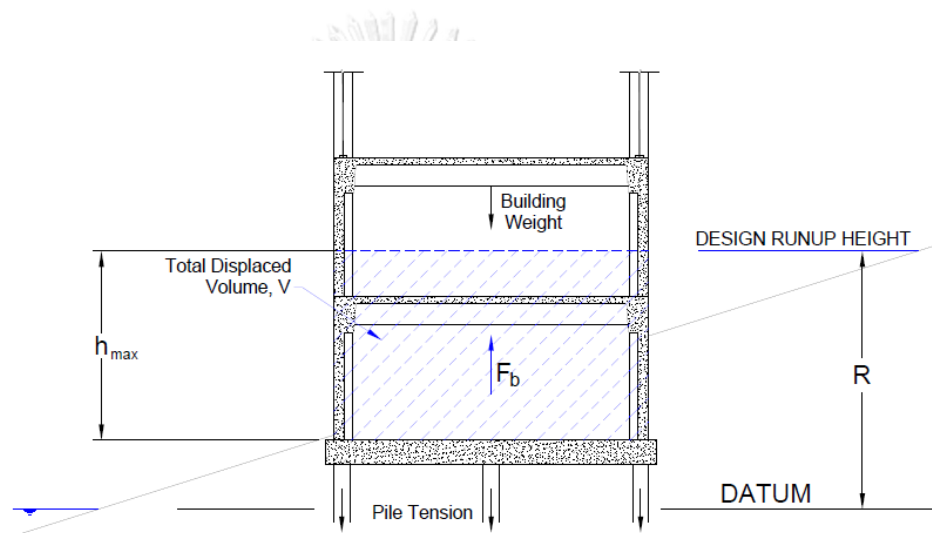
Figure 2.3 Buoyant forces on an overall building with watertight lower levels [1]

2.2.4 Surge Force

The leading edge of the incoming flooding water moves towards the structure as the bore-like wave or a bore causes the surge forces that impact the structure. [4] adopted from Dames & Moore (1980) provide the surge force equation for the walls that heights are greater than or equal to 3h (See Eq. (2.6)). However, the walls that heights are less than 3h need surge forces to be calculated using an appropriate combination of hydrodynamic force and hydrostatic force equations for different situation.

$$F_s = 4.5 p g h^2 \tag{2.6}$$

Where

Fs = surge force

ρ = density of the water

g = acceleration due to gravity

h = surge height

In 2009, [7] discussed the tsunami-induced force components in which surge force is obtained from the summation of hydrodynamic and hydrostatic components at the time of tsunami bore impacts a structure. The resulting surge force is equal to the same magnitude by the [4]. As the CCH assumes that the velocity used in the calculation of surge force is greater than that used in hydrodynamic force. Thus, it can be concluded that the velocity of the leading edge of the tsunami bore is greater than that of the semi-steady flow around the structure. An experimental investigation was conducted by [9]. It was observed that for 0.5, 0.75 and 0.85 m impounded depth, the surge force is not over the drag force in the case of the cylindrical structure. But for an impounded depth of 1 m, the surge force was greater than the drag force.

The relationship between a hydraulic bore and free-standing structures which are rhomboidal, rectangular, and circular sections were studied by [10] for impounded depths up to 0.3 m using the experiments on a dry bed condition. It was observed that for a square column, surge force overshot the hydrodynamic force for small-bore heights but in a circular or rhomboidal column, no overshot surge forces are observed shown in Figure 2.4.
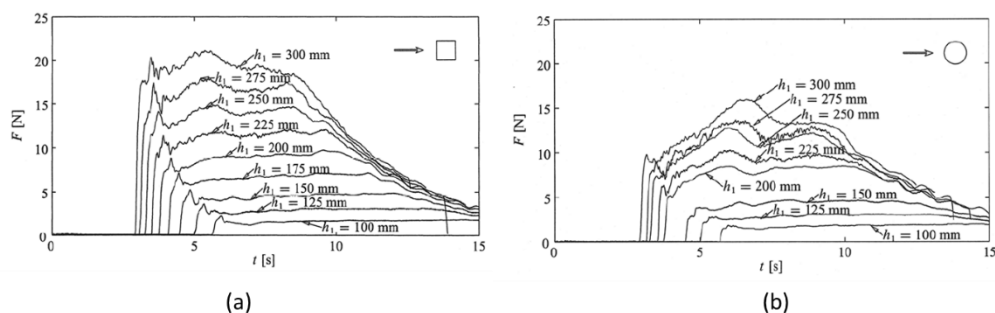
Figure 2.4 Time history of exerted force on (a) the square structure (b) the circular structure due to bores of varying heights [10]

According to [3], the maximum inundation depth is used as a height of the surge front used in the CCH surge force equation. [11] studied that the surge forces calculated from the CCH code give overestimated values compared with the surge

forces from the experiment under nominal wave conditions of 80mm. However, in the case of a dry bed surge, there is a constant increase in tsunami force before getting to the quasi-steady state. It is observed that no surge force overshoot the hydrodynamic force during the initial impact by [12], and these observations are the same as discussed by [2]. According to this reason, it can be concluded that for dry bed surge, surge force can be neglected.

2.3 Impact force due to debris

When a tsunami comes, the flooding water carries debris such as containers, ships, automobiles, parts of the structures, and even ships. The impact force due to these water-borne debris affects the structure seriously and leading to damage to the structure Figure 2.5. However, it is not easy to estimate this force accurately. When considering the structures which are constructed in the tsunami-prone region, the possibility of tsunami debris is assessed under these facts: (1) the potential distribution of debris and types of debris and (2) the forces generated by the impact. Debris types can be generally divided into three groups: small debris, moderate debris, and large debris shown in Figure 2.6 and Figure 2.7. Small debris is represented as objects that impact cannot affect the structure very much and moderate debris is generally defined as objects that impart a typical impact on the structure. Large debris is defined as objects that generate excessive forces on the structure and create a significant impact on the structure. If an object is specified as one of these groups, the characteristic of mass, size, stiffness, and buoyancy are identified first. Each characteristic directly affects the potential of debris that impacts the structure [13].

To estimate the debris impact force, three approaches are used as basic models. These approaches are (i) impulse-momentum, (ii) constant-stiffness and (iii) work-energy. These approaches depend on the mass and velocity of debris. Each approach needs their corresponding parameters such as impulse-momentum needs stopping time of debris after impact and time history of impact, constant-stiffness requires stiffness between debris and structure and then for work energy, distance traveled from where initial contact occurs to where debris stops. Background

information concerning the development of this force is provided by some codes and some researchers and discuss below.

Figure 2.5 Car and Boat as debris impact March 2011, Japan Tsunami
(Sourcehttp://www.thelargest.net)

Figure 2.6 Debris categories
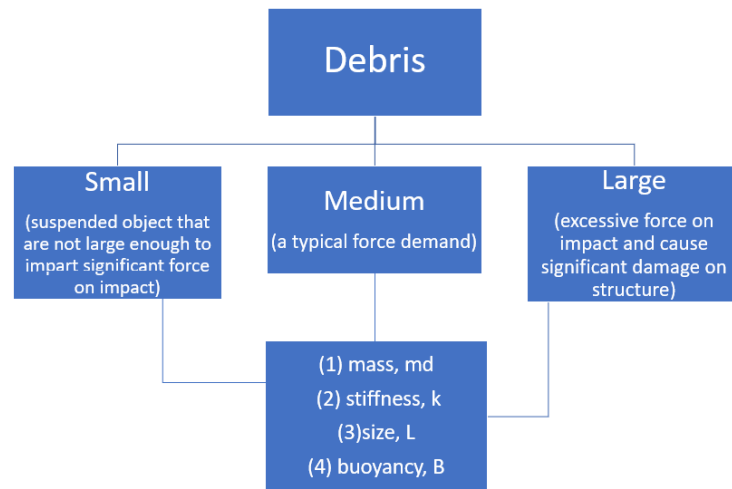
Figure 2.7 Small, moderate and large debris categories [13]

For the equation of debris impact forces, [4] code provides the following equation Eq. (2.7) based on the impulse-momentum concept. However, there is uncertainty to assess the impact duration, Δt. In this code, Δt assumes that 1.0 sec for a wooden structure, 0.5 sec for a steel structure, and 0.1 sec for a concrete structure respectively. The assumption of the impact duration times can cause a significant fluctuation in maximum impact load.

$$F_I = m\frac{du}{dt} = m\frac{u}{\Delta t} \qquad (2.7)$$

Where,

F_I = debris impact force

m = mass of impact body

u = velocity of the body

t = time

Depending on the size, shape, and weight of debris and flow velocity, the debris impact force is proposed by [3] using simplify equation of ASCE 7-10, Commentary C5 and can be seen in Eq. (2.8).

$$Fi = WVC_DC_BC_{str} \qquad (2.8)$$

Where

Fi = impact force acting at the still water elevation (lb)

W = weight of the object (lb)

V   = velocity of water (ft/sec), approximated by $1/2(gd_s)^{1/2}$

C_D = depth coefficient (see Table 2.1)

C_B = blockage coefficient (see Table 2.2)

C_{Str} = Building structure coefficient (use ASCE 7-10 Commentary equation)

Table 2.1 Depth Coefficient (C_D) by Flood Hazard Zone and Water Depth [3]

Flood Hazard Zone and Water Depth	C_D
Floodway[a] or Zone V	1.0
Zone A, stillwater flood depth $\geq$ 5 ft	1.0
Zone A, stillwater flood depth = 4 ft	0.75
Zone A, stillwater flood depth = 2.5 ft	0.375
Zone A, stillwater flood depth $\leq$ 1 ft	0.00

Table 2.2 Values of Blockage Coefficient CB [3]

Degree of Screening or Sheltering within 100 Ft Upstream	C_B
No upstream screening, flow path wider than 30 ft	1.0
Limited upstream screening, flow path 20-ft wide	0.6
Moderate upstream screening, flow path 10-ft wide	0.2
Dense upstream screening, flow path less than 5-ft wide	0.0

From the generalized equation of ASCE 7 based on the constant-stiffness approach, the debris impact force for flooding case can be estimated and provided in [1] which do not account to consider the orientation effects of debris but take into account to consider the hydrodynamic mass coefficient. In contrary to other tsunami forces, debris impact force can apply on a single structural element at water flooding level shown in Figure 2.8. The debris impact force equation according to ASCE 7 is shown in Eq. (2.9).

$$F_i = 1.3 u_{max} \sqrt{km_d(1+c)} \qquad (2.9)$$

Where

1.3 = important factor for debris impacts that is specified by [14]for Risk Category IV structures

u_{max} = maximum flow velocity of debris

c = hydrodynamic mass coefficient which depends on the shape, size, and orientation of the debris concerning the flow direction

k = the combination of effective net stiffness (the debris stiffness and the stiffness of the impacted structural elements), (see Table 2.3)

m_d = debris mass, (see Table 2.3)
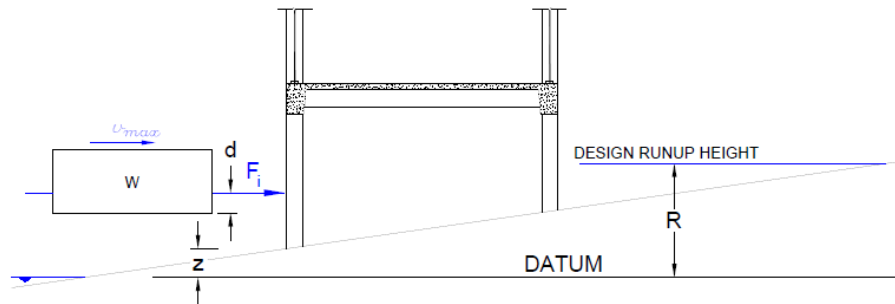
Figure 2.8 Debris impact force due to tsunami [1]

Table 2.3 Mass and stiffness categories for some debris [1]

Type of Debris	Mass (m_d) in kg	Hydrodynamic Mass Coefft. (c)	Debris Stiffness (k_d) in N/m
Lumber or Wood Log – oriented longitudinally	450	0	2.4×10^6 *
20-ft Standard Shipping Container – oriented longitudinally	2200 (empty)	0.30	85×10^6 **
20-ft Standard Shipping Container – oriented transverse to flow	2200 (empty)	1.00	80×10^6 **
20-ft Heavy Shipping Container – oriented longitudinally	2400 (empty)	0.30	93×10^6 **
20-ft Heavy Shipping Container – oriented transverse to flow	2400 (empty)	1.00	87×10^6 **
40-ft Standard Shipping Container – oriented longitudinally	3800 (empty)	0.20	60×10^6
40-ft Standard Shipping Container – oriented transverse to flow	3800 (empty)	1.00	40×10^6

* Haehnal and Daly, 2002; ** Peterson and Naito, 2012

If the stiffness and natural period of the structure and the stiffness and mass of the debris are determined, the impact force equation is provided by ASCE 7-16. The

nominal instantaneous debris impact force, F_{ni}, and the design instantaneous debris impact force, F_i are given in this code and shown below. However, in the case of shipping container impact, F_{ni} is not greater than 220 kips (980 kN) [14]. If an equivalent elastic static analysis is performed, the design F_i is needed to multiply with the appropriate dynamic response factor, R.

The nominal instantaneous debris impact force equation, F_{ni} is

$$F_{ni} = u_{max} = \sqrt{km_d} \qquad (2.10)$$

The design instantaneous debris impact force equation, F_i is

$$F_i = I_{tsu}C_oF_{ni} \qquad (2.11)$$

Where

I_{tsu} = Importance Factor (given in Table 2.4)

C_o = Orientation coefficient, equal to 0.65 for shipping containers

u_{max} = Maximum flow velocity at the site occurring at depths enough to float the debris

k = Effective stiffness of the impacting debris or the lateral stiffness of the impacted structural element(s) deformed by the impact, whichever is less

m_d = Mass (W_d/g) of the debris

Table 2.4 Tsunami importance factors for hydrodynamic and impact loads

Tsunami Risk Category	I_{tsu}
II	1.0
III	1.25
Tsunami Risk Category IV, Vertical Evacuation Refuges, and Tsunami Risk Category III Critical Facilities	1.25

[15] conducted the small-scale experiment generating surge as well as bore and full-scale experiment about impact force produced by driftwood on a rigid structure. In the full-scale experiment, wooden logs hit a frame in the open air, and then, impact forces produced were estimated. All scaling effects are considered in a full-scale experiment in design. However, in the small-scale experiment, the added mass of water is only considered in the design. Therefore, the estimated impact forces

from the full-scale experiment can vary with real tsunami because of neglecting the added-mass of water. [15] provided a formula for the impact force due to wooden logs based on his regression analysis and as follows in Eq. (2.12).

$$\frac{F}{\gamma_w D^2 L} = 1.6 C_M \left(\frac{u}{\sqrt{gD}}\right)^{1.2} \left(\frac{\sigma_f}{\gamma_w L}\right)^{0.4}$$ (2.12)

Where

r_w = specific weight of the wood or log

D = diameter of the wood or log

L = length of the wood or log

C_M = added-mass coefficient (1.7 for bore or surge and 1.9 for steady flow)

u = velocity of the wood or log at impact

δ_f = yield stress of the wood or log

[16] analyzed a single degree of freedom model (Figure 2.9) to evaluate the woody debris impact force for a rigid structure based on three approaches such as (i) impulse-momentum, (ii) constant-stiffness, and (iii) work-energy. They showed that the formulae of three approaches derived from the single degree of freedom model are identical and yield the maximum impact force and the equation for debris impact can be seen in Eq (2.13):

$$F_I = Max.(kx) = u\sqrt{km}$$ (2.13)

In which the effective stiffness, k is derived by the following equation.

$$\frac{1}{k} = \frac{1}{k_d} = \frac{1}{k_s}$$ (2.14)

Where

u = debris velocity

m = debris mass

k_d = debris stiffness

k_s = structure stiffness
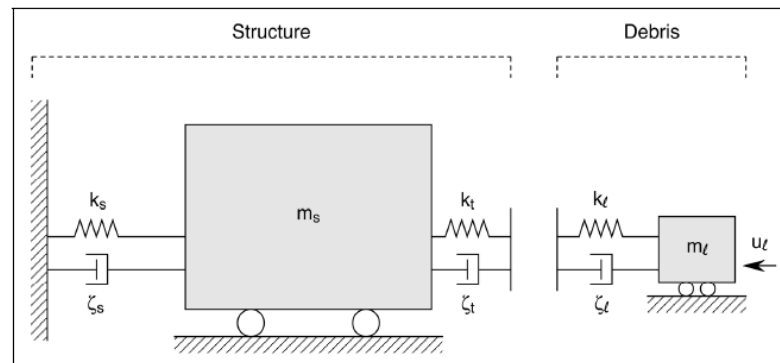
Figure 2.9 Impact of a single debris element with a structure [16]

They also found that the resulting debris impact force is a function of impact velocity, debris mass, and effective stiffness of the collision between the woody debris and the structure. Hence the formula is not depending on the properties of the structure if the structure is considered rigid. They also investigated the influence of added-mass of the water and eccentric and oblique collision in which the maximum impact force was found when the log (major axis of the log parallel to the flow direction and perpendicular to the structure) hits the structure. Figure 2.10 shows the orientation effect of the debris impact.
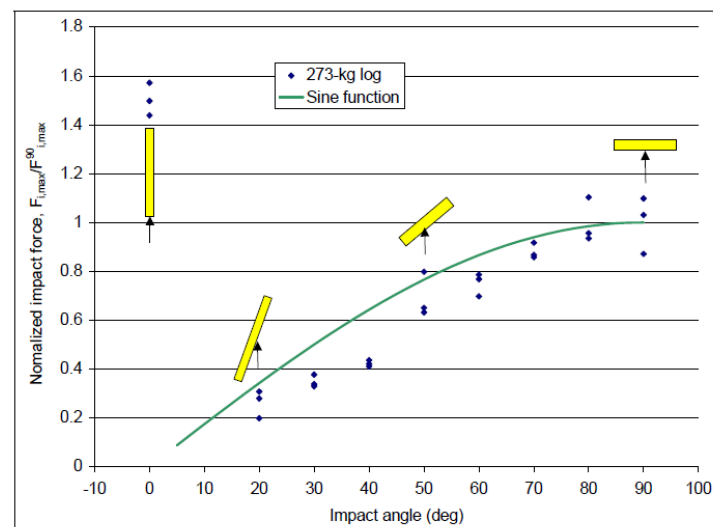
Figure 2.10 Effects of orientation on impact force [16]

[17] presented numerical simulations to study the behavior of debris impact load on wood panels such as exterior and interior walls. They used the exact

experimental results based on [16] small scale tests to compare their numerical results. The comparison results of the impact forces between experimental and numerical modeling are shown in Table 2.5. The results based on numerical modeling were within the range of the experimental results and thus these results were validation for conducting the parametric studies. Various parameters used in their study are flow velocity, inundation depth, debris size, and debris density. They found that as the flow velocity and debris mass increase, the impact force on the exterior wall panel increase in Figure 2.11. However, for the interior wall panel when the flow velocity and debris mass increase with mass constant, reduction in debris impact force was investigated.

Table 2.5 Comparison of debris impact forces between numerical and experimental results [17]

Velocity (m/s)	Contact-Stiffness force $1550u\sqrt{m}$ (N)	Numerical modeling force (N)	Difference (%)
0.381	2621	3218	54.3
0.533	3667	3218	12.2
0.800	5504	4037	26.6
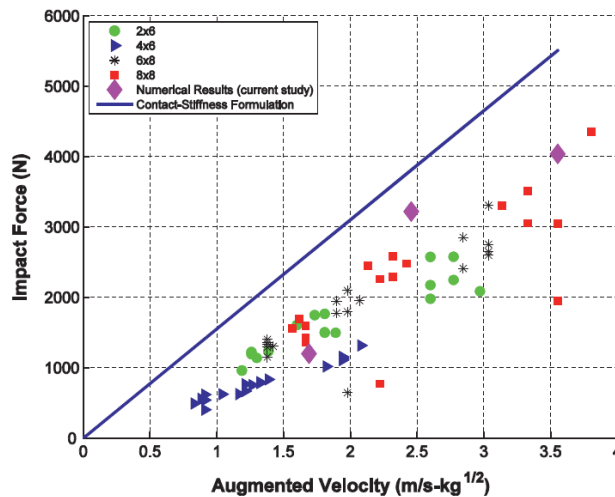
Figure 2.11 Comparison of numerical and experimental results for debris impact forces [17]

The response of reinforced concrete columns impacted by tsunami dispersed shipping containers (20 and 40 ft) are studied by [18]. The difference in peak impact forces estimated between FEMA-P646 and ASCE 7-10 is quite large for 20 and 40 ft

containers shown in Figure 2.12. Therefore, there is needed for further investigations of estimated peak impact forces.
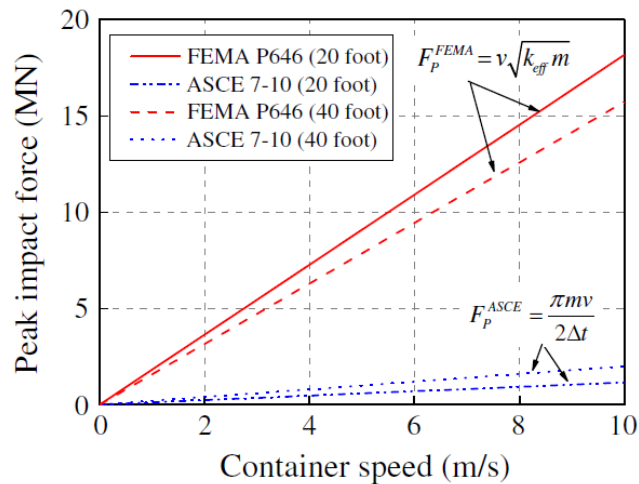
Figure 2.12 Comparison of estimated peak impact force for 20' and 40' containers [18]

Square and circular columns were used for each container with different column-container impact configurations as shown in Figure 2.13. The peak impact force for a square and a circular column for a 20 ft container was found in L3 and C1 configurations respectively. On the other hand, the peak impact forces for 40 ft container were found in the L2 configuration in both columns. In these cases, the peak impact force for 40 ft container was greater than that for 20 ft container because of the mass of the container and the structural system of the container (additional stiffness). They found that for most impact configurations, the peak impact force is larger in the square column than in the circular column since the container-column contact area is wider in the square column. They also formulated the average impact duration and effective contact stiffness for both types of columns of 20 and 40 ft containers respectively. The average impact duration and effective constant stiffness are used to calculate the impact force equation from FEMA p-646 and ASCE 7-10.
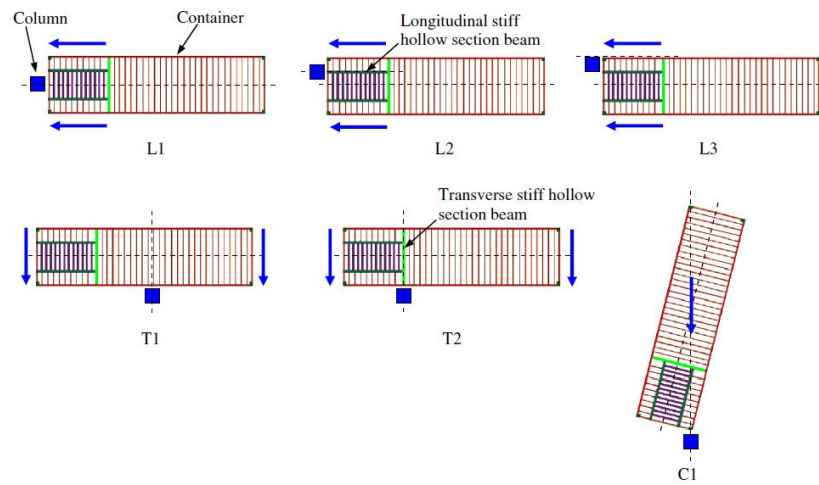
Figure 2.13 40 ft container-column impact configurations [18]

The effect debris attached with the nonstructural mass (NSM) and the maximum impact force and duration were investigated by [19]. Empty and loaded shipping containers were used in the experiments and to validate the results, a nonlinear dynamic finite element model was established. The equivalent nonstructural-mass-spring-bar model as an SDOF system was used to account for the connection between NSM and container Figure 2.14. The effects of NSM, amount of payload mass, and impact velocity were used as parametric studies. They explored that the maximum primary impact force and duration are not influenced by the NSM as shown in Figure 2.15. They also found that the equivalent model allows for an accurate prediction of the maximum impact force for all three cases.
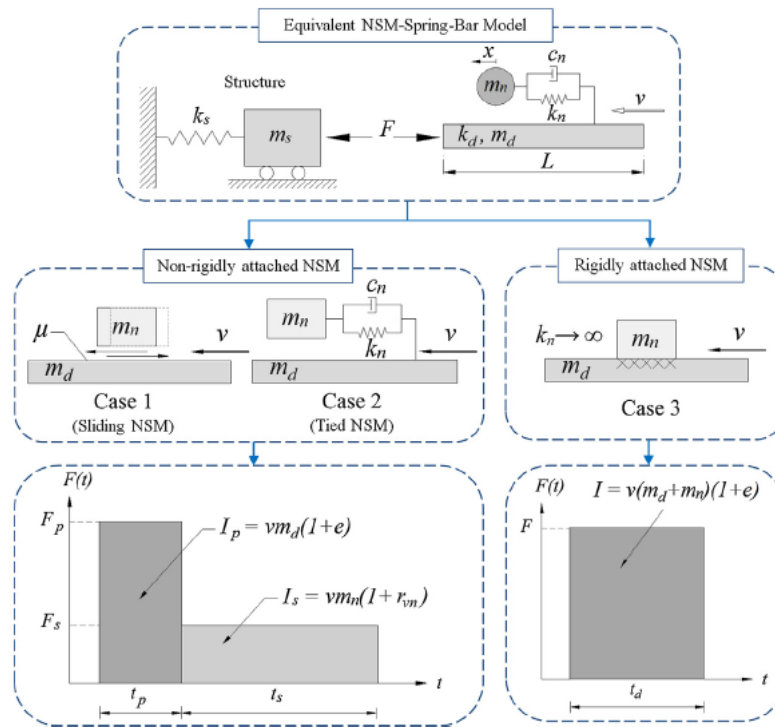
Figure 2.14 Idealized force-time histories due to the impact of debris [19]
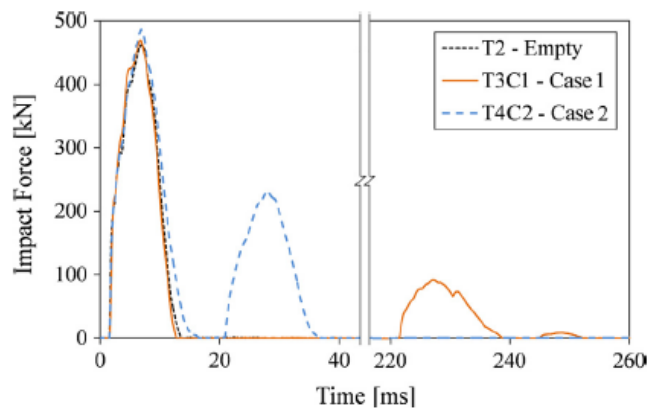
Figure 2.15 Measured impact force-time histories for empty and loaded container tests at 1.0 m/s. [19]

[20] tested the effect of transverse impact form tsunami driven object using a full-scale standard container, steel bar (solid bar and hollow tube) sections. Axial and transverse impact configurations for orientally shipping containers are shown in Figure 2.16. Analytical models for transverse members were considered as elastic and inelastic SDOF dynamic model to evaluate the impact duration and maximum impact force. Finite element simulation was performed to study the effect of transverse debris

impact and then validated with experiments. In comparisons of the experimental peak impact results with the estimated peak impact values for shipping containers provided by FEMA P-646 and ASEC 7/10, FEMA P-646 got over-conservative values especially for high impact velocities and however peak impact values obtained from ASCE 7/10 were unconservative in case of the elastic model. The comparison results are shown in Figure 2.17.

(a)   (b)

Figure 2.16 (a) Axial and transverse impact configurations for a shipping container and (b) damaged shipping containers under the transverse impact [20]
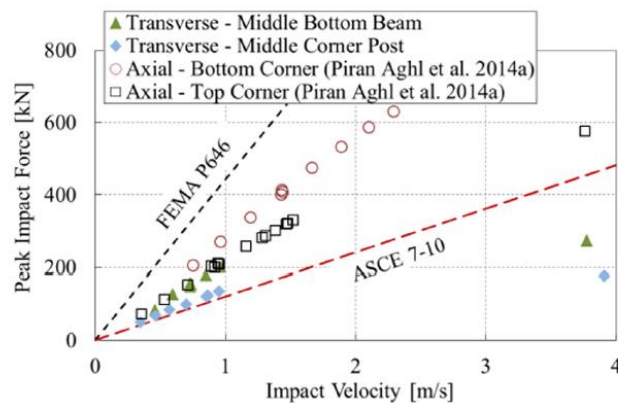
Figure 2.17 Measured shipping container peak impact force

[21] investigated the linear response of a transverse horizontal beam hitting a fixed-end column for elastic case only shown in Figure 2.18. Consideration of impacting velocity was 3-5 m/s since they only focused on elastic behavior. The initial peak impact force equation was formulated using the Timoshenko beam theory in an analytical impact model. They considered multiple impact cases i.e. contact phase and separation phase were also considered in the collision event. Results of the

analytical method were examined with the numerical method. The results of both methods are comparable. They explored that the peak impact force of the beam that hit the column can be 1.5 times than the initial peak force. They investigated the domination of shear deformation in the pole and the column due to multiple impacts.
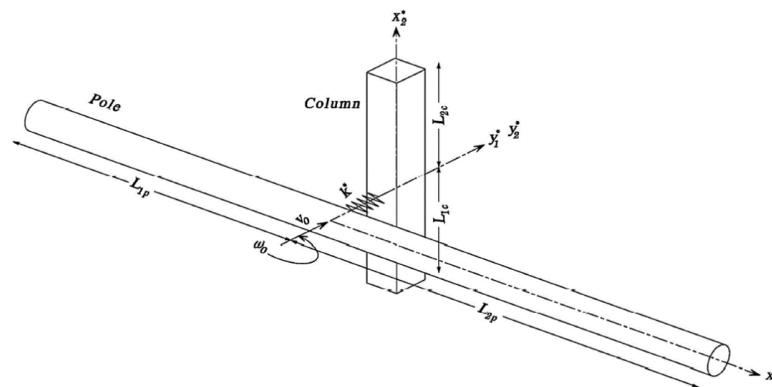
Figure 2.18 Schematic of pole and column [21]

[22] studied the design procedures to evaluate the extreme impact loads on structures such as shipping vessels, containers, and even wood poles. In their case study, flow velocity and flow depths are estimated using three methods: (1) Energy grade line method and (2) Modified energy grade line method and (3) Site-specific inundation analysis which are needed to estimate the impact force. However, for estimating equivalent static impact force, ASCE 7/16 provided the two approaches: (1) an alternative simplified approach and (2) impact force and duration equation approach. By comparing the equivalent static impact force from the two approaches, there was a negligible difference between these approaches. They recommend that the modified energy grade line method was appropriate to estimate inundation depth and flow velocity for tsunami inundated regions.

2.4 Study of flow velocity
        The velocity of the flooding water can differ significantly during tsunami events. Differences in calculating tsunami forces as well as debris impact forces are due to the differences in estimating flow velocity. There is less information concerned

with flow velocity during these events. The magnitude and direction of flow velocity can vary significantly during the tsunami. Flood water can reach a site from one direction at the beginning of the tsunami event and then move to another direction. Variation of flow velocity can be found by flooding water that reaches a low-lying region. Hence, the flow velocity can vary from zero to higher velocity during a single tsunami event. The general form of the flow velocity due to the tsunami is shown in Eq. (2.15).

$$U = \alpha\sqrt{gh} \tag{2.15}$$

Where

U = the flow velocity, m/s

α = constant-coefficient

h = the inundation depth, m

Several codes and researchers have investigated the flow velocity in terms of inundation depth. The FEMA (2003) assumes that a constant coefficient of flow velocity can be 2 but Yeh (2007) supposed that this is too high. Under the real load test on a minor damaged building in Khao Lak, Thailand, [23] calibrated with the tsunami loading based on FEMA P-55 and found that the suitable flow velocity as $1.2\sqrt{gh}$ - $1.36\sqrt{gh}$.

[11] studied the relationship between the velocity and flow depth using a small-scale model experiment with the impact of a tsunami-induced bore. They used the velocity with the equation of $1.5\sqrt{gh}$, $2\sqrt{gh}$ and $2.5\sqrt{gh}$ and they found that the computed maximum velocities using the equation of $2\sqrt{gh}$ are approximately the same as the measured velocities Figure 2.19. However, they said that the constant coefficient may be less than 2 when the beach slope is steeper.
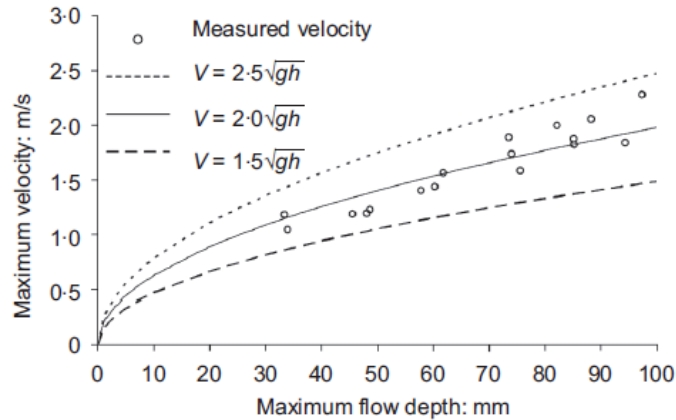
Figure 2.19 Comparison of the measured velocity and the computed velocity [11]

In 2016, [24] studied the impact of tsunami bores on a square model using an experiment. To calculate the bore flow velocity, they used some equations to compare the measured values Figure 2.20. The velocity equation, u is equal to $\alpha\sqrt{gh}$ in which α=1.7 is within 7% and 10% of the values of Murty (1977) and FEMA (2012) respectively.
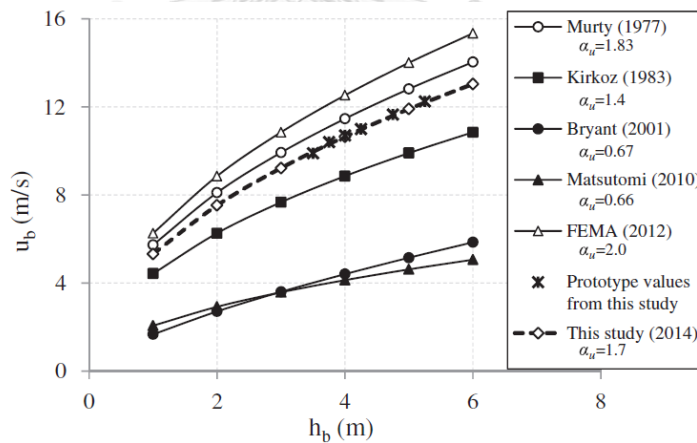
Figure 2.20 Relationship between bore velocity and bore height for different studies [24]

Due to the influence of the parameters such as wavefront celerity and velocity profiles to estimate the impact forces, the average front celerity from dry bed surges was compared with the formula design codes and practices by [25]. They found that the waves produced from the proposed experiment (Vertical release generation

technique) had celerity values at α = 1.25 and correlated with other investigations Figure 2.21.
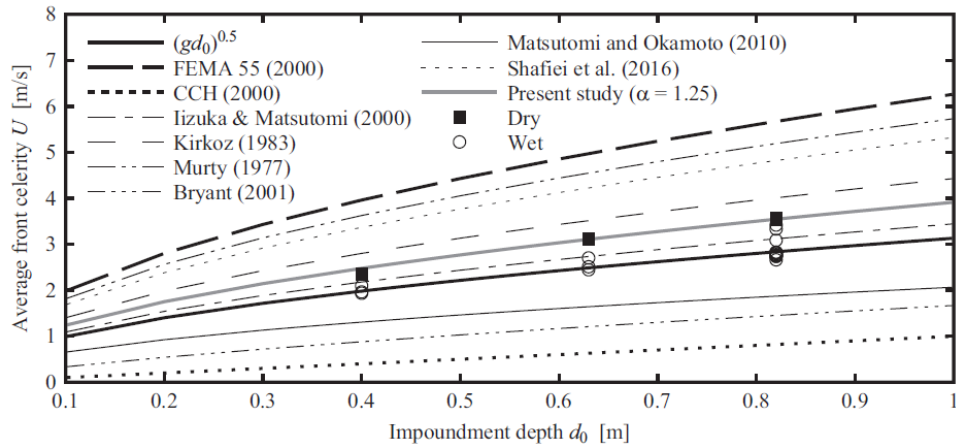
Figure 2.21 Comparison of the measured average front celerity [25]

2.5 Configuration of the structure under the response of tsunami

The configuration of the building is very important for potentially tsunami inundated regions. Irregular building shape suffers more significant tsunami forces than the shape of the regular building, especially undesirable torsional effects occur in structural elements. Therefore, a simple regular shaped building is more suitable over an irregular shape as shown in Figure 2.22.
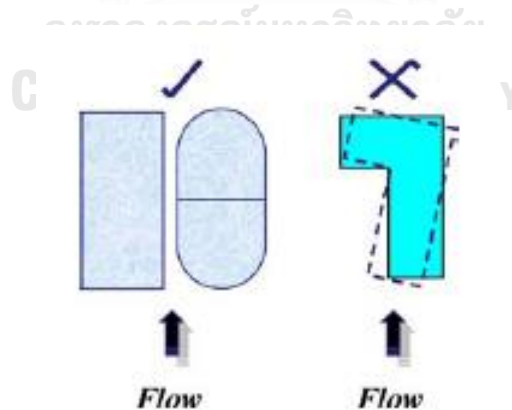
Figure 2.22 Shapes of regular and irregular Building

[26] studied that the rectangular and circular building shapes which consist of the provision of stilt columns and opening to protect the tsunami waves. According to his conduction, the increase in the opening of the building increases the stability of the building. However, he recommended that the percentage of the opening should be

up to 50% so that it can care for the stability of the structure. He also concluded that the circular building is better than a square building to withstand tsunami impact loads. The prototype of the circular building is shown in Figure 2.23.
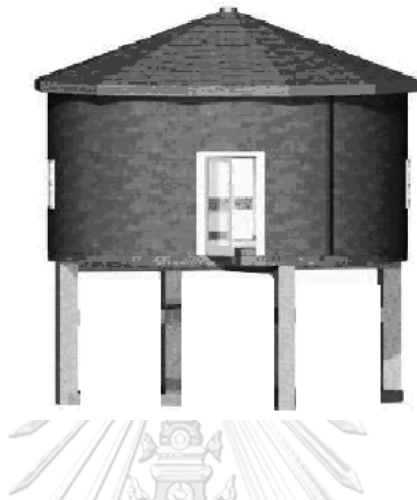
Figure 2.23 Circular shaped building [26]

[26] used the stilt columns and there are no partitions between the column because these allow the free flow of tsunami waves. Hence, no partition walls or breakable walls are a considerable aspect of tsunami case. The performance of a structure with a strong wall and the breakable wall is illustrated in Figure 2.24. As we can see, there is minimal damage that occurred in the breakable wall however, due to the loading transferred effects of the strong wall, structural elements significantly suffer tsunami impact.

Figure 2.24 Performance of strong wall and the breakable wall [27]

The effect of openings is also important for the structure to reduce the incoming tsunami impact forces. As we can see in Figure 2.25, the area of the tsunami inundated region is damaged by the tsunami wave, but the mosque still survived from tsunami wave because of the effect of opening and good structural configuration system. [28] conducted the effect of openings for a reinforced concrete building using a small-scale building model approaching with broken wave such as a bore. The result of the tsunami forces with the different openings is shown in Table 2.6. Based on the experiment of their results, 15% to 25% reduction has resulted in a 25% opening configuration and 30% to 40% reduction are in the case for 50% opening configuration, respectively.

Figure 2.25 Rahmatullah Lampuuk Mosque stands unhurt after the 2004 tsunami hit the area in Lhoknga, near Banda Aceh, Indonesia

Table 2.6 Tsunami force (N) on a square model with different opening configurations [28]

Opening	Nominal Wave height								
	40 mm			60 mm			80 mm		
	PF0	PF1	PF2	PF0	PF1	PF2	PF0	PF1	PF2
0%	2.65	1.23	0.49	3.96	2.08	1.11	4.36	3.10	2.30
25%	2.80	1.04	0.33	4.56	2.04	1.19	4.61	2.71	2.14
50%	2.99	1.16	0.13	4.94	1.93	1.26	4.66	3.07	2.40

[29] investigated the effect of opening and protection on building to reduce the tsunami impact forces. They simulated an experiment using the dam break model to obtain the wave forces on building with various openings. They clearly show that the openings significantly reduced the tsunami forces on the building, shown in Figure 2.26 and Figure 2.27.
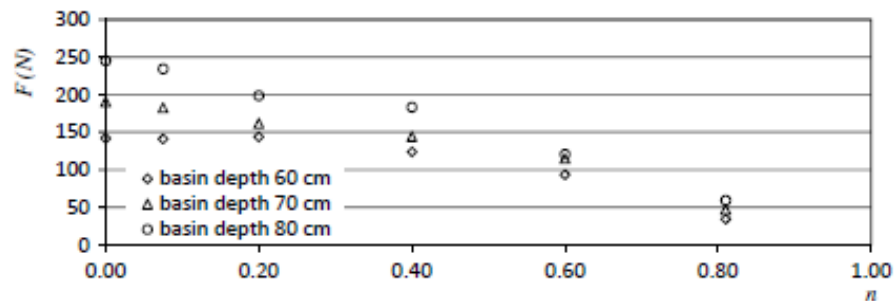
Figure 2.26 Tsunami force on building with various openings [29]
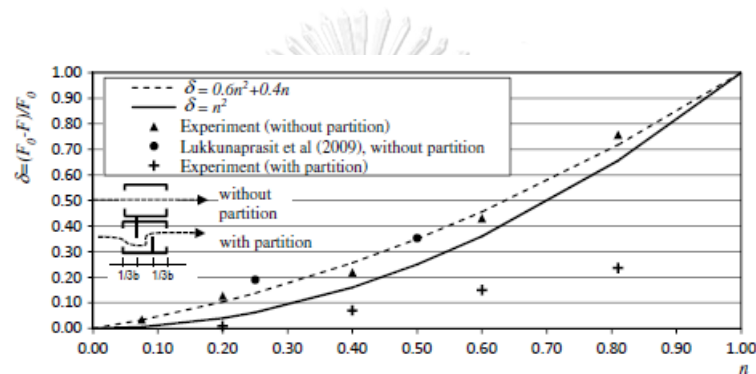
Figure 2.27 Force reduction due to opening [29]

The influence of openings on building and building shape is investigated by [11] using a small-scale model under the same condition at Khao Lak, Thailand. They observed that the square and rectangular-shaped buildings were approximately the same results of tsunami force. However, for an octagonal building, the tsunami force per unit width was reduced by 20 percent compared with a square-shaped building. The condition of the tsunami wave force on different building shapes is shown in Table 2.7. The results of the wave force acting on the building with the opening configuration of 25% and 50% were reduced about 10 to 30% and 40 to 60% of the tsunami wave force respectively shown in Table 2.8.

Table 2.7 Tsunami force on building with different configuration: S, square; R, rectangular; O, octagonal [11]

Nominal wave condition: mm	Force: N		
(a) Khao Lak (K), Phang Nga, Thailand	KS	KR	KO
30	8·24	11·71	6·85
60	16·97	21·77	11·07
80	23·25	36·42	16·70
(b) Kamala, Phuket (P), Thailand	PS	PR	PO
40	6·84	10·68	6·08
60	18·15	29·28	14·11
80	36·98	59·68	26·93

Table 2.8 Different openings under various wave condition [11]

Opening	Nominal wave condition		
	30 mm	60 mm	80 mm
0%	9·8 (100%)	17·8 (100%)	23·1 (100%)
25%	6·8 (69%)	14·7 (83%)	21·0 (91%)
50%	4·1 (42%)	8·8 (50%)	13·2 (57%)

[30] investigated the pressure distribution on the wall due to the impact of tsunami bore for various wave heights using a tsunami wave basin. Maximum pressure distributions were found at the base of the wall of the building for various wave heights. The results of the experiment for typical wall pressure distribution are illustrated in Figure 2.28. They concluded that if nonstructural walls are used in the building, they will easily break away under these loads and as a result, can reduce tsunami loads.
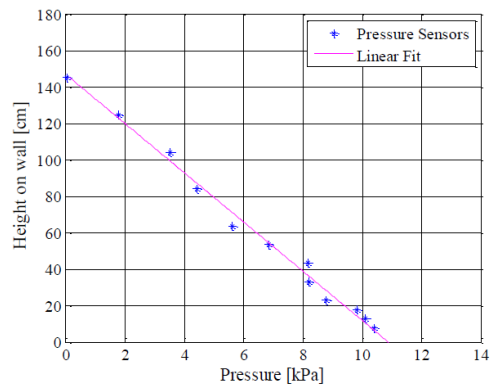
Figure 2.28 Pressure distribution on a typical wall due to peak impact load of 120.5 cm wave with 5 cm standing water

2.6 Protection system to reduce large impact forces

Fender is the pile or frame attached with energy absorption devices such as rubber fender in the marine system shown in Figure 2.29 and Figure 2.30. The function of the fender is to protect the berth structure against damaged caused by the ship approach by absorbing the kinetic energy of the ship. Fender system to prevent damages due to ship impact is carefully designed on the coastal region by using timber, rubber, and metallic fender types.

In the previous literature review, the governing forces that are considered for the design of building in tsunami inundation regions are studied according to some guidance and researchers. However, most of the collapsed buildings have come from the impact of large debris forces such as shipping boats, shipping containers, etc. Sizes of structural members should be large to resist these large impact forces however it can be uneconomical and impractical. Therefore, the design of the fender system is considered as a tsunami shelter for debris impact loads and hydrodynamic pressure.
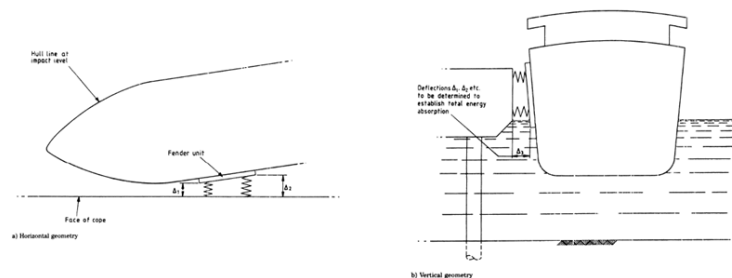
Figure 2.29 Fender geometry impact [31]

Figure 2.30 Marine fenders

To design the fender system, [27] introduced the design of the evacuation shelter due to tsunami in two categories namely (i) small to moderate debris impact and (ii) large debris impact. The configurations of the evacuation building used for both types of debris are shown in Figure 2.31.

For small to moderate debris impact, the structures may be rigid to resist tsunami loads and hence no energy absorption devices are necessary because of the sizes of debris. However, to resist the impact of large debris, inner and outer structures are considered, and the inner structure is the main building, and the outer structure is such a fender locating at the side of the seashore to protect the inner one. Therefore, energy-absorbing devices are proposed to resist the large debris impact relying on the work-energy principle to balance the kinetic energy of the movement of large debris masses with the potential energy absorbed by devices shown in Figure 2.32. These devices are installed outside of the main building on every floor level connect with a rigid beam. The height of the outer structure is determined by the inundation depths because it only needs in lower levels of the main building to protect from debris. The outer structure should displace over a large distance to accommodate the deformation of energy-absorbing devices and hence the foundation should be designed to allow such movement. Pimanmas et al. (2010) concluded that they provided the design concept as a guideline for tsunami evacuation shelters in a tsunami-prone area.
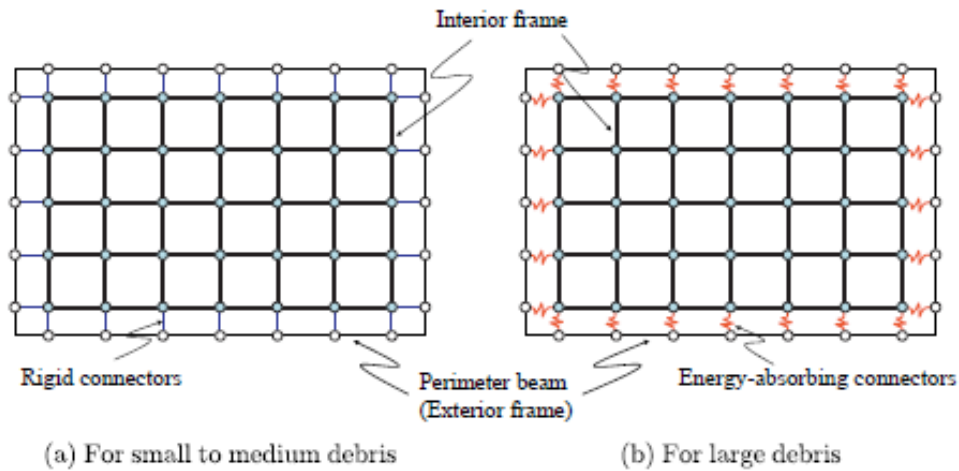
Figure 2.31 Schematic structural system for resisting tsunami [27]
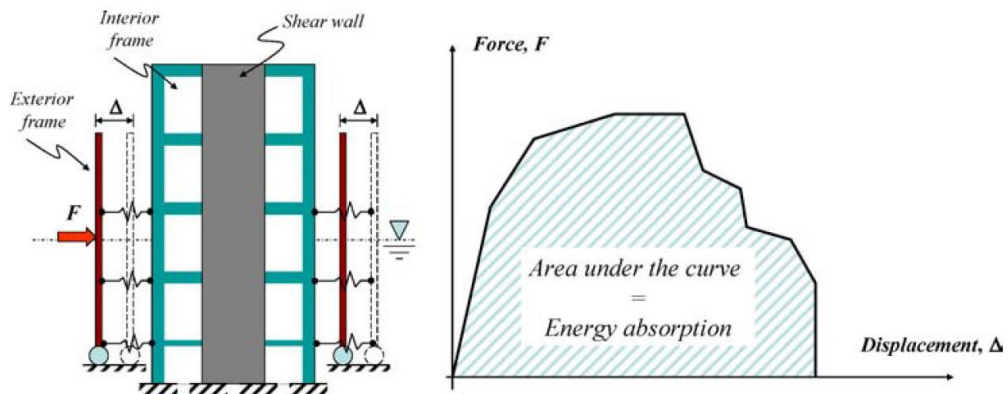
Figure 2.32 Relationship between force and deformation and capacity curve [27]

[32] proposed the tsunami evacuation building surrounded by fender piles to absorb the impact of moving debris shown in Figure 2.33 by using numerical simulation and experimental testing. Not only tsunami wave force but also the collision of tsunami driftage with the building is considered. The influence of fender pile due to tsunami wave forces is investigated in two conditions: with and without fender piles. According to numerical simulation and experimental testing, fender piles can effectively reduce the tsunami wave forces when tsunami driftage strikes shown in Figure 2.34.
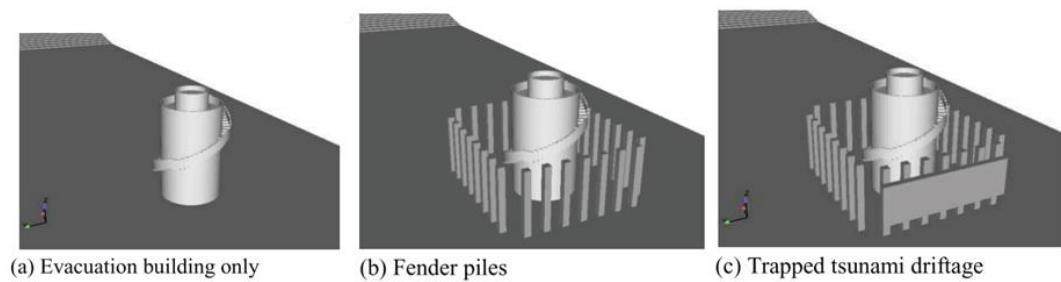
(a) Evacuation building only   (b) Fender piles   (c) Trapped tsunami driftage

Figure 2.33 Building model setups
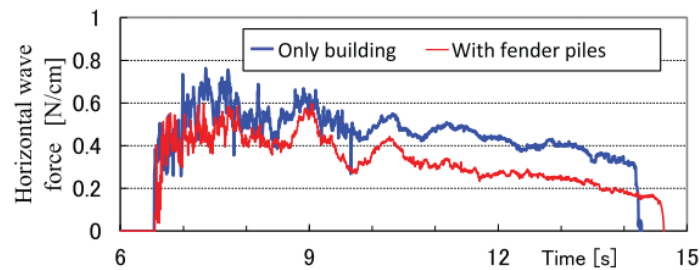
Figure 2.34 Tsunami wave force acting on tsunami evacuation building

With the help of energy absorption devices to reduce large debris impact based on the work-energy principle, [33] studied the behavior of 4-story RC buildings under tsunami loads and debris impact loads. The building consists of the main building and an outer protecting building shown in Figure 2.35. Nonlinear static analysis is used to investigate the effectiveness of the protection frame over the main building with energy-absorbing devices (Cone type fender devices). Types of debris impact forces applied to the building are categorized in Table 2.9.

Table 2.9 Comparison of types of debris impact depending on its sizes applied to building [33]

Comparison	Small to medium debris	Large debris
Types of object	Cars, logs, trees	Large fishing boats, shipping containers
Mass (KN)	5 tons	784 tons
Impact force equation	$F_i = \dfrac{W_i v_i}{gt}$	$KE = \dfrac{1}{2}mv^2$
The position of the impact loading	The critical position of the building	

Based on the work-energy principle, the kinetic energy of the moving debris is balanced with the potential energy absorbed by the connection and the equation is provide in Eq. (2.16). This principle is simple and rational to use with energy absorption devices.

$$KE = W$$
$$\frac{1}{2}mv^2 = \int f(x)dx \tag{2.16}$$

Where

KE = kinetic energy of debris mass

W = potential energy by the energy dissipation devices

m = mass of debris

v = flow velocity

f(x) = the reactive force (fender)

x = deformation (fender)

The energy absorption device is used as a connection between the inner and outer structure and can absorb the high impact energy by losing the elastic form of itself and resulting in little reaction force. The inner structure should be designed to be in the elastic range under the reaction force that is sent from the connector. If the strength of the inner structure is weaker than the connectors, large inelastic deformation cannot be controlled by the connectors.

The connectors are modeled as nonlinear elements and the force-deformation response of the nonlinear link can be attained from the manufacture or laboratory test.

The connection between the column and the beam of the outer structure is used as pinned and rigid types. The ability of the energy absorption of the building with and without the fender systems are shown in Figure 2.36 and Figure 2.37.
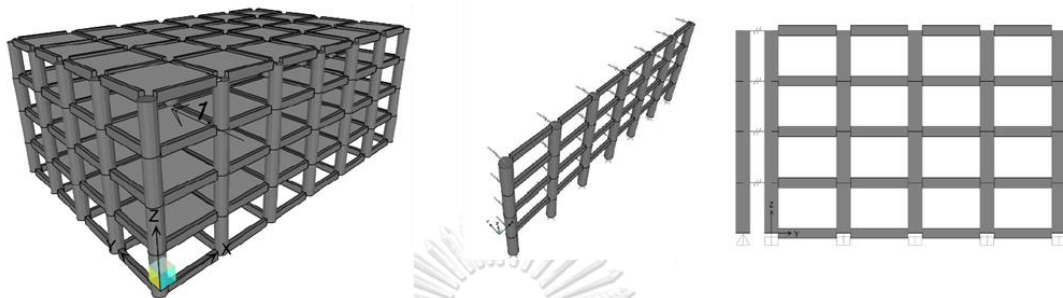
Figure 2.35 3D and elevation view of the main building with the energy absorption devices [33]
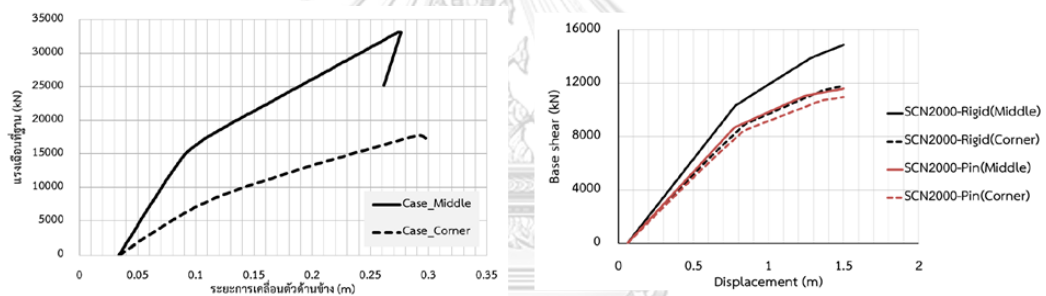
Figure 2.36 Relationship between base shear and displacement of the building without and with energy-absorption devices [33]
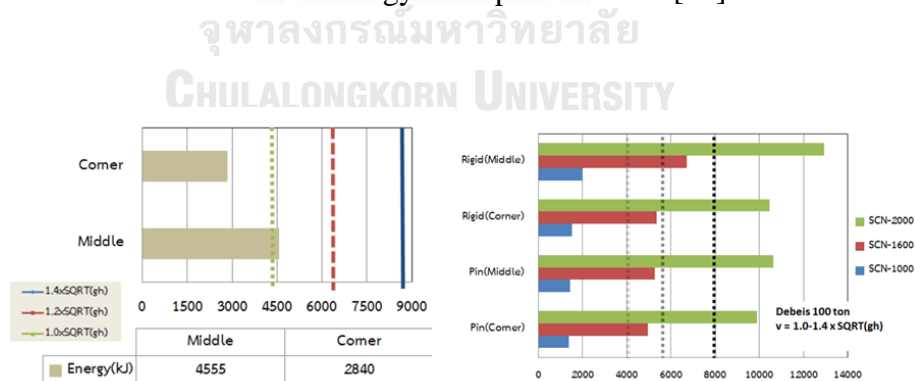
Figure 2.37 Ability of energy absorption without and with fender system [33]

Magada [34] addressed the benefits of the interaction between a marine rubber fender and a steel pile structure of a berthing dolphin. By using the interactive treatment method (ITM), the proper selection of the minimum required size of the steel structure was evaluated by diving the absorbing energy into two components

such as fender and steel structure. According to this author, the fender selection and the mass and stiffness of steel pile structure are the influence parameters for the economical point of view. A general group of berthing dolphins with a steel pile substructure was illustrated in Figure 2.38. To calculate the kinetic energy of moving vessels, Eq. (2.17) was used in the study [31, 35].

$$E_{ka} = \frac{Mv^2}{2} C_m C_e C_s C_c F_a \qquad (2.17)$$

where

Eka = abnormal berthing kinetic energy of the vessel to be absorbed by dolphin elastic deflection (kilojoules); M = displacement of the vessel (tons); v = approach velocity of the vessel perpendicular to the berthing line (meters per second); Cm = added mass coefficient (virtual mass coefficient); Ce = eccentricity coefficient; Cs = softness coefficient; Cc = berth configuration coefficient; and Fb = abnormal impact safety factor.
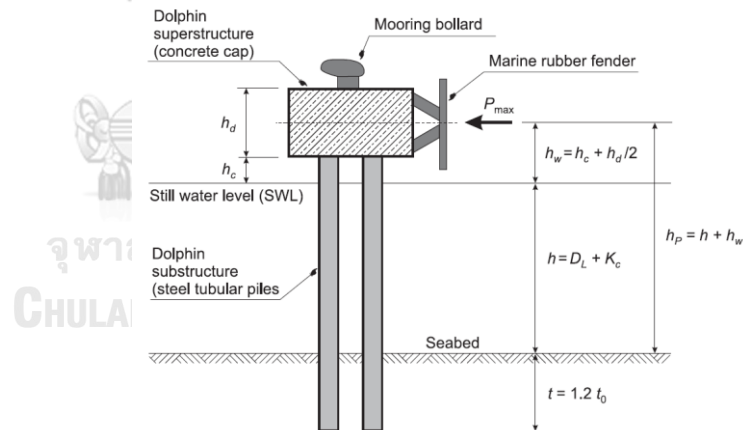
Figure 2.38 General view of the berthing dolphin

[36] described that the performance-based approach for the flexible breasting dolphins. In this study, the coupled behavior of the flexible structure-fender system and the energy absorption capacities of each component were investigated. The energy absorbed by each component was described in Figure 2.39 and 40.
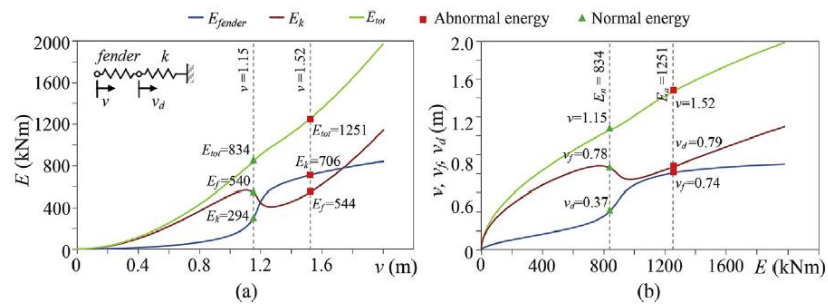
Figure 2.39 (a) Energy absorbed by the system components vs the global displacement v; (b) displacements of dolphin vd, of fender vf and global displacement v vs the absorbed energies
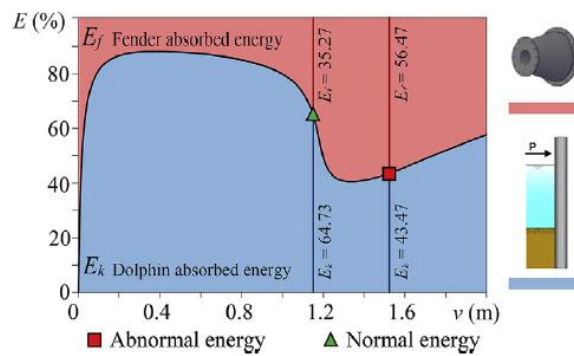
Figure 2.40 Percentage of energy absorbed by the system components

It was observed that the contribution of the flexible dolphin in absorbing the impact energy of the normal berthing is higher than the fender contribution, while the fender contribution is essential in abnormal conditions.

2.7 Energy absorption devices

Fender systems on the coastal region to prevent damages due to ship impact are designed carefully by using timber, rubber, and metallic fender types. Energy-absorption devices used in marine fender systems are mostly made of rubber with various kinds of shapes such as cone shape fender. The primary objective of the rubber fender is to absorb collision energy during the berthing process. The structure of the fender system consists of the main fame which is made of steel or concrete or timber and in which the impacted area is comprised of energy-absorbing elements such as rubber elements, metallic elements, and so on.

Rubber fender and steel damper can be used as energy absorption units to absorb the energy of moving debris depending on their sizes. Fender elements can absorb the energy from impact by deforming by themselves which will be attached to the rigid structure. The fender system can be comprised of a single energy absorbing unit or several energy absorbing units together to absorb impact. Types of rubber fender-element used in the fendering system are shown in Figure 2.41 according to [37]. The deformation of the fenders is depending on the types of the fender which are available in the commercial catalog. In cone shaped-fender type, the ultimate deformation is 72 % of fender length while in the cell fender, the deformation is 52.5% of its length.
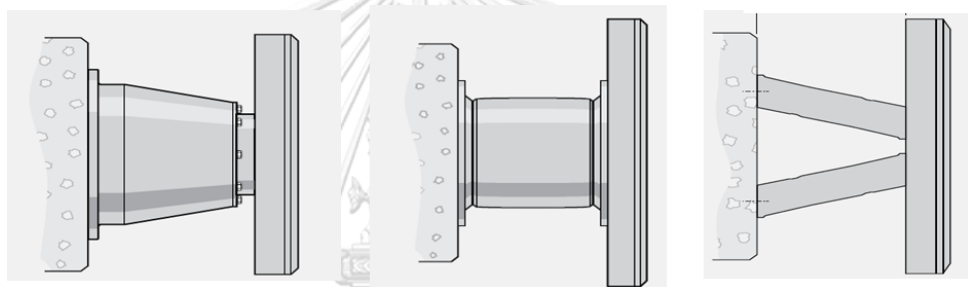
Figure 2.41 Types of the fender by commercial catalog

2.8 Tsunami pushover analysis

Few studies have focused on the tsunami pushover analysis for the hydrodynamic load pattern. In 2014, Macabuagi et al. [38] presented that the tsunami fragility function using the tsunami pushover analysis using the force-controlled method. The tsunami loading based on the codes that are considered in this literature is illustrated in Table 2.10. The resultant pushover curve according to these loading conditions is shown in Figure 2.42. According to these results, it was found that the applied load distributions are very sensitive to the tsunami pushover curve.

Table 2.10 Load cases to generate pushover curve

Tsunami PO Curve Ref	Design Standards	Description of Loading
1	MLIT 2570	Equivalent hydrostatic pressure. No shelter from the incoming wave.
2	MLIT 2570	Equivalent hydrostatic pressure. >500m from the water source with shelter from the incoming wave.
3	MLIT 2570	Equivalent hydrostatic pressure. <500m from the water source with shelter from the incoming wave.
4	FEMA 646	Impulse loading based on the maximum momentum flux at each inundation depth. Uniform vertical distribution. Runup taken as that of the maximum credible tsunami at the site, assumed as 10m for the purpose of this investigation.
5	FEMA 646	Impulse loading based on the minimum momentum flux at each inundation depth. Uniform vertical distribution.
6	ASCE 7-16	Simplified pseudo-static approach. Hydrostatic pressure distribution with density multiplied by 3.
7	ASCE 7-16	Hydrostatic drag (no bore impact).
8	ASCE 7-16	Bore impact over standing water. At each step of inundation depth (h_i), bore height = 50% of inundation depth and standing water is assumed to a depth of 15% of the bore height.
9	ASCE 7-16	Bore impact over a dry bed. At each step of inundation depth (h_i), bore height = 50% of inundation depth.
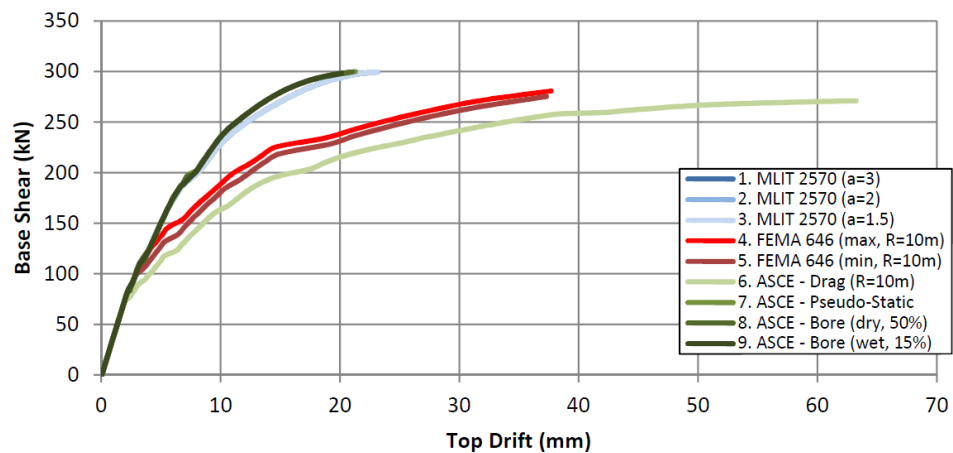
Figure 2.42 Relationship of base shear and displacement for different tsunami loading pattern

In 2017, [39] determined the most reliable method for the evaluation of structural performance under tsunami action. In this literature, two different types of tsunami pushover methods were considered such as constant high pushover (CHPO) and variable high pushover (VHPO) methods. The validation of these methods was compared with the time history method. CHPO is the displacement-controlled and VHPO is the force-controlled. The hydrodynamic load pattern for these two methods is described in Figure 2.43.
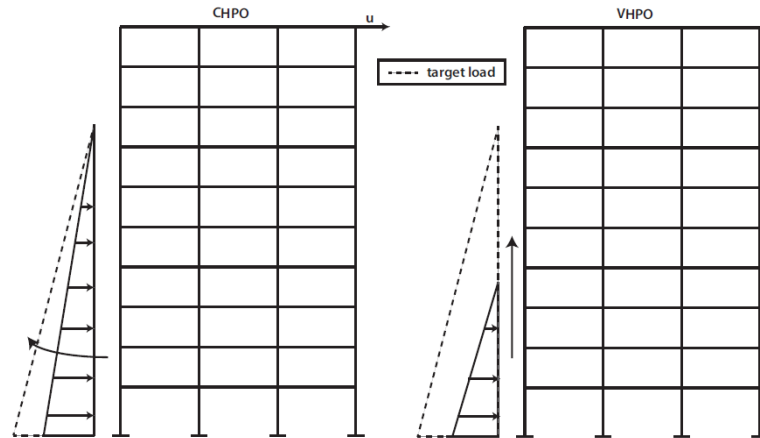
Figure 2.43 Evolution of the load patterns in CHPO and VHPO for a given target load.

In this literature, the sensitivity analysis was conducted due to the nonuniform load pattern. According to Figure 2.44, pushover analysis is a good prediction for time history analysis in which VHPO (force-controlled) is a better prediction than CHPO (displacement-controlled) by comparing with time history. However, VHPO analysis is not suitable to investigate the post-peak behavior when the structure exhibits a softening behavior.

(a)   (b)
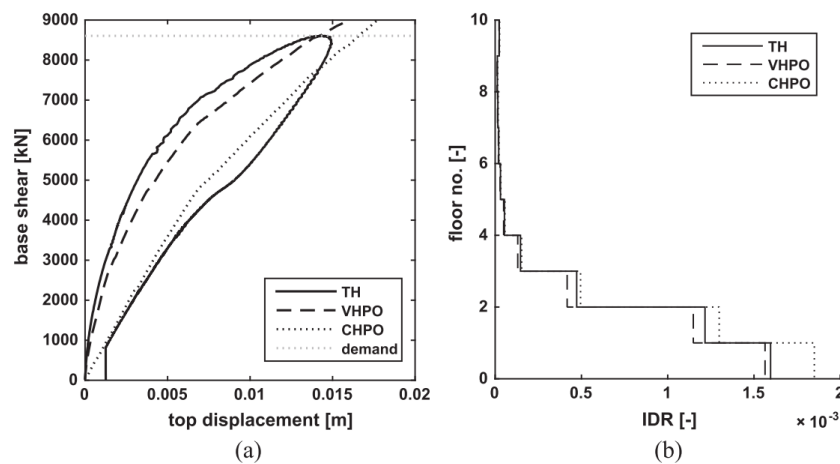
Figure 2.44 Time-history vs pushover analyses for two different tsunami wave traces: (a) force-displacement envelope; (b) maximum inter-story drift demand

In 2019, [40] presented a comprehensive comparison of different approaches for assessing the structural performance of buildings under sequential earthquakes and tsunami. Different approaches considered to assess the structural response under earthquake and tsunami are shown in Table 2.11. Three steps were considered to analyze the building under tsunami and earthquake (Figure 2.45). It was observed that for regular structures with the first mode dominated response under earthquake loading, a double pushover approach (PO-FC-VDPO) can be used to reduce computational effort.

Table 2.11 Different approaches to assess structural response under earthquake and tsunami

Earthquake (EQ)	Unloading (UNL)	Tsunami (TS)	Abbreviation
Nonlinear response history analysis (DY)	Transient free vibration (FV)	Nonlinear response history analysis (TDY)	DY-FV-TDY
DY	FV	Static variable depth pushover (VDPO)	DY-FV-VDPO
DY	FV	Static constant depth pushover (CDPO)	DY-FV-CDPO
Static nonlinear pushover analysis (PO)	FV	VDPO	PO-FV-VDPO
PO	FV	CDPO	PO-FV-CDPO
PO	Static force controlled (FC)	VDPO	PO-FC-VDPO
PO	FC	CDPO	PO-FC-CDPO
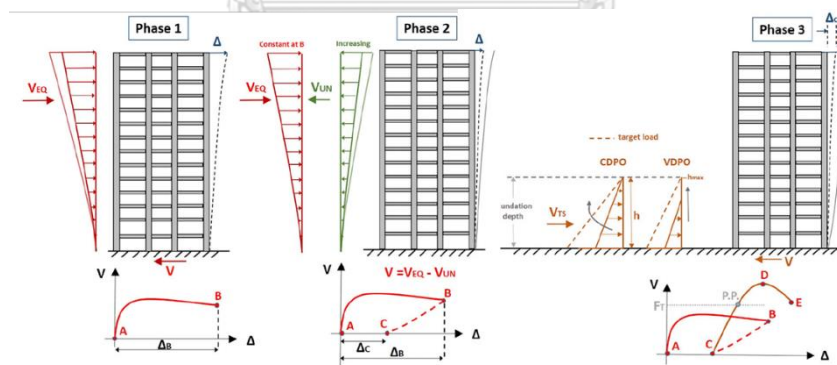
Figure 2.45 Illustration of the three phases of earthquake and tsunami loading

2.9 Plastic hinge length

The inelastic response of the element is a function of the plastic hinge length and the properties of the cross-sections. A plastic hinge length is an essential tool for the relationship between curvature and rotation of the structural element. The plastic rotation is defined as the difference between the ultimate and the yield curvature (curvature ductility) multiplied by the plastic hinge length [41] is shown in Figure

2.46. In which ϕy and ϕp are yield and plastic curvatures, respectively. My and Ie are yield moment and effective moment of inertia, respectively. Lp is the length of the plastic hinge.
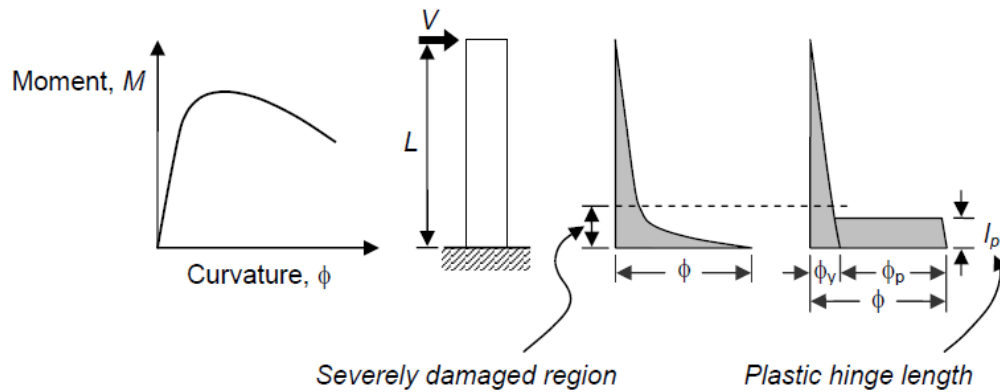
Figure 2.46 Definition of plastic hinge length [41]

The plastic hinge length, lp, of RC members depends on several parameters, including the definition of yielding and ultimate curvatures, section geometry, material properties, longitudinal and transverse reinforcement properties, the stress-strain curve for the concrete, bond-slip characteristics between concrete and the reinforcing steel, support conditions and the magnitude and type of loading, axial force, and shear span ratio.

[42]tested full-scale concrete column with different section sizes and confinement conditions under (i) axial load only and (ii) axial and cyclic lateral load. They proposed the plastic hinge length equation based on their test results. The proposed plastic hinge length equation and plastic hinge length from the experiment are shown in Eq. (2.18) and Table 2.12. The first expression especially yielded for column bending, while the second yielded for bar slip due to the longitudinal bar's elongation. However, they did not reveal any relation of lp on longitudinal reinforcement ratio and axial load ratio.

$$L_p = 0.08L + 6d_b \qquad (2.18)$$

Where Lp = Equivalent plastic hinge length

L = distance from column base to point of contra flexure

d_b = bar diameter

Table 2.12 Experimental and predicted plastic hinge length [42]

Researchers Reference		Column aspect ratio, $L/_D$ or $L/_h$	Section width, D or h, mm	Longitudinal bar diameter, d_b, mm	Plastic hinge length L_p		
					Experiment	Predicted [Eq. (20)]	Experiment / Predicted
Davey et al.	25	3.5	D = 500	13	0.54D	0.44D	1.23
		5.5	D = 500	13	0.58D	0.60D	0.97
Munro et al.	26	5.5	D = 500	13	0.45D	0.60D	0.76
Ng et al.	27	4.0	D = 250	13	0.58D	0.64D	0.91
Gill et al.	6	2.18	h = 550	24	0.44h	0.44h	1.00
		2.18	h = 550	24	0.34h	0.44h	0.77
		2.18	h = 550	24	0.40h	0.44h	0.91
		2.18	h = 550	24	0.50h	0.44h	1.13
Potangaroa et al.	5	2.0	D = 600	24	0.35D	0.40D	0.88
		2.0	D = 600	24	0.35D	0.40D	0.88
		2.0	D = 600	24	0.37D	0.40D	0.93
		2.0	D = 600	24	0.42D	0.40D	1.05
Ang et al.	7	4.0	D = 400	16	0.54D	0.56D	0.96
		4.0	D = 400	16	0.61D	0.56D	1.09
		4.0	h = 400	16	0.73h	0.56h	1.30
		4.0	h = 400	16	0.55h	0.56h	0.98
Mander et al.	4	4.27	h = 750	10	0.37h	0.42h	0.88
		4.27	h = 750	10	0.38h	0.42h	0.90
		4.27	h = 750	10	0.40h	0.42h	0.95
		4.27	h = 750	10	0.41h	0.42h	0.98

Average 0.97

[43] proposed the equation based on the UWPEER Structural performance in which a full-scale test of 37 circular columns is included. These columns met the design criteria that the axial load ratio is less than or equal to 3, the spiral pitch of the column is 6db or less, the effective confinement ratio is greater than or equal to 0.05, the depth of concrete cover is less than or equal to 0.1D, longitudinal reinforcement ratio is less than or equal to 4%. Based on the error function of 37 columns, they proposed the following Eq. (2.19).

$$lp = 0.05L + 0.1 f_y d_b L \sqrt{f_c'} \, (MPa)$$

$$lp = 0.05L + 0.008 f_y d_b L \sqrt{f_c'} \, (psi) \qquad (2.19)$$

Where lp = column plastic-hinge length

L = column length from point of the maximum moment at column base to point of zero moments at the column top

f_y = yield strength of column longitudinal reinforcing steel

f_c' = concrete compressive strength

d_b = bar diameter

[44] experimentally conducted the parametric study on the influences on lp of various parameters using four full-scale RC columns. The details of the tested column are shown in Table 2.13. The effect of axial load ratio, shear span ratio, and

reinforcement ratio was accounted for in their experiments and the equation Eq. (2.20) was proposed.

$$\frac{lp}{h} = \left[0.3(\frac{P}{P_o}) + 3(\frac{A_s}{A_g}) - 0.1\right](\frac{L}{h}) + 0.25 \geq 0.25 \tag{2.20}$$

Where lp = column plastic-hinge length

L = column length from point of maximum moment at column base to point of zero moment at column top

h = overall depth of column

P = applied axial force

P_0 = nominal axial load capacity as per ACI 318-05

A_g = gross area of concrete section

A_s = area of tension reinforcement

Table 2.13 Details of test specimens [44]

Specimen	b x h, in. x in. (mm x mm)	f'_c, ksi (MPa)	Longitudinal steel			Transverse steel					
			Size	ρ_l, %	f_{yl}, ksi (MPa)	Size	s_h, in. (mm)	ρ_s,* %	f_{yh}, ksi (MPa)	$A_{sh}/A_{sh,ACI}$	P/P_o†
S24-2UT	24 x 24 (610 x 610)	63 (43.4)	No. 7-1 (22M-1)	1.25	73 (50.3)	No. 4-1 (13M-1)	3-3/4 (95)	2.04	62 (42.7)	1.09	0.5
S17-3UT	17.25 x 17.25 (440 x 440)	6.3 (43.4)	No. 5 (16M)	1.25	72 (49.6)	No. 3-1 (10M-1)	3-3/8 (86)	1.76	72 (49.6)	1.12	0.5
24-4UT	24 x 24 (610 x 610)	5.3 (36.5)	No. 7-2 (22M-2)	1.25	58 (40.0)	No. 3-2 (10M-2)	6 (152)	0.72	66 (45.5)	0.44	0.2
S24-5UT	24 x 24 (610 x 610)	6.0 (41.4)	No. 7-2 (22M-2)	1.25	58 (40.0)	No. 4-2 (13M-2)	6 (152)	1.30	63 (43.4)	0.74	0.2

*ρ_s = volumetric ratio of transverse reinforcement to concrete core.
†$P_o = 0.85 f'_c A_c + f_{yl} A_s$.

[45] also conducted the parametric study including axial load level, slenderness ratio, and transverse reinforcement ratio using the two different rectangular sections with twenty-four column specimens. The criteria of these parameters are such that slenderness ratio is 5 and 7.27, the axial load level is 11%, 16%, 22% and 27% of nominal sectional concrete strength and the transverse reinforcement ratio has three levels: 0.6%, 0.95%, and 1.3%. Using the effect of these factors on twenty-four column specimen, they provide the following equation Eq. (2.21).

$$\frac{L_p}{h} = \begin{cases} \dfrac{0.03}{n_G} + 0.04\rho_{sv} + 0.3 \\ \dfrac{0.05}{n_G} + 0.12\rho_{sv} + 0.5 \end{cases} \tag{2.21}$$

In which

$$n_G = \frac{P}{f'_c A_g}$$

Where, Lp =column plastic-hinge length

P = axial compressive load

A_g =gross area of concrete section

f_c' = concrete compressive strength

ρ_{sv} = transverse reinforcement ratio in critical region

CHAPTER (3)
EFFECTS OF TSUNAMI FORCES ON BUILDINGS

3.1 General

With the aim of reducing the loss of life and property in low-lying coastal areas especially tsunami hazard areas, all buildings and structures should be constructed by methods and practices that minimize tsunami damage. To ensure safety structures, flood, wind, and seismic hazards are considered in the design. Floodwaters can create a variety of loads on building components. According to FEMA guidelines, hydrostatic including buoyancy or flotation effects, breaking wave, hydrodynamic force, and debris impact forces are considered to apply to the structure.

3.2 Mitigation concept of the hydrodynamic forces and debris impact

A tsunami can cause a massive flooding loading and it is impossible to design all structures to resist. Therefore, mitigation is necessary for building to resist the tsunami. The regular building can reduce undesirable forces such as torsion in structural members other than irregular building. The height of the building is required to be elevated above an elevation of the estimated tsunami inundation level or the building should be located on natural terrain above the regulatory flood elevation on natural undisturbed ground. The column foundation of the tsunami-resistant building should be used as a fixed condition for pile foundations that are capable of resisting lateral loads and can protect scouring effects. The column of the building should be selected as a circular column to reduce the hydrodynamic loading. The lowest floor of the building has been chosen as no wall to allow free flow of flooding water and the elevated floors have chosen to use breakable walls in such an event that they should be strong enough to resist wind or other normal environmental loads. The percentage of openings is also considerable condition to reduce the tsunami impact forces on the structure. For the impact forces due to tsunami such as hydrodynamic load and buoyancy load, the above conditions are acceptable but for large debris impact forces, there is necessary to protect the building i.e., shelter or fender.

3.3 Proposed buildings

3.3.1 Modeling of the buildings

In this study, the 5 stories reinforced concrete building is considered. The size of the building and the number of the story are depending on the area of the district where tsunami mostly occurs and the required minimum area per evacuees. A structural system of moment resisting frame is used in the building system.

The configurations of the structure are octagonal and square buildings. The area of both buildings is designed as 850 m^2 to accommodate 850 evacuees per floor. The highest wave height has been found at 12 m in Thailand on 26 December 2004 [33]. The average sea level is 3 m and hence, the design inundation depth is considered as 9 m. Therefore, the height of the building considered is 15 m (3 m for each floor level) shown in Figure 3.1.

The plan, elevation, and three-dimensional view of the proposed building are shown in Figures 3.2 and 3.3.
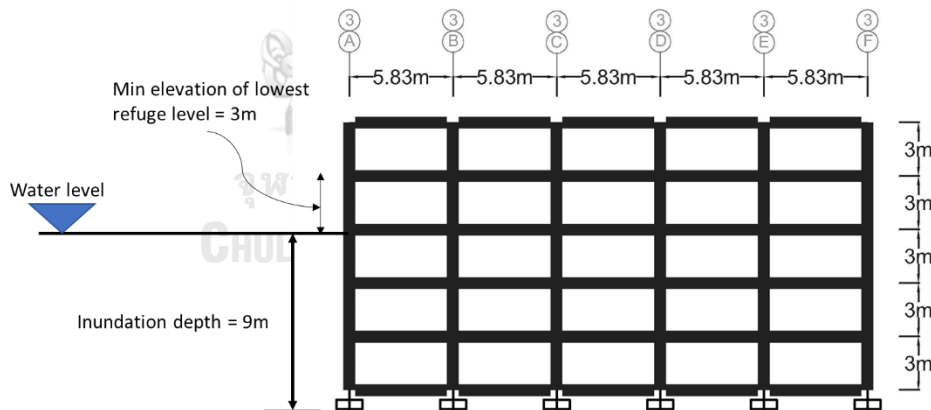
Figure 3.1 Dimension of propose building with minimum refuge elevation
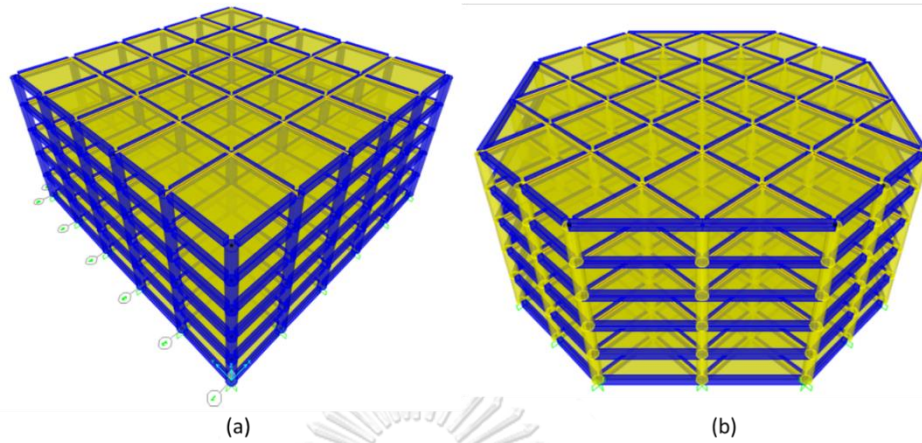
Figure 3.2 Three-dimensional view of the proposed buildings
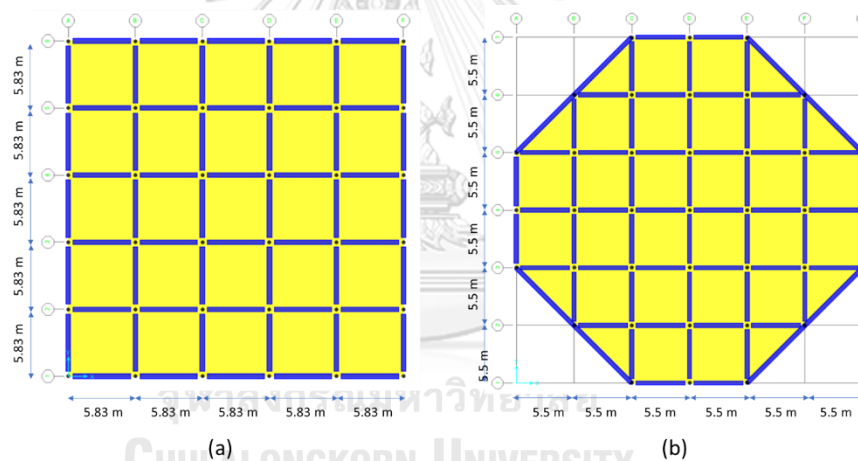
Figure 3.3 Plan view of the proposed buildings

3.3.2 Material properties of the structural elements

The properties of column, beam, and slab and material properties of concrete and steel for the proposed structure are shown in Table 3.1.

Table 3.1 Property of materials

Material Properties		
Concrete material	Concrete compressive strength, fc' (MPa)	35
	Modulus of elasticity, Ec (MPa)	25700
Steel material	Steel yield strength, fy (MPa)	500
	Modulus of elasticity, Es (MPa)	200,000

3.4 Consideration of gravity and tsunami loads for analysis

3.4.1 Gravity load

Gravity loading according to ASCE 7-16 for the proposed structure used in the analysis is shown in Table 3.2.

Table 3.2 Gravity loads

No	Description of loads	Loads (kN/m^2)
1	Live load, LL	4.8
2	Superimposed dead load, SDL	1.5

3.4.2 Tsunami loads

Flood water can create a variety of loads on building components. Loads from the tsunami that are considered in this study are hydrodynamic and buoyance loads. According to literature from the previous chapter, hydrostatic load and surge load are not considered because the proposed building is considered as no wall or breakable wall, and surge forces are smaller than the hydrodynamic load under dry bed conditions. Tsunami forces considered in this study are as follows and are shown in Figure 3.4 and the parameters that are used to evaluate the tsunami forces are shown in Table 3.4.

3.4.2.1 Hydrodynamic Force

Using the parameter of drag coefient and flow velocity, the hydrodynamic force can be computed according to [4]. The formula of the hydrodynamic force is as Eq. (3.1). The application of load is used as a uniform load pattern according to [1, 14].

$$F_d = \frac{pC_d A u^2}{2} \tag{3.1}$$

Where F_D = hydrodynamic or drag force acting in the flow direction

C_d = drag coefficient (1.2 for circular column by FEMAP-55, 2.0 for square column by CCH and FEMAP- 55 and 1.5 for wall section)

ρ = density of the water

u = flow velocity

A = proposed area of the structure perpendicular to the direction of flow

3.4.2.2 Buoyant Force

The buoyant force is significant for a structure that is less resistant to upward force especially for basements, empty tanks located above or below ground, swimming pools, components designed considering only gravity loads. The buoyant force is obtained from the specific weight of water and the volume of water.

$$F_b = \rho_s gV \qquad (3.2)$$

Where Fb = buoyant force (FEMA P-646 and CCH)

ρ_s = density of the water (1200 kg/m^3)

g = acceleration due to gravity

V = the volume of the water displaced by the submerged structure

3.4.3 Consideration of debris impact load due to tsunami

For the case of impact forces that can cause severe damages to the building, the shipping container impact case is considered in this study. Most of the debris impact equations are formulated based on the impulse-momentum concept, work-energy approach, and constant stiffness approach.

Unlike the other tsunami forces, the floating container can be assumed to impact the single member of the structure at the inundation level [1, 14]. The impact energy of the moving container can be achieved based on the kinetic energy approach[35].

Kinetic energy of moving debris = $\frac{1}{2}mu^2$ \qquad (3.3)

Where u is the maximum flow velocity at the site occurring at depths enough to float the debris, m is the mass of the debris. The calculation of tsunami forces is shown in Appendix.
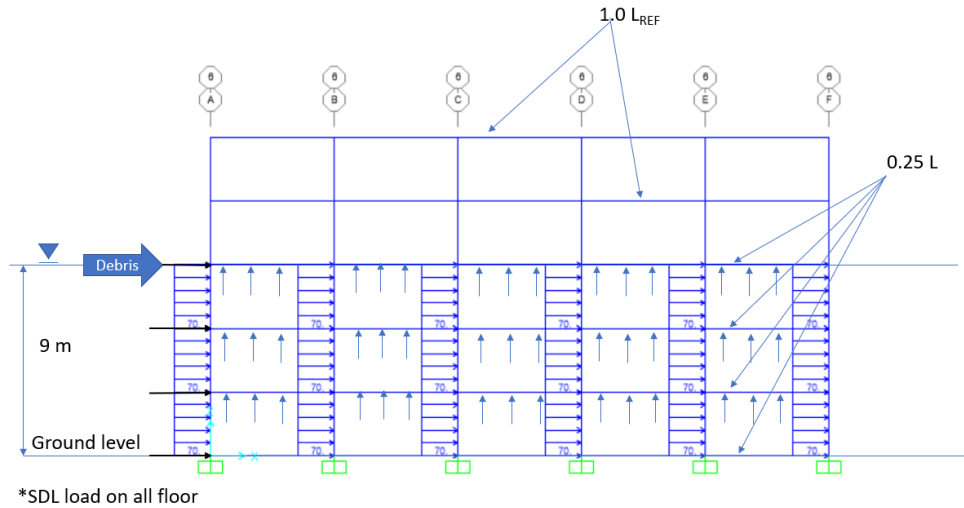
Figure 3.4 Tsunami forces applied to the building

3.5 Consideration of tsunami flow velocity

The tsunami flow velocity can be estimated based on the relationship between inundation flow velocity and inundation depth. The general equation of tsunami flow velocity is

$$U = \alpha\sqrt{gh} \tag{3.4}$$

Where U = flow velocity, m/s

α = velocity coefficient

g = acceleration due to gravity

h = inundation depth, m

The velocity coefficient, α is very important in the relationship of flow velocity and can be verified through several experiments and tsunami events. The following Table 3.3 is the study of the velocity coefficient based on the literature review.

Table 3.3 Review of flow velocity based on past tsunami and research

Literature review	Study method	Velocity coefficient
Matsutomi (2010)	Experiment	0.42 - 1.2
Lukkunaprasit et al. (2010)	2004 Tsunami, Thailand	1.2 - 1.36
Chinnarasri et al. (2013)	Experiment	2
Shafiei et al. (2016)	Experiment	1.7
Wüthrich et al. (2018)	Experiment	1.25
Ghodoosipour et al, 2019	Experiment	1.2

According to the literature review of the velocity coefficient of tsunami flow velocity, the value is between 1.2 and 1.7. Since the hydrodynamic, surge, and debris impact forces are proportional to the tsunami-induced velocity, and uncertainties in estimating flow velocity induce large differences in estimating forces, and hence velocity coefficient of 1.25 is used as unbiased.

Table 3.4 Parameters for calculation of tsunami forces applied to building

No	Parameters	Values
1	Design inundation depth, h	9 m
2	Velocity coefficient, α (Wüthrich (2018)	1.25
3	Acceleration due to gravity, g	9.81 m/s2
4	Flow velocity, u	11.75 m/s
5	Drag coefficient, Cd (ASCE 7-16)	1.2 (for circular element) 2 (for rectangular element)
6	Seawater mass density, ρ_{sw} (ASCE 7-16)	1025 kg/m3
7	Min fluid density for tsunami load, $\rho_s = k_s \rho_{sw}$	1127.5 kg/m3
8	ks (fluid density factor) (ASCE 7-16)	1.1
9	Mass of 20 ft standard shipping container (ASCE 7-16, FEMAP 646)	2270 kg (empty) 13150 kg (loaded)
10	Mass of 40 ft standard shipping container (ASCE 7-16, FEMAP 646)	3810 kg (empty) 17240 kg (loaded)

3.6 Application of tsunami forces on buildings

Using the parameters in Table 3.4, the calculated tsunami forces are shown in Table 3.5 below. Although the same load pattern of buoyant forces is applied to the

floor area of the building, the behavior of hydrodynamic load distributions is not the same for two buildings that are facing the flow direction. The application of hydrodynamic forces on the buildings is shown in Figure 3.5.

Table 3.5 Tsunami forces applied to the RC buildings

	Description of tsunami forces	Values
1	Hydrodynamic load	80 kN/m (for column)
2	Hydrodynamic load	93 kN/m (for beam)
3	Buoyancy load	2.21 kN/m^2

(a)   (b)
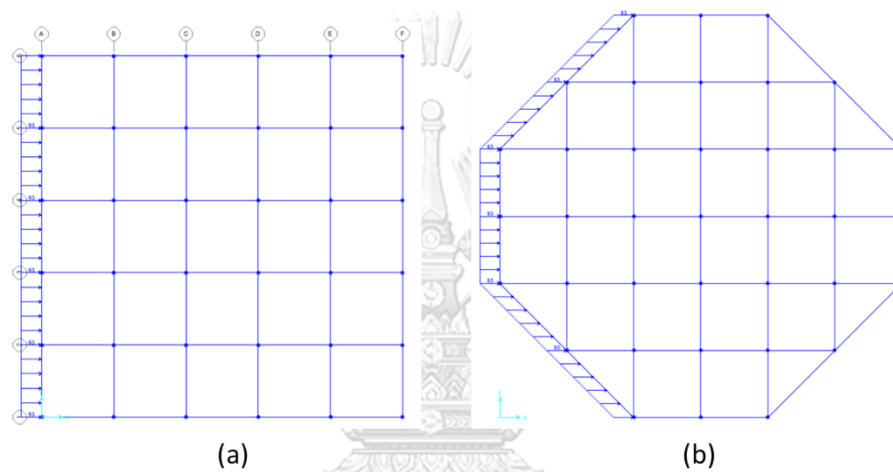
Figure 3.5 Hydrodynamic load applied on building (a) square building and (b) octagonal building

3.7 Load combination

The resulting tsunami load is combined with gravity load effects according to FEMA 646 and the load combination is described in Table 3.6.

Table 3.6 Load combination

Name	Load combination
U1x	1.2 (DL+SDL)+ + 0.25 LL + 1(Drag X+Buoyancy)
U2x	0.9 (DL+SDL)+ 1(Drag X+Buoyancy)

3.8 Equivalent force distribution and fundamental period

3.8.1 Equivalent force distribution

Before analyzing with pushover analysis, the building is analyzed with linear static analysis, and the gravity loads, and tsunami loads applied to the building are check with static equilibrium condition.

The lateral force distribution due to hydrodynamic load and the vertical force distribution due to buoyant, super dead load, and live load is exhibited by using the equilibrium condition in previous Figure 3.5. The summation of distributed lateral force is equal to the base shear of the building and the summation of distributed vertical force is also equal to the axial force at the base of the building. The model is checked not only for lateral force but also for vertical force distribution on the building with hand calculation and compared with Sap 2000 value. The detailed hand calculations are described in the Appendix. Table 3.7 and Table 3.8 shows the check of the model with horizontal distributed and vertical distributed loads using equilibrium condition.

Table 3.7 Horizontal and vertical distributed loads check for the model (Square building)

Loads	Hand calculation (kN)	Sap 2000 (kN)	Difference (%)
Superimposed dead load	7641	7648	0.09
Live load	12226	12236	0.08
Buoyancy load	5628	5633	0.09
Hydrodynamic load	36764	36764.8	0

Table 3.8 Horizontal and vertical distributed loads check for the model (Octagonal building)

Loads	Hand calculation (kN)	Sap 2000 (kN)	Difference (%)
Superimposed dead load	7623	7623	0
Live load	12194	12196.8	0.02
Buoyancy load	5615.8	5615.6	0
Hydrodynamic load	42308.64	42305.9	0.006

3.8.2 Fundamental period

The natural period of vibration is the fundamental parameter for the assessment of the structure. The natural period of building is obtained from the modal analysis of Sap 2000 and the obtaining result is compared by the approximate fundamental period from ASCE 7/16. The model period and mode shape of the buildings are shown in Table 3.9, Table 3.10, Figure 3.6, and Figure 3.7.

Table 3.9 Model period of the square building

OutputCase	StepType	StepNum	Period	UX	UY	UZ	SumUX	SumUY	SumUZ
MODAL	Mode	1	0.565837	0.00024	0.80037	1.858E-20	0.00024	0.80037	1.858E-20
MODAL	Mode	2	0.565837	0.80037	0.00024	0	0.80062	0.80062	2.311E-20
MODAL	Mode	3	0.532867	0	0	0	0.80062	0.80062	2.381E-20
MODAL	Mode	4	0.164397	0.10334	0.01138	0	0.90396	0.812	2.719E-20
MODAL	Mode	5	0.164397	0.01138	0.10334	2.273E-17	0.91534	0.91534	2.276E-17

Table 3.10 Model period of the octagonal building

OutputCase	StepType	StepNum	Period	UX	UY	UZ	SumUX	SumUY	SumUZ
MODAL	Mode	1	0.548196	0.000003934	0.77712	4.743E-12	0.000003934	0.77712	4.743E-12
MODAL	Mode	2	0.548038	0.77714	0.000003949	8.076E-12	0.77714	0.77712	1.282E-11
MODAL	Mode	3	0.52201	0.000003224	0.000003068	3.782E-10	0.77715	0.77712	3.91E-10
MODAL	Mode	4	0.160594	9.068E-08	0.10983	6.074E-11	0.77715	0.88695	4.517E-10
MODAL	Mode	5	0.160553	0.10983	9.121E-08	8.657E-11	0.88697	0.88695	5.383E-10
MODAL	Mode	6	0.152796	3.534E-07	0.00000034	1.822E-09	0.88697	0.88695	2.361E-09
MODAL	Mode	7	0.08125	7.302E-07	0.04656	2.026E-09	0.88698	0.93352	4.387E-09
MODAL	Mode	8	0.081232	0.04656	7.307E-07	3.311E-09	0.93354	0.93352	7.697E-09

Check the period of the structure according to ASCE 7/16

Approximate fundamental period, $Ta = Ct\ h^x$ (3.5)

$Ct = 0.0466$ (Concrete moment resisting frame) (Table 12.8-2 from ASCE 7/16)

$x = 0.9$ (Table 12.8-2 from ASCE 7/16)

$h = 15$ m (Total height of the building)

$Ta = 0.0466 \times 15^{0.9} = 0.533$ sec

The modal period from Sap 2000 are approximately the same with the period from ASCE 7/16.

(a) Mode shape 1   (b) Mode shape 2   (c) Mode shape 3
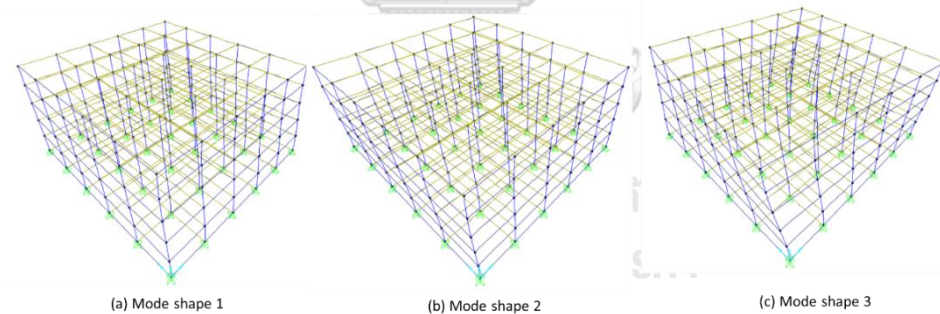
Figure 3.6 First three-mode shaped of the square building

(a) Mode shape 1   (b) Mode shape 2   (c) Mode shape 3
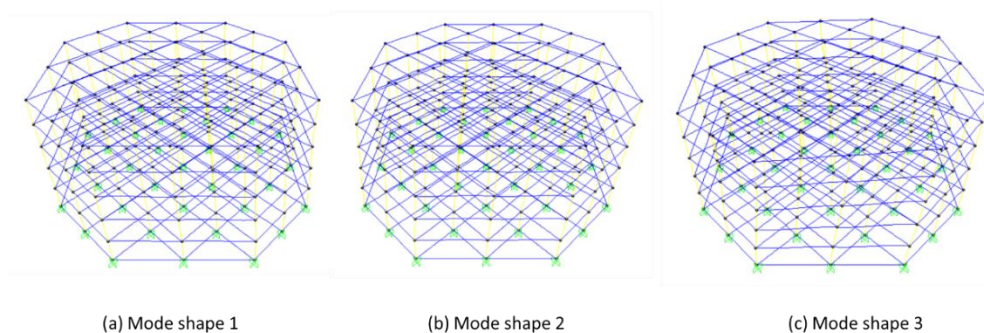
Figure 3.7 First three-mode shaped of the octagonal building

3.8.3 Design of structural members

The column and beam for both square and octagonal buildings are designed according to tsunami load combinations so that the building can resist the tsunami loads under design inundation depth. Constant column and beam size are used throughout the building (for both square and octagonal building).

3.8.3.1 Design of column

Considering the strength of the column to support the tsunami loads, confirmation of column size is needed before analyzing with Pushover analysis. Trial column sizes are firstly used in square building to conduct the strength of the column caused by tsunami load and gravity load shown in Table. The strength of the column is checked by utilizing the P-M interaction diagram.

The tsunami load based on the sample size of column 80 cm diameter is first chosen and then the capacity of the column is checked with PM interaction diagram. The vertical reinforcement ratio for all trial column sizes is chosen within the limitation of 1% to 8% adopted by ACI 318-14. According to the figure, even though the column size is enough for the axial and bending moment, the failure mode is a flexural-shear failure because the prediction of failure mode is needed to assign the plastic hinge for nonlinear analysis. Checking of failure mode is done using the equation of [46]. Column size is reduced slowly to obtain the suitable column size for gravity loads and tsunami loads and to obtain the flexural failure mode. Not only to avoid shear failure and usage of larger steel size but also for the plastic hinge length in nonlinear modeling, the strength of the concrete must be increased, and hence concrete strength of 35 MPa is used for the continued study. According to the analysis of the column under varying sizes shown in Table 3.11 and Figure 3.8, the suitable column size is 85 cm diameter for a square building.

For octagonal building, the selected column size (85 cm diameter) from the square building is utilized, and then check the capacity of the column for the gravity loads and tsunami loads. As shown in Figure 3.9, an 85 cm diameter column size can also be utilized for both buildings.

Table 3.11 Analysis of column varying size

No	Column size	Concrete strength (MPa)	Longitudinal steel	Transverse steel	Longitudinal steel ratio	PMM failure	Failure mode prediction
1	700 mm	30	21 DB 32mm	12 mm @ 100 mm spacing	0.044	Yes	-
2	750 mm	30	24 DB 32mm	12 mm @ 100 mm spacing	0.044	No	Flexural-shear failure
3	800 mm	30	25 DB 32mm	12 mm @100 mm spacing	0.04	No	Flexural-shear failure
4	800 mm	35	25 DB 32mm	16 mm @100 mm spacing	0.04	No	Flexural-shear failure
4	850mm	35	28 DB 28mm	16 mm @ 100 mm spacing	0.03	No	Flexural failure
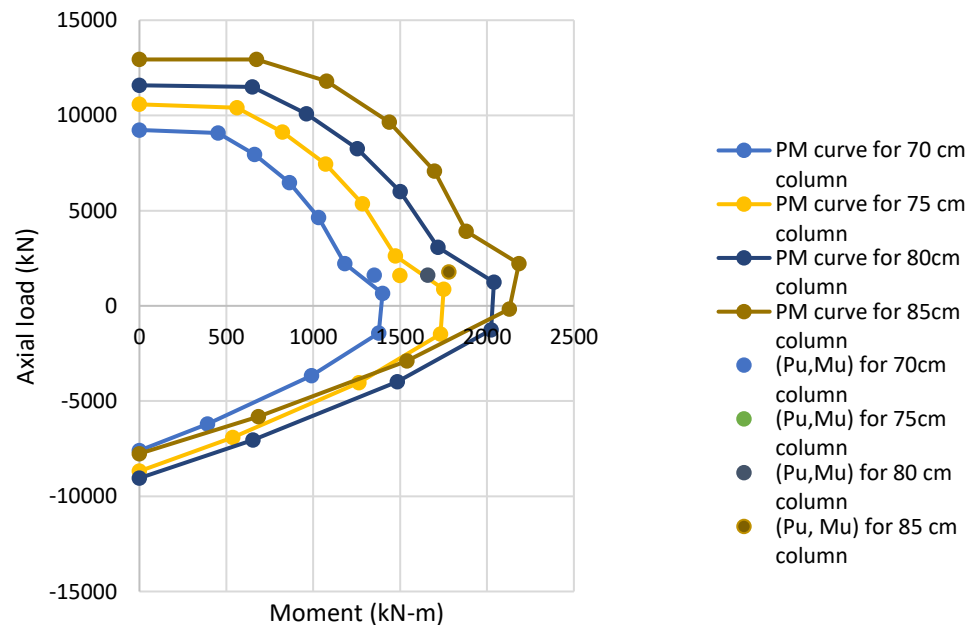
Figure 3.8 Checking capacity of various column sizes for the square building
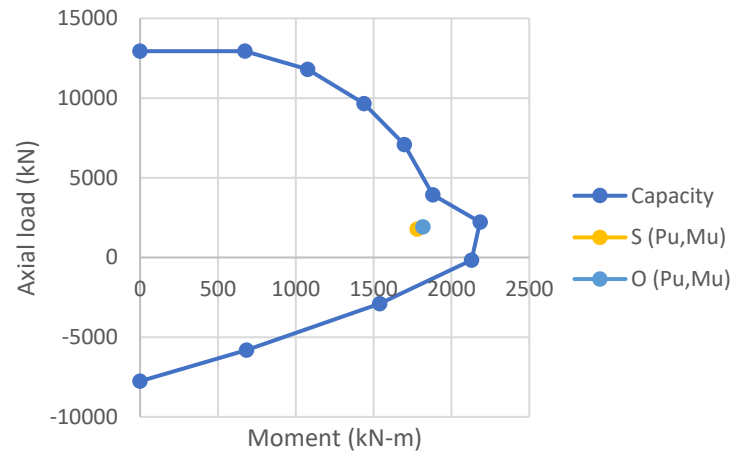
Figure 3.9 Capacity checking for both buildings

3.8.3.2 Check the beam capacity

The beam size should be enough to resist the flexural and shear failure caused by the gravity and tsunami loads. For sufficient shear and flexural reinforcement, ACI 318-14 is adopted to check the proposed beam size. Detail design checking for the beam 40x60 cm is provided in the Appendix. The maximum demand of the beam due to the static analysis is lower than the nominal strength of that beam according to ACI 318-14 and shown in Table 3.12. Therefore, the proposed beam size of 40x60 cm is used for the continued study.

Table 3.12 Demand and design strength of the beam

Beam Internal forces	Square building	Octagonal building	ACI 318-14
V_{max} (kN)	137	231	360
M_{max} (kN-m)	316	370	505

3.9 Comparison of internal forces and displacement between square and octagonal building

In this section, the comparison of internal forces between square and octagonal buildings is presented. Even though the area of the buildings is the same, the internal forces are larger in the octagonal building than in the square building (See Figure 3.10 and Figure 3.11) because the water contact area of the building subjected to the tsunami in the octagonal building is greater than the area in the square building. The evaluation of tsunami forces for both buildings is shown in Table 3.13. Furthermore,

the inter-story drift ratio in the octagonal building is slightly larger than that of the square building and can be seen in Figure 3.12.
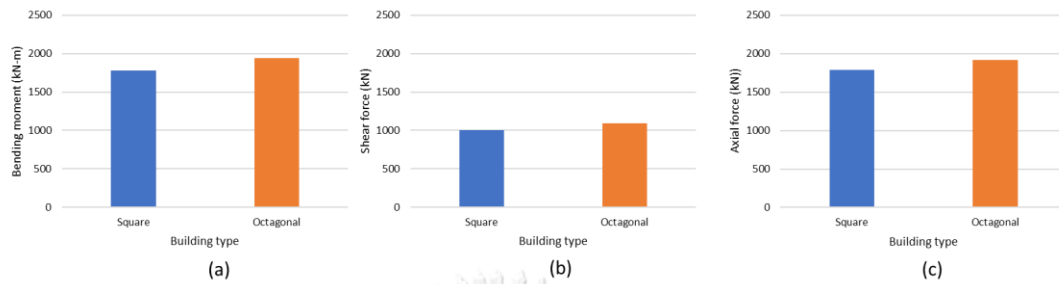
Figure 3.10 (a) Maximum bending moment (b) maximum shear force and (c) maximum axial force of the column
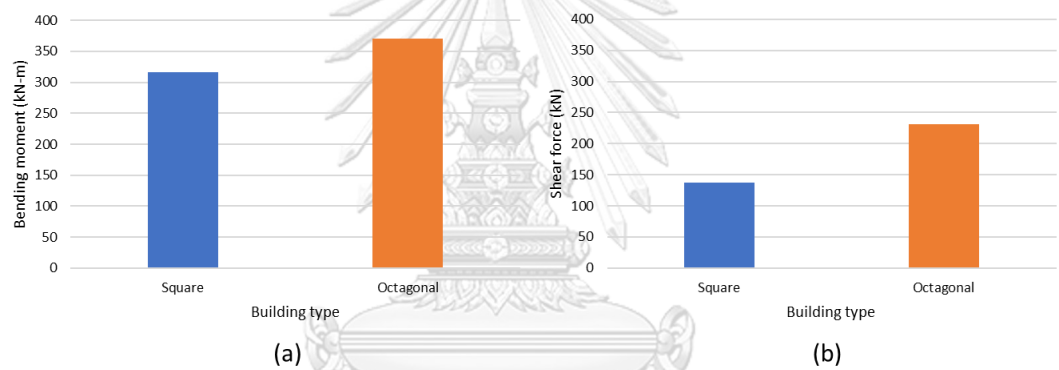
Figure 3.11 (a) Maximum bending moment and (b) maximum shear force of the beam
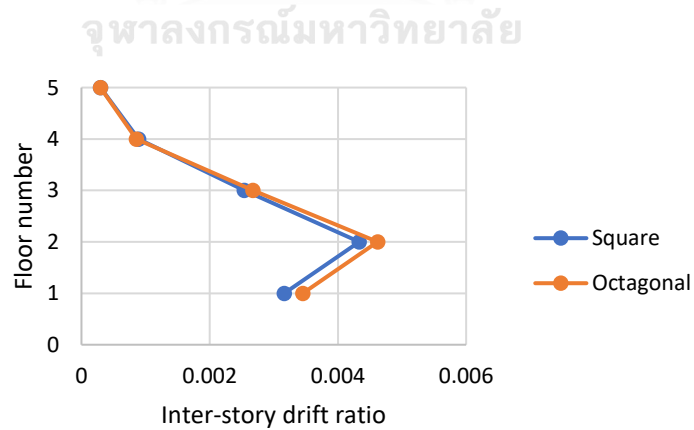
Figure 3.12 Comparison of inter-story drift ratio, IDR of the buildings

Table 3.13 Comparison of gravity and tsunami forces on the buildings

Tsunami forces	Square building	Octagonal building
Superimposed dead load	7647 kN	7623 kN
Live load	12236 kN	12196 kN
Buoyancy forces	5633 kN	5615 kN
Hydrodynamic forces	36764 kN	42306 kN

3.10 Response of the buildings due to tsunami forces under tsunami pushover analysis

3.10.1 Nonlinear modeling for the building system

After analyzing the building with linear static analysis, a column size of 85 cm diameter and beam size of 40 x 60 cm are chosen depending on tsunami load combinations. To investigate the real capacity and performances of the buildings, pushover analysis is conducted. Before analyzing with pushover analysis, beams and columns are modeled as nonlinear frame elements with lump plasticity at the start and the end of each structural member to detect the behavior of the structure when tsunami load and debris impact load come. Modeling of nonlinear elements is depending on the nonlinear material properties of the structural members.

Concrete

Mander's concrete model [47], shown in Figure 3.13 is adopted to model the material stress-strain relationship of confined concrete. Mander's concrete stress-strain curve calculates the compressive strength and ultimate strain values as a function of the confinement (transverse reinforcing) steel. The stress-strain relationship of the concrete model proposed by Mander is given by the following expression.

$$f_c = \frac{f'_{cc}\, xr}{r - 1 + x^r}$$

(3.6)

where

$$x = \frac{\varepsilon_c}{\varepsilon_{cc}} \qquad \varepsilon_{cc} = \varepsilon_{cc}\left[1+5\left(\frac{f'_{cc}}{f'_{co}}-1\right)\right] \qquad f'_{cc} = Kf'_{co} \qquad r = \frac{E_c}{E_c - E_{\sec}}$$

$$E_{\sec} = \frac{f'_{cc}}{\varepsilon_{cc}} \qquad \varepsilon_{cu} = 0.004 + \frac{1.4\rho_s f_{yh}\varepsilon_{sm}}{f'_{cc}}$$

Where,

f_c = the longitudinal compressive concrete stress

f'_{cc} = compressive strength of confined concrete

f'_{co} = the unconfined concrete strength

f_{yh} = yield strength of the hoop reinforcement

E_c = modulus of elasticity of the concrete

E_{sec} = concrete secant modulus elasticity

K = confinement ratio of concrete

ρ_s = ratio of the volume of rectangular steel hoops to the volume of concrete core measured to the outside of the peripheral hoop

ε_c = longitudinal compression strain of concrete

ε_{cc} = compression strain at maximum concrete stress of confined concrete

ε_{cu} = ultimate compression strain of confined concrete

ε_{sm} = steel strain at maximum tensile stress
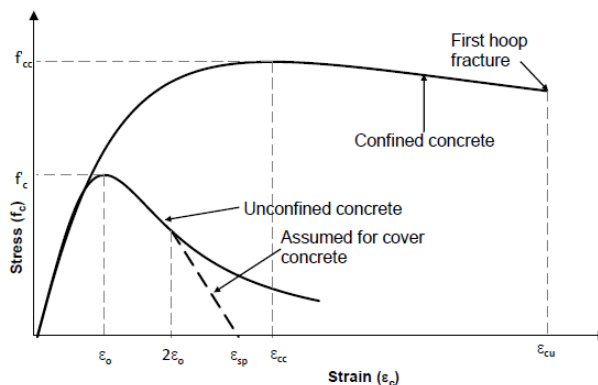
Figure 3.13 Stress-strain model for concrete [47]

Reinforcing steel

The typical reinforcing steel with a strain hardening ratio of 1 % is adopted. The ultimate strain of the steel is adopted as 0.1. The nominal yield strength of 500 MPa corresponding to the ultimate strength of 625 MPa is used and the inelastic

stress-strain relationship of reinforcing steel used in this study is presented in Figure 3.14.
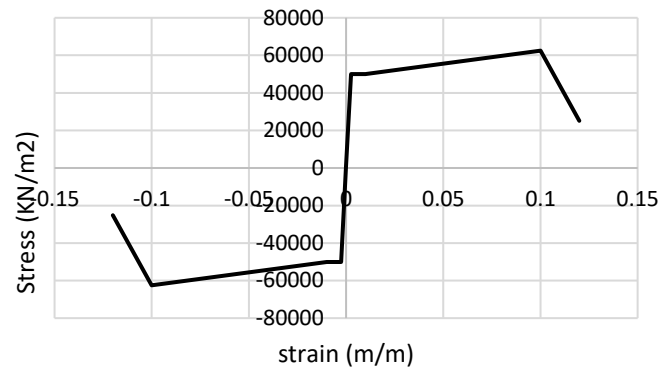
Figure 3.14 Stress-strain relationship of reinforcing steel

3.10.2 Plastic hinge for nonlinear modeling

The plastic hinge can be assigned in Sap 2000 through two types such as automatic hinge and user-defined hinge. Automatic hinge is section dependent in which the program generates automatically to the final hinge properties. The automatic hinge properties for concrete members are based on [48]. User-defined hinge properties can be modified in automatic hinge properties or can be defined by the user. Now, ASCE 41/17 [49] can be available as a modification code of ASCE 41/13 but cannot use in Sap 2000 directly, and hence, user-defined plastic hinge properties according to ASCE 41/17 are used in this study. As shown in Figure 3.15, the force–deformation behavior of a plastic hinge is defined as five points generally A, B, C, D, and E.

Since the lateral hydrodynamic forces and debris impact forces are considered for nonlinear analysis of the building and the maximum axial applied load is 10 % of its nominal compressive strength, hence M3 hinges for column and beams are adopted in this study.
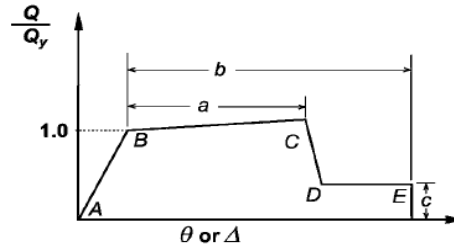
Figure 3.15 Force–deformation relationship of a typical plastic hinge

3.10.2.1 Plastic hinge properties according to ASCE 41/17

For assigning the plastic hinges in each structural element, calculation of modeling parameters is needed in which the flexural yielding moment and curvature are obtained from the moment-curvature analysis using section designer in Sap 2000. From this analysis, moment and curvature for the column and beam at yield point are obtained based on the procedure of [50] (Figure 3.16) in which the axial load from the column is used as maximum axial load under tsunami load combination. The initial effective stiffness value between point A and B is taken as 0.7 for column and 0.35 for beam [51].

Plastic moment–curvature normalized concerning the yield moment and curvature is needed when defining the frame hinge properties in nonlinear modeling of the building. Notably, axial loads in the beam are assumed to be zero. Accordingly, the moment hinge of the column and the beam is only established in this study. The modeling parameters for the beam and the column according to ASCE 41/17 are shown in Table 3.14 and Table 3.15.

The modeling parameters from ASCE 4/17 are accessible as a moment-rotation relationship instead of the moment-curvature relationship. Plastic hinge length is needed to develop from yielding curvature to yielding rotation. Several plastic hinge lengths have been proposed in the literature. For the calculation, plastic hinge length from [43] is reasonable such that the parameters used in their experiment (such as longitudinal steel ratio, transverse steel ratio, axial load ratio, shear span ratio) are compatible with the parameters that have been used in this study. The

detailed calculation of modeling parameters is implemented in the Appendix. The plastic hinge properties for the column and the beam assigned in nonlinear modeling of the building are presented in Figure 3.17.

(a)

(b)

Figure 3.16 Moment-curvature curves for (a) the column and (b) the beam

Table 3.14 Modeling parameter and acceptance criteria for the nonlinear plastic hinge for column [49]

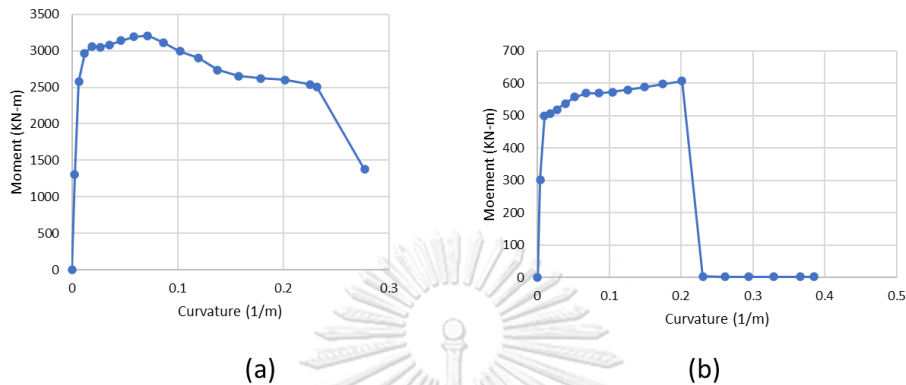| Modelling Parameters		Acceptance Criteria		
		Plastic Rotation Angle (radians)		
		Performance Level		
Plastic Rotation Angles, a and b (radians) Residual Strength Radio, c		IO	LS	CP
Columns not controlled by inadequate development or splicing along the clear height [a] $a= (0.06 - 0.06\frac{NUD}{Agf'cE} + 1.3\rho t - 0.037\frac{VyE}{VColOE})\geq 0.0$ $For\ \frac{NUD}{Agf'cE} \leq 0.5 \{b = \frac{0.65}{5+\frac{NUD}{0.8 Agf'cE}\frac{1}{\rho t} \frac{f'cE}{fytE}}\cdot$ $c = 0.24 - 0.4\frac{NUD}{Agf'cE} \geq 0.0$		0.15a ≤ 0.005	0.5 b [b]	0.7 b [b]
Columns controlled by inadequate development or splicing along the clear height [c] $a = (\frac{1\rho t fytE}{8\rho t fylE})\ \begin{matrix}\geq 0.0\\ \leq 0.025d\end{matrix}$ $b = (0.012 - 0.085\frac{NUD}{Agf'cE} + 12\rho te)\ \begin{matrix}\geq 0.0\\ \geq a\\ \leq 0.06\end{matrix}$ $c = 0.15 + 36\rho t\ \leq 0.4$		0.0	0.5 b	0.7 b

Notes: ρ_t all not be taken as greater than 0.0175 in any case nor greater than 0.0075 when ties are not adequately anchored in the core.
Equations in the table are not valid for columns with   small ρ_t n 0.0005
shall not be taken as less than 0.2
N_{UD} shall be the minimum compressive axial load accounting for the effects of lateral forces as descirbed in Eq. (7-34)
Alternatively, it shall be permitted to evaluate N_{UD} based on a limit-state analysis.
[a] b shall be reduced linearly for $N_{UD}/(Agf'_{cE})$>0.5 from its value at $N_{UD}/(Agf'_{cE})$=0.5 to zera at $N_{UD}/(Agf'cE)$=0.7 but shall not be smaller than a
[b] $N_{UD}/(Agf'_{cE})$ shall not be taken as smaller than 0.1.
[c] Columns are considered to be controlled by inadequate development or splices where the calculated steel stress at the splice exceeds the steel stress specified by Eq. (10-1a) or (10-1b). Modelling parameter for columns controlled by inadequate development or splicing shall never exceed those of columns not controlled by inadequate development or splicing.
[d] a for columns controlled by inadequate development or splicing shall be tabken as zero if the splice regions not crossed by at least two tie groups over its length.
[e] ρ_t shall not be taken as greater than 0.0075

Table 3.15 Modeling parameter and acceptance criteria for the nonlinear plastic hinge for beam [49]

Conditons			Modelling Parameters[a]			Acceptance Criteria		
			Plastic Rotation Angle (radians)		Residual Strength Radio	Plastic Rotation Angle (radians)		
						Performance Level		
			a	b	c	IO	LS	CP
Conditon i. Beams controlled by flexure[b]								
$\frac{\rho - \rho'}{\rho bal}$	Transverse reinforcement[c]	$\frac{Vd}{bwd\sqrt{f'cE}}$						
≤0.0	C	≤3(0.25)	0.025	0.05	0.2	0.01	0.025	0.05
≤0.0	C	≥6(0.5)	0.02	0.04	0.2	0.005	0.02	0.04
≤0.5	C	≤3(0.25)	0.02	0.03	0.2	0.005	0.02	0.03
≤0.5	C	≥6(0.5)	0.015	0.02	0.2	0.005	0.015	0.02
≤0.0	NC	≤3(0.25)	0.02	0.03	0.2	0.005	0.02	0.03
≤0.0	NC	≥6(0.5)	0.01	0.015	0.2	0.0015	0.01	0.015
≤0.5	NC	≤3(0.25)	0.01	0.015	0.2	0.005	0.01	0.015
≤0.5	NC	≥6(0.5)	0.005	0.01	0.2	0.0015	0.005	0.01
Condition ii. Beams controlled by shear[b]								
Strrip spacing ≤ d/2			0.0030	0.02	0.2	0.0015	0.1	0.02
Strrip spacing > d/2			0.0030	0.01	0.2	0.0015	0.005	0.01
Condition iii. Beams controlled by inadequate development or spacing along the span[b]								
Strrip spacing ≤ d/2			0.0030	0.02	0.0	0.0015	0.01	0.02
Strrip spacing > d/2			0.0030	0.01	0.0	0.0015	0.005	0.01
Condition iv. Beams controlled by inadequate embedment into beam-column joint[b]								
			0.015	0.03	0.2	0.01	0.02	0.03

Note $f'cE$ in lb/in2 (MPa) units

[a] Values between those listed in the table should be determined by linear interpolation

[b] Where more than one of conditons i. ii. iii. and iv occur for a given component, use the minimum appropriate numerical value from the table.

[c] "C" and "NC" are abbreviations for comforming and noncomforming transverse reinforcement, respectively. Transverse reinforcement is comforming if, within the flexural plastic hinge region, hoops are spaced at ≤ d/3, and if, for components of moderate and high ductility demand, the strength provided by the hoops (Vs) is at least 3/4 of the design shear. Otherwise, the transverse reinforcement is considered noncomforming.

[d] V is the design shear force from NSP or NDP.

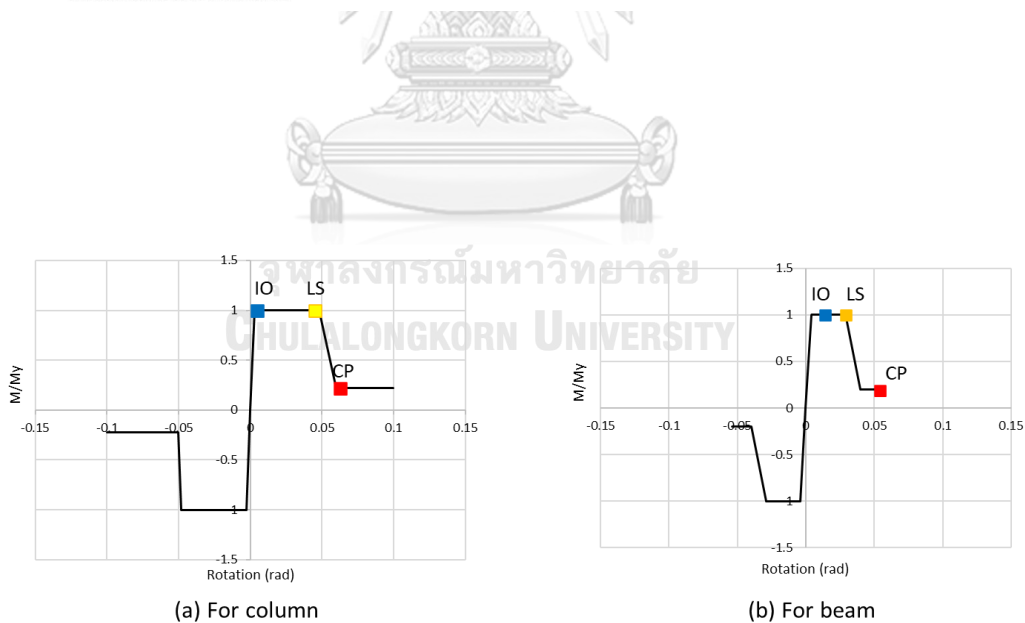(a) For column   (b) For beam

Figure 3.17 Plastic hinge properties for (a) the column and (b) beam

3.11 Tsunami pushover analysis

Tsunami forces on the RC frame building are assessed by the pushover method. In the existing literature of tsunami pushover paper [38, 40, 52, 53], hydrodynamic forces as tsunami forces on the buildings are mainly focused on considering the lateral load distribution pattern for different inundation depth ranges. According to the literature, tsunami pushover analysis can be evaluated by two methods: (i) displacement-controlled method and (ii) force-controlled method. For the tsunami pushover analysis in this study, actual hydrodynamic forces are used as force-controlled method and debris impacts are used as displacement-controlled method to study the behavior of buildings due to debris after applying hydrodynamic forces. In this study, there are two cases in the building analysis namely case (I) building without fender structure and case (II) building with a fender structure as shown in Figure 3.18. The capacity of the buildings under different cases are obtained using both the force-controlled and displacement-controlled methods. From these capacity curves, the remaining energy due to the debris after the application of actual hydrodynamic forces on the building can be evaluated (Figure 3.19). The behavior of this procedure is that the building experienced hydrodynamic forces when the debris impacts the building. The resistance of the building can be evaluated using the work–energy method, in which the kinetic energy of the moving debris is absorbed by the potential energy of the building.
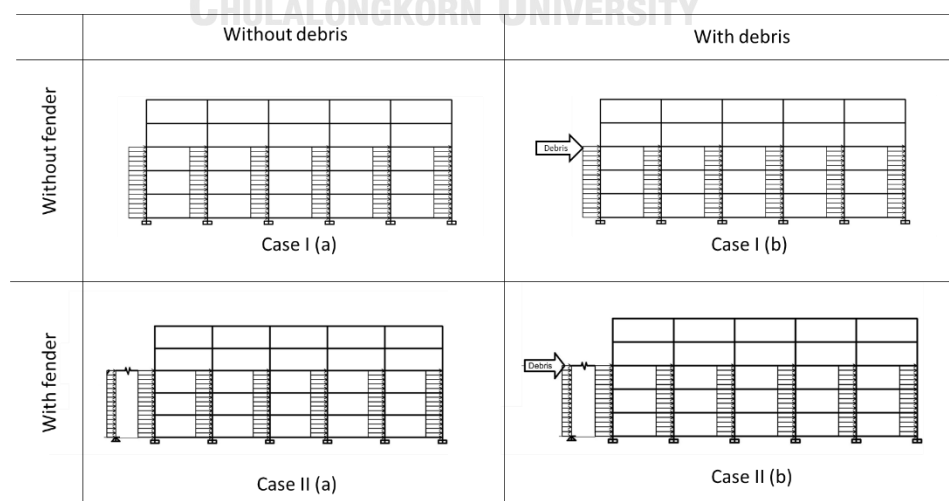

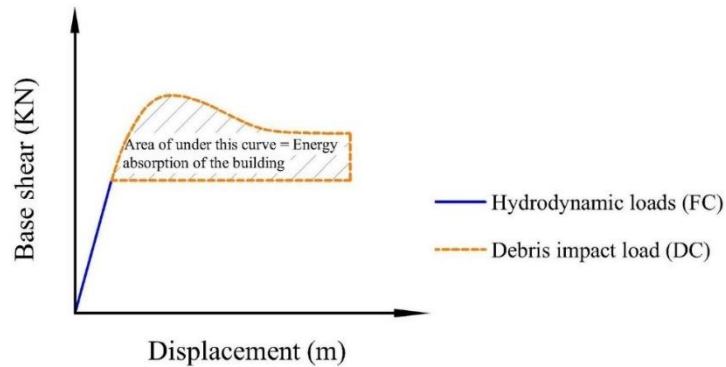Figure 3.18 Building structures under different cases

Figure 3.19 Energy absorption area due to debris after hydrodynamic loads

3.12 Energy absorption of the buildings due to debris after actual hydrodynamic forces (Case I (a) and Case I (b))

The energy absorption of the building is evaluated using capacity of the building. Before conducting with nonlinear analysis, the debris impact location is first chosen for the case study of the building. Both square and octagonal buildings are symmetrical building, and hence the impact locations are selected from one side of the buildings. The selected locations are shown in Figure 3.20.

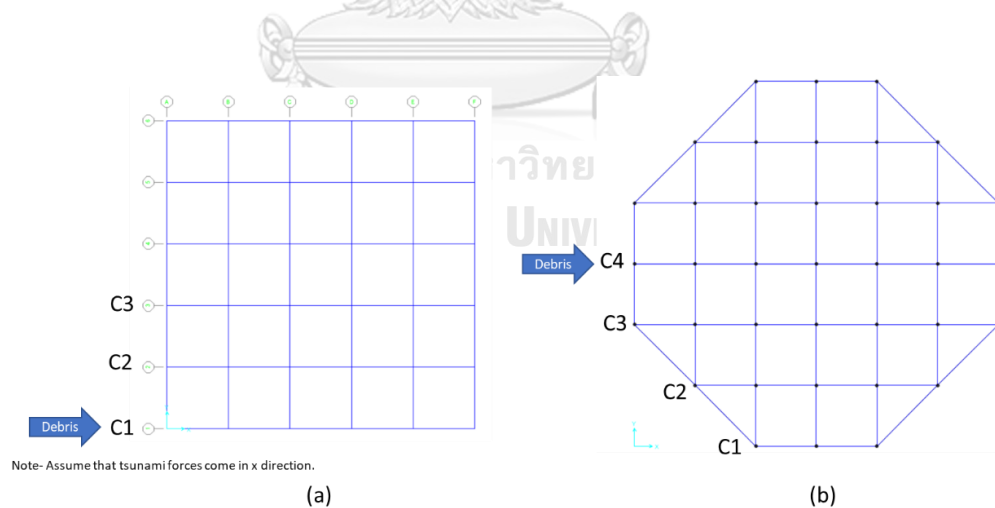Figure 3.20 Debris impact locations for (a) square and (b) octagonal building

Although the tsunami forces are influenced by both inundation depth and flow velocity, constant inundation depth is used for assessing the structural performance under tsunami actions. The hydrodynamic forces as uniform load patterns acting on all columns of the building below the level of inundation depth are examined. Four

percent of the height of the building as target displacement is considered at each debris impact location.

Step by step plastic hinge formation for all cases is shown in Figure 3.21 and Figure 3.22. Member's flexural moment due to lateral hydrodynamic forces did not reach the yield state because the building was designed using the tsunami load combination including hydrodynamic forces. For the case of debris impact, firstly, significant beam failure is found before column failure with plastic hinge formations of LS state, as a result, this failure mechanism constitutes the confirmation of strong column weak beam concept.
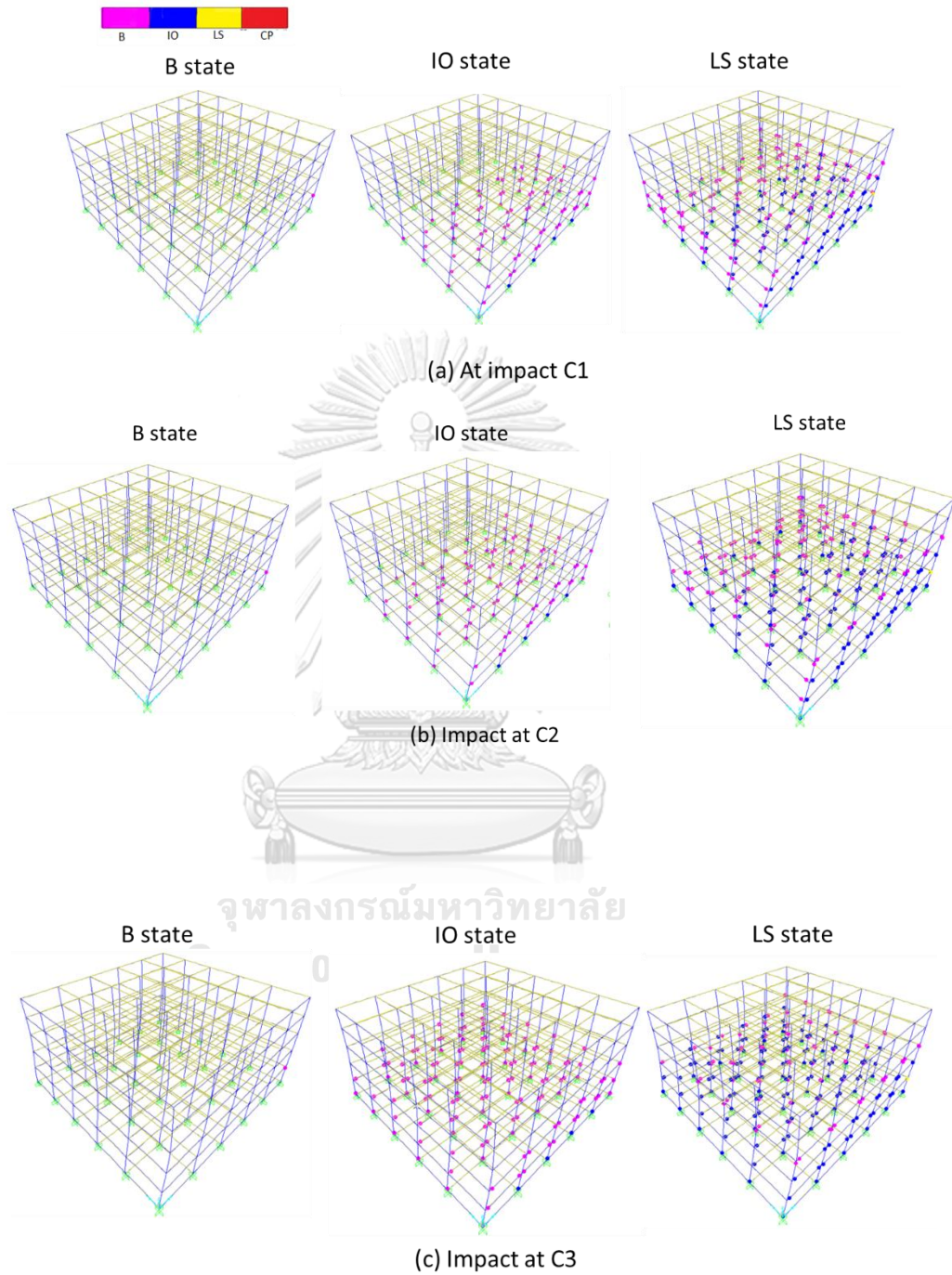
Figure 3.21 Step by step plastic hinge formation at different impact location for square building (a) Impact at C1, (b) Impact at C2, and (c) Impact at C3
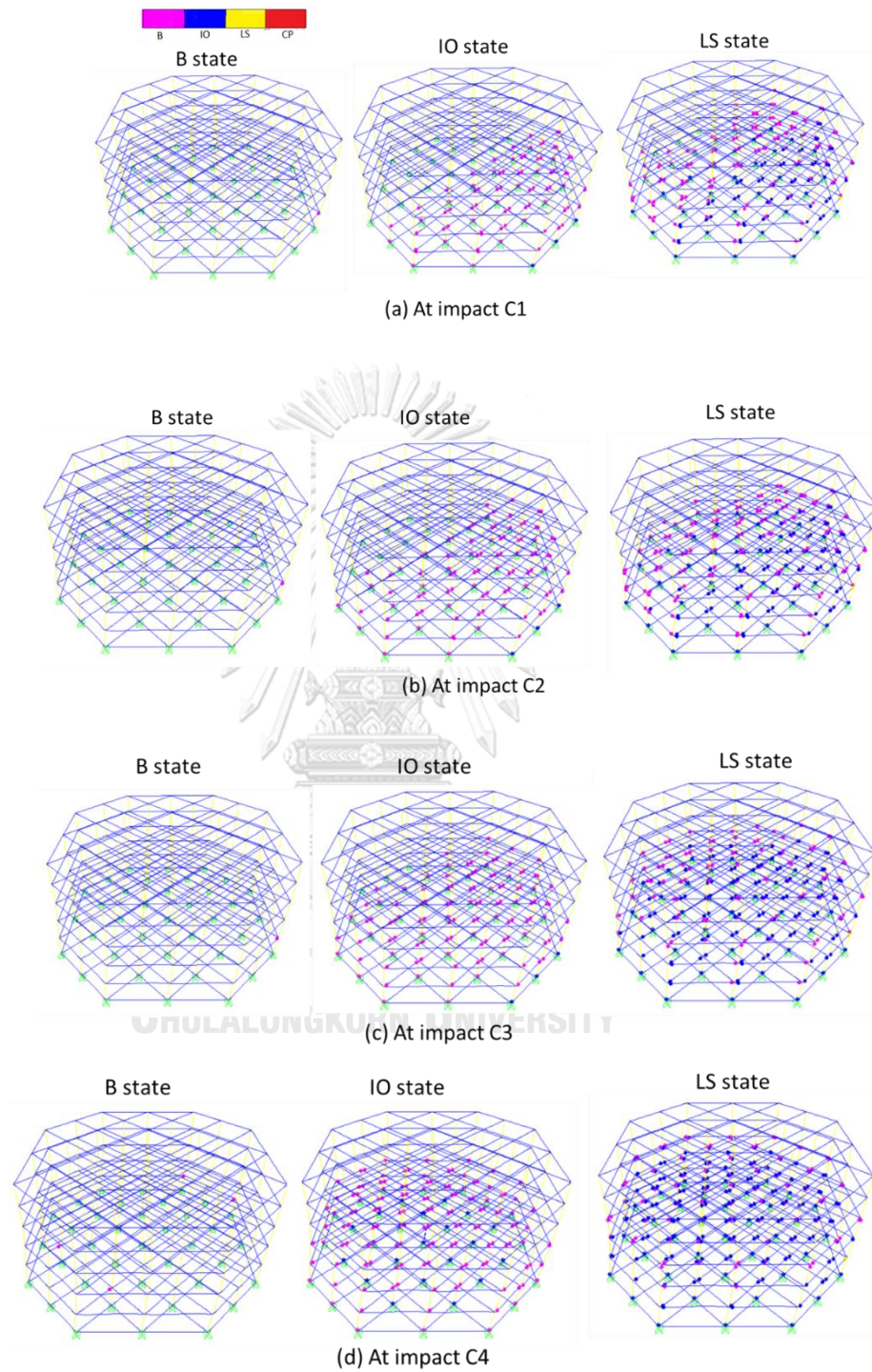
Figure 3.22 Step by step plastic hinge formation at different impact location for octagonal building (a) Impact at C1, (b) Impact at C2, and (c) Impact at C3

The force-deformation relation due to actual hydrodynamic forces is obtained using the force-controlled method and shown in Figure 3.23 and Figure 3.24. Since the same hydrodynamic forces are applied to the building for different impact locations, the load-deformation due to hydrodynamic forces are the same. On the other hand, the forces due to hydrodynamic forces are not the same for the square (36764 kN) and octagonal building (42306 kN) because as described in the previous section, the hydrodynamic forces are larger in the octagonal-shaped building than the square-shaped building.

The performance of the building is observed with no plastic hinge formation due to the hydrodynamic forces under constant inundation depth, however, the building has displaced at a certain distance due to hydrodynamic forces on columns. The remaining capacity for the impact of debris is evaluated after applying actual hydrodynamic forces, through pushover, displacement-controlled method. The capacity curve of the buildings are shown in Figure 3.23 and Figure 3.24.
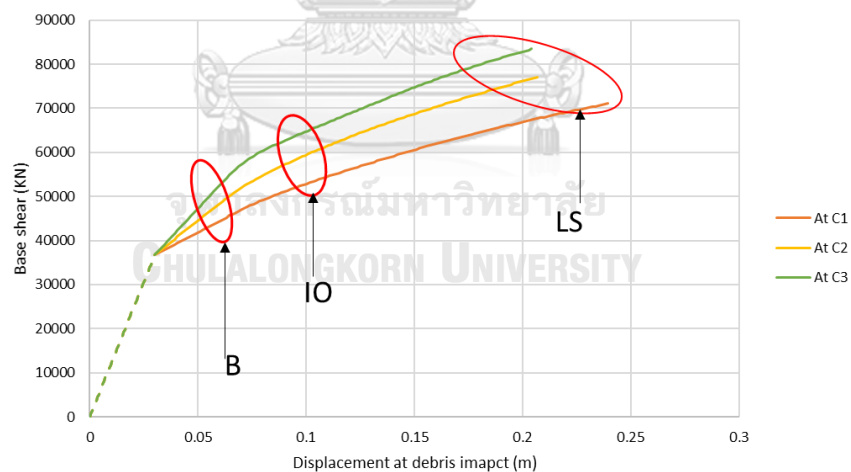

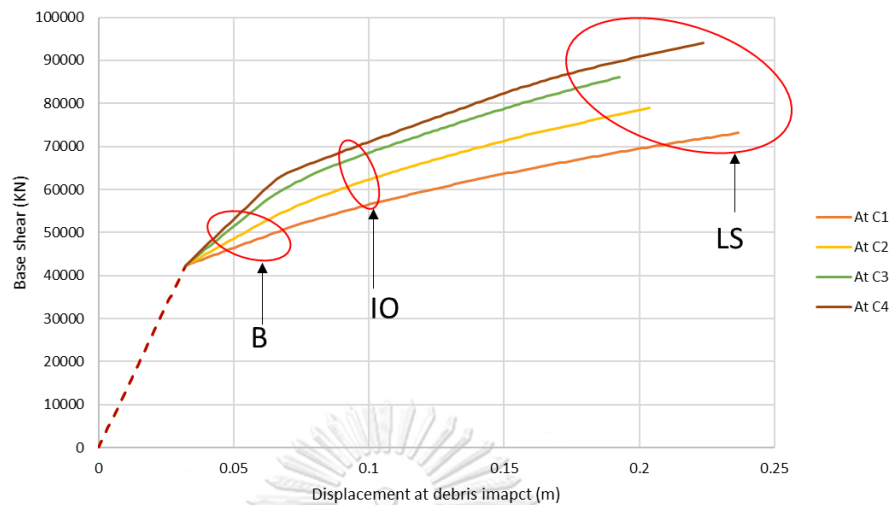Figure 3.23 Capacity of the square building at each performance state

Figure 3.24 Capacity of the octagonal building at each performance state

The evaluation of energy absorption based on the desired performance is needed to examine the resistance of the building through the work-energy method. Therefore, the energy of the building is calculated based on the LS performance state of the buildings. The energy absorption of the building due to debris impact cases for different impact locations are shown in Table 3.16.

As in the case of the square building, the impact location at C3 is the largest energy absorption because of the distribution of structural members' capacity. The lowest energy absorption is caused by the impact location at C1 because of the corner column impact.

For the impact locations C1, C2 and C3, the energy absorption in square building are larger than that in octagonal building. For the impact location C4, energy absorption cannot compare because the square building has 5 spans, and the octagonal building has 6 spans.

Therefore, due to the capacity of the building, energy absorption, hydrodynamic forces conditions, simple profile to install fender system, the square-shaped building is selected for the upcoming section for the building with fender system.

Table 3.16 Energy absorption of the buildings

Building type	Square building			Octagonal building			
Impact location	C1	C2	C3	C1	C2	C3	C4
Energy (kN-m)	4129	4311	5118	3686	3754	4334	6325

CHAPTER (4)
EFFICIENCY OF FENDER STRUCTURE

4.1 Mitigation concept of debris impact

When the tsunami comes, not only the flooding water but also debris such as containers, ships, automobiles, and even ships can impact the buildings. Debris types can be generally divided into three groups: small debris, moderate debris, and large debris, depending on the characteristic of mass, size, stiffness, and buoyancy. Generally, small-size debris cannot completely affect the structure however, field investigations have shown that the structural failure mostly occurs from moderate and large debris strikes [13]. Therefore, the design of the building where the potential inundation level is greater than 3 m or higher, near coastal region has resistance not only the tsunami water wave forces but also debris impact forces especially large debris.

For the consideration of the conceptual design concept to reduce large debris impact forces such as shipping containers, the protection system is needed to resist large debris impact. In this study, the building with a fender structure is considered to resist the shipping container impacts. Energy absorption devices such as super cone fenders are considered for the connection between the inner and outer fender structure to absorb the kinetic energy of flowing debris through their elastic deformation. The main building is used to live for evacuees and the outer fender structure is only considered to protect the inner one without occurring failures by absorbing the kinetic energy of the debris. The configuration of the inner structure is the same (square-shaped building) as described in the previous chapter. The height of the fender structure connected with the main building is determined by the inundation depth. For the fender structure to resist the large debris impact, steel frame structure with the pinned based condition is used to allow the flexibility of the fender units. The proposed building with a fender structure is shown in Figure 4.1. It should be noted that the distance between the building and the fender structure must allow for the deformation of the fender, otherwise, the main building can suffer several damages without utilizing the advantages of the fender structure.
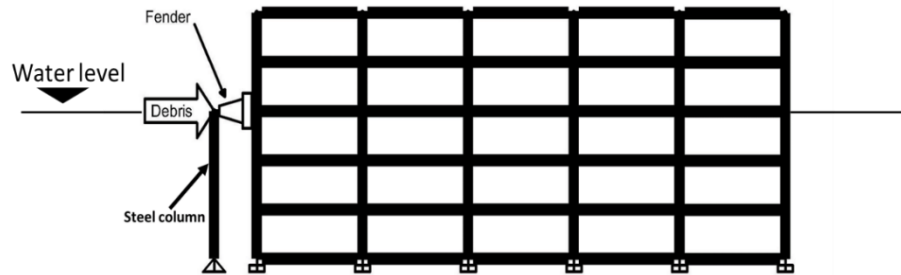
Figure 4.1 Building with fender structure

4.2 Response of the building with a fender system (2D frame analysis)

4.2.1 Two-dimensional analysis of building without a fender structure (Case I (a) and Case I (b))

Firstly, to under the behavior of the building with a fender structure under tsunami pushover analysis, a two-dimensional analytical model of the original building, is created as a representative of the whole building, Figure 4.2. Before considering the building with a fender structure, the building without fender is needed to analyze with tsunamic pushover analysis for the detailed behavior of the system. The nonlinear behaviors of the structural elements are the same as the previous chapter. The procedure of the tsunami pushover methods applied to the building is the same as the previous chapter.

The hydrodynamic forces as uniform load pattern acting on all columns of the building below the level of inundation depth are examined by using pushover, force-controlled method. Four percent of the height of the building as target displacement at debris impact location is considered in the pushover analysis.
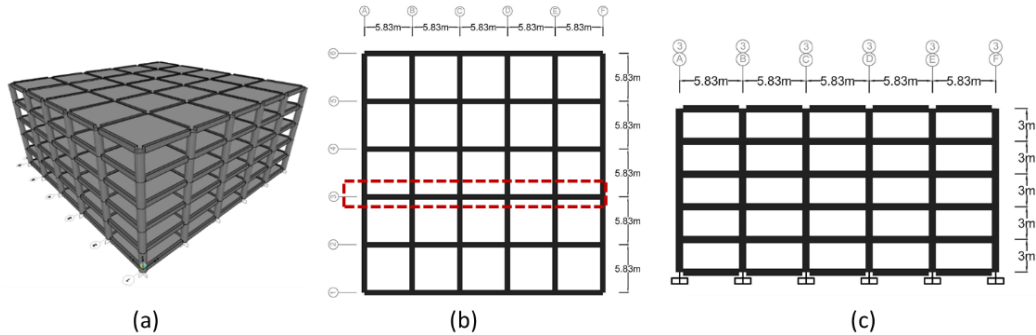
Figure 4.2 Selected 2-dimensional structure from the proposed building (a) Three-dimensional, (b) plan and (c) elevation view

The force-deformation relation due to actual hydrodynamic forces is obtained using the force-controlled method and shown in Fig. The performance of the building is observed with no plastic hinge formation due to the hydrodynamic forces with certain inundation depth, however, the building has displaced at a certain distance due to hydrodynamic lateral loads on columns. The remaining capacity for the impact of debris is evaluated after applying actual hydrodynamic forces, through pushover, displacement-controlled method. The evaluation of energy absorption based on the desired performance is needed to examine the resistance of the building through the work-energy method. The base shear forces at B, IO, and LS states are respectively set to 1140, 2052, and 2488 kN respectively, (Figure 4.3) to evaluate the performance of the building for the debris impact forces.
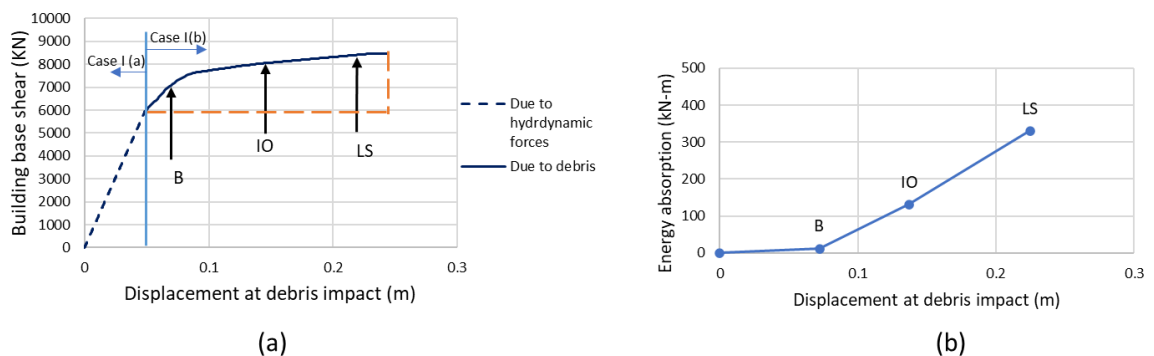

Figure 4.3 (a) Capacity curve due to debris after hydrodynamic forces and (b) relationship between energy absorption and displacement of the building

Figure 4.4 shows the deformation of the building due to actual hydrodynamic forces and the step-by-step plastic hinge formation due to debris after the application of hydrodynamic forces. Failure mechanisms are not observed in the building due to actual hydrodynamic forces. The flexural moment of members due to lateral hydrodynamic forces did not reach the yield state because the building was designed using the tsunami load combination including hydrodynamic forces. For the case of debris impact, beam failure is initially found before column failure with plastic hinge formations starting from the LS state. Consequently, this failure mechanism constitutes the confirmation of the strong column–weak beam concept. After reaching the LS state, the building shows extensive damages in beams when the flexural moment reached its ultimate capacity. Accordingly, the evaluation of building energy absorption should be conducted before the LS performance state in nonlinear analysis. For the performance of the building, the investigation of the inter-story drift ratio is one of the most influential parameters in the displacement-based engineering system. The inter-story drift ratio of the building due to debris impact at each performance state is shown in Figure 4.5.
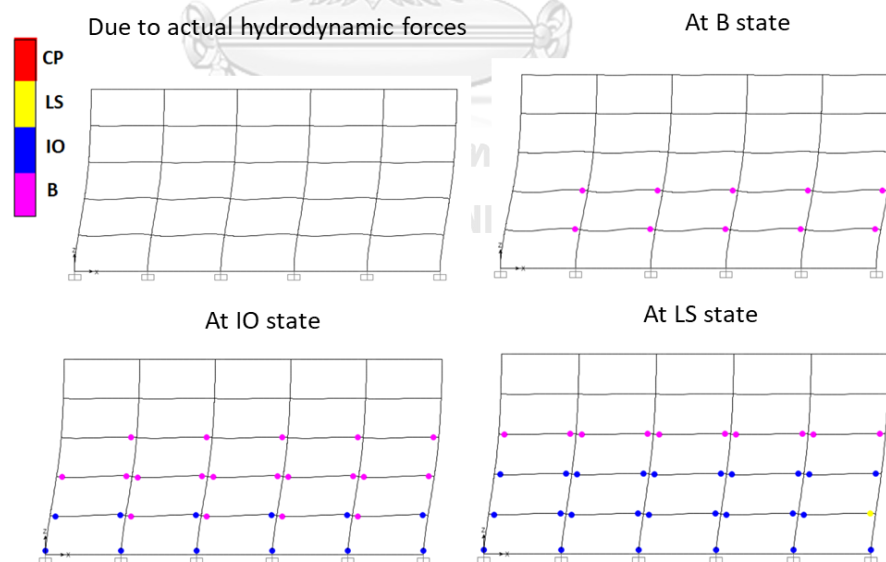

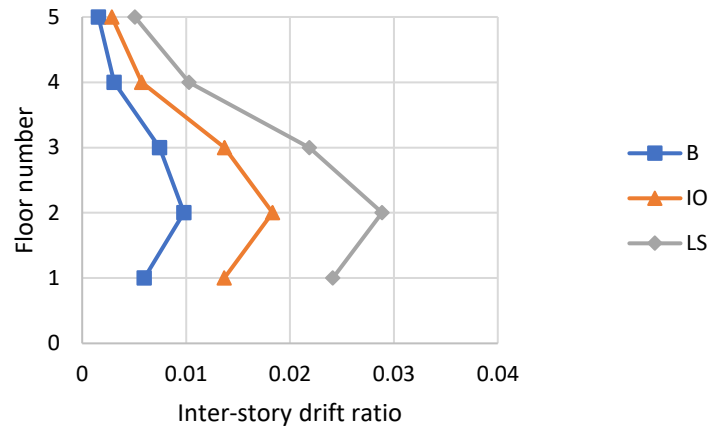Figure 4.4 Plastic hinge formation due to debris after actual drags

Figure 4.5 Inter story drift ratio due to debris after hydrodynamic loads

The remaining energy of the building is evaluated using the capacity curve through the displacement-controlled method. The evaluated energy of the building is compared with the kinetic energy of different kinds of shipping container. The resistance of the building compared with the debris impacts is described in Figure 4.6. This figure shows that the building can only resist the empty shipping container impact. If the loaded container impacts the building, then the building cannot resist these impact types. Therefore, the strength of the building must be increased using some protection systems, especially for the large debris impact cases.
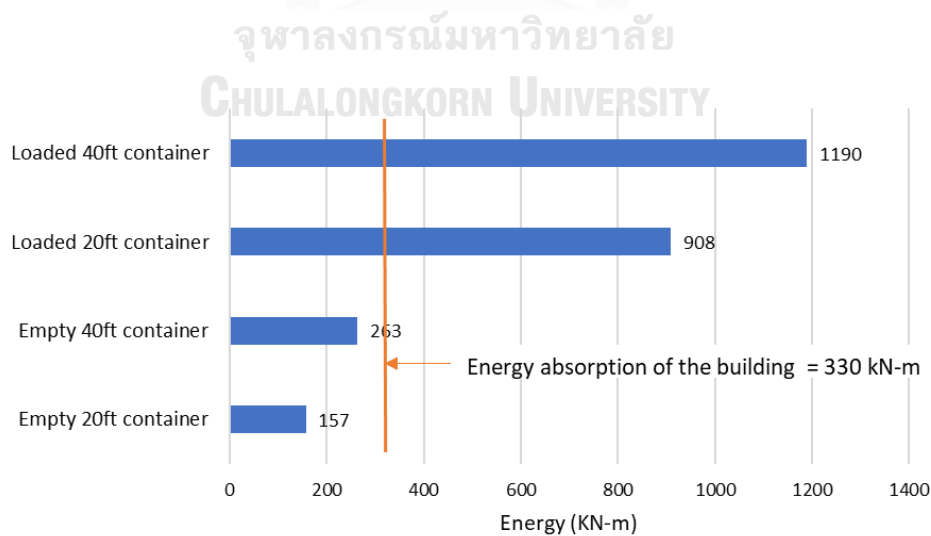

Figure 4.6 Comparison of energy absorption of the building

4.2.2 Building with fender structure (Case II (a) and Case II (b))

4.2.2.1 Selection of the fender

Energy absorption of the building to resist tsunami wave forces and large debris impact forces can be increased by using the marine fender that absorbs large energy using large inelastic deformation. The general concept of the building with a fender structure was described in section 4.1. To understand the efficiency of the fender system, variation of fender reaction is considered as a parameter. The 100 % energy of the fender can be assessed when the fender reaches its ultimate deformation [35, 37]. The ultimate fender deformation is depending on the type of available fender in the commercial catalog. In this study, the inelastic deformation of the fender is based on the super cone fender. The yield and ultimate fender deformation are considered as 33 % and 72 % of fender length to obtain 100 % of the fender's energy (see Figure 4.7). The idealized fenders used in the building are shown in Figure 4.8. A multilinear elastic element is used as a fender model in nonlinear modeling of the building.

For the variation of fender reaction, the selected fender reaction forces are chosen lower than the LS state of the building (i.e., 2260 kN). The corresponding fender lengths are taken as 1.6, 1.8, and 2 m. The parameters used in the fender structure are shown in Table 4.1.

Table 4.1 Parameter for the fenders

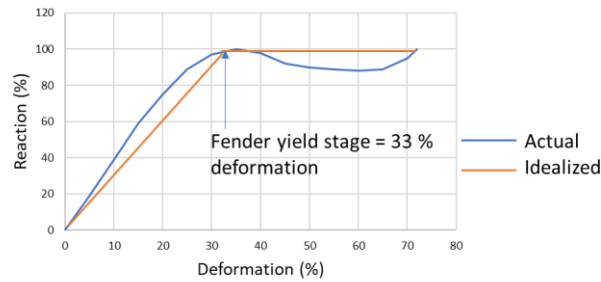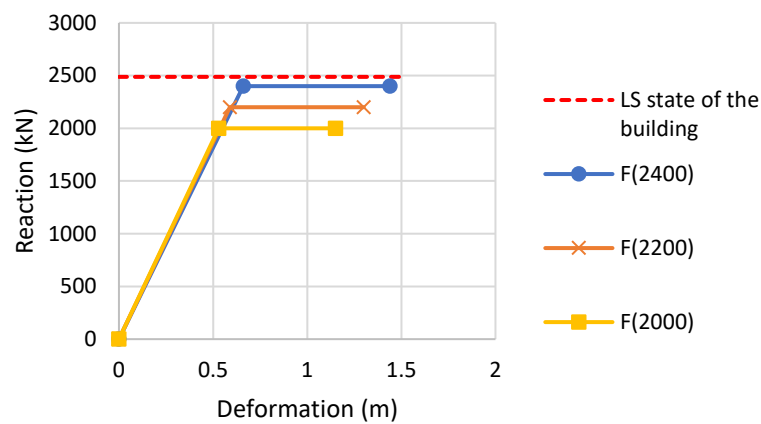| Case | From a commercial catalogue | | | | Idealized fender | | Remark (LS state of base shear) (kN) |
	Fender length, L_f (m)	Fender deformation (33% of L_f) (m)	Reaction (kN)	Stiffness (kN/m)	Idealized initial stiffness (kN/m)	Idealized reaction (kN)	
$F_{(2000)}$	1.6	0.53	2012	3796	3700	2000	2488
$F_{(2200)}$	1.8	0.59	2204	3735	3700	2200	2488
$F_{(2400)}$	2	0.66	2369	3589	3700	2400	2488

Figure 4.7 Performance curve of a fender

Figure 4.8 Idealized force-deformation of the fenders

For the capacity of the building, the hydrodynamic forces are applied to the building including fender structure, Figure 4.9. The procedures of the analysis method, in which the tsunami forces are applied to the building, are the same as those presented in Section 3.11. The location of target displacement is considered at debris impact location, and the target displacement is currently used as the ultimate fender deformation.
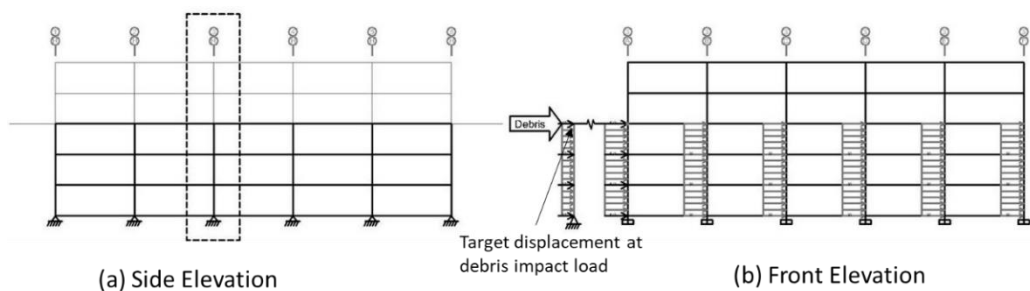

Figure 4.9 Application of tsunami forces on building with fender system (a) side elevation and (b) front elevation

The fender stiffness is considered to be the same. Thus, the global force–deformation curves for all fenders are also the same due to hydrodynamic forces. However, the hydrodynamic forces in the building with a fender system are approximately 6705.5 kN, which is larger than the hydrodynamic forces from the building without a fender system (that is, 5946 kN). This finding is due to the hydrodynamic forces from the fender structure (Fig. 18). Therefore, the hydrodynamic forces are crucial in this system. After applying the hydrodynamic forces, the capacity of the building due to debris is obtained through the displacement-controlled method. The displacement of the capacity curves is distinct because of the different ultimate fender deformations. As can be seen in Figure 4.10, the building with the fender, $F_{(2400)}$ is the largest deformation.

The same fender stiffness and hydrodynamic forces are considered for the performance of the fender system. Thus, the force–deformation results of all fenders are the same as the application of the hydrodynamic forces to the building. After applying the hydrodynamic forces with the force-controlled method, fenders are found to absorb half of these forces from the fender structure and then transfer to the main building (i.e., 759.5 kN). Moreover, the maximum base shear of the building due to debris after hydrodynamic forces at each fender size depends on the fender yield force values; i.e. maximum base shear of the building for the usage of fender $F_{(2000)}$, $F_{(2200)}$ and $F_{(2400)}$ are 1240.5 kN, 1440.5 kN, and 1640.5 kN respectively.

In Figure 4.10 (d) (e) and (f), the fender $F_{(2000)}$, $F_{(2200)}$ and $F_{(2400)}$ use their performance completely. Whether the fenders completely use their energy for all tsunami forces, the energy absorption by the fenders can be evaluated on the basis of their performance due to debris impact.
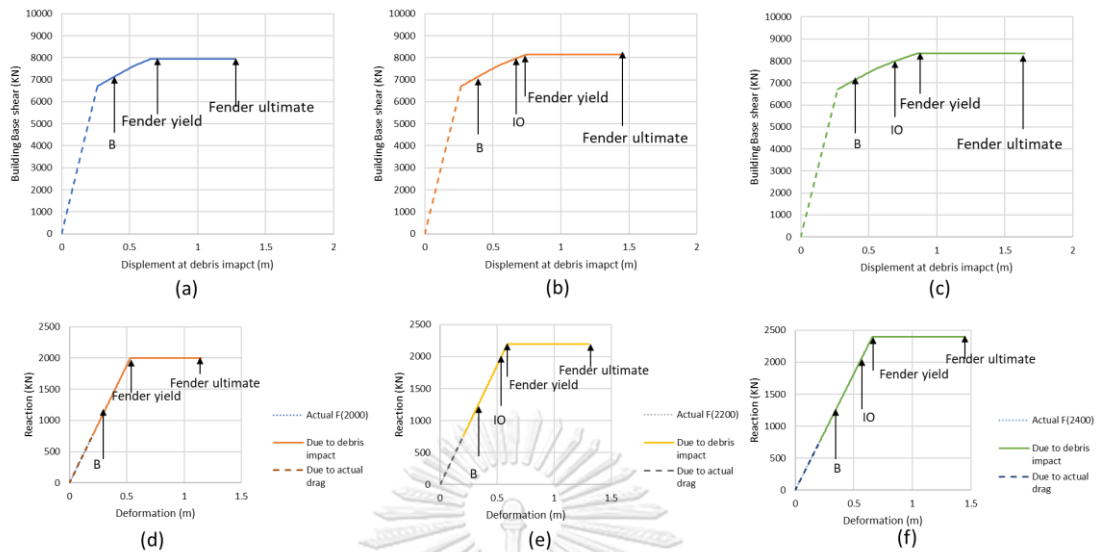
Figure 4.10 Capacity curve and performance of the fenders due to debris after hydrodynamic forces (a) building with fender, $F_{(2000)}$, (b) building with fender, $F_{(2200)}$ and (c) building with fender, $F_{(2400)}$, (d) Fender, $F_{(2000)}$, (e) Fender, $F_{(2200)}$ and (f) Fender, $F_{(2400)}$

Figure 4.11 shows the step-by-step plastic hinge formation of the building with a fender system. No plastic hinge formation is found due to hydrodynamic forces for all fender cases. For the debris impact case, the building without a fender system showed up to the failure behavior. However, in Figure 4.11, due to the efficiency of the fender system, the building does not occur the failure behavior. This is the advantage of the fender structure using fender. As in the case of a building connected with a fender structrue, continuous plastic hinge formation appeared in the building is found only before reaching the fender yield state, and after reaching the yield state, there is no plastic hinge formation. Simultaneously, the fender leads to the large inelastic deformation from its yield to its ultimate state. According to this observation, the fender which is lower than the maximum capacity of the building (LS state) can absorb the energy using its inelastic deformation without inducing damages to the main building starting from the fender yield state.
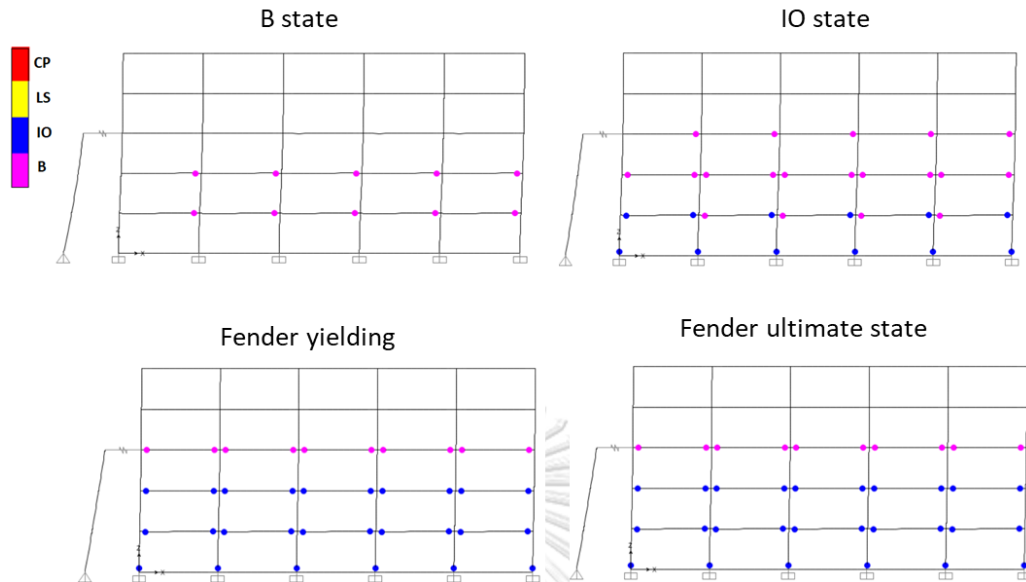
Figure 4.11 Step by step plastic hinge formation of the building with the fender system

As shown in Figure 4.12, the building with F$_{(2000)}$ has occurred no IO state while the other two systems reached the IO state of the building.
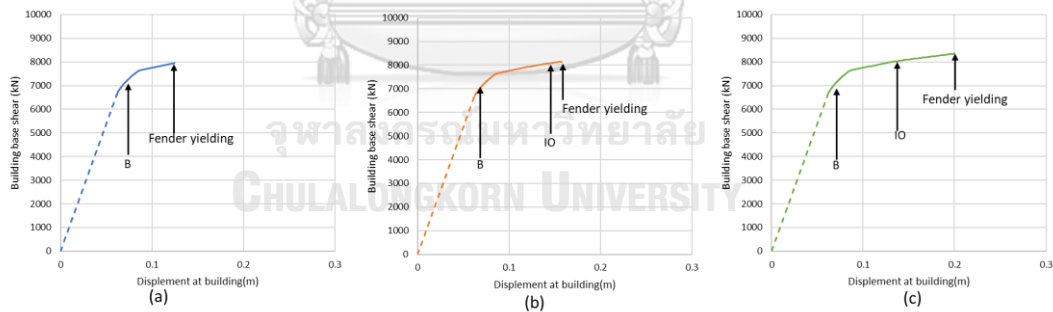

Figure 4.12 Relationship between base shear and building displacement (a) building with fender, F$_{(2000)}$, (b) building with fender, F$_{(2200)}$ and (c) building with fender, F$_{(2400)}$

Figure 4.13 shows the step-by-step inter-story drift ratio (IDR) of the building with and without a fender structure. As can be seen in Figure 4.13, the IDR of the building with and without the fender structure is the same at the performance state of B. Additionally, it was found that the fender yield force of F$_{(2000)}$ i.e 2000 kN is lower than the base shear of the building at the IO state i.e 2052 kN, consequently, the IDR ratio is lower than that of the building without a fender system at IO state.

Furthermore, it was also found that the fender yield force of $F_{(2200)}$ and $F_{(2400)}$ i.e 2200 kN and 2400 kN are lower than the base shear of the building at LS state i.e 2488 kN and therefore the IDR values are lower than that of the building without fender system at LS state. The IDR ratio of fender $F_{(2000)}$, $F_{(2200)}$, and $F_{(2400)}$ systems remain stable starting from the fender yield state. From this observation, the performances of plastic hinge formation and the deformation of the building are related to the fender yield force values.
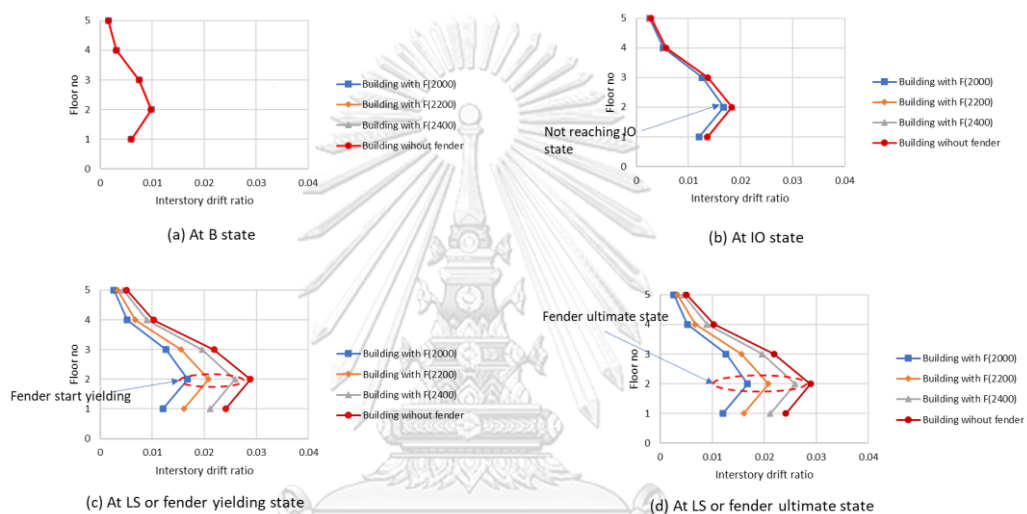

Figure 4.13 Inter-story drift ratio (IDR) of the building

The energy absorbed by the building for both conditions (with and without the fender system) due to debris impact load is illustrated in Figure 4.14. As can be seen, the building without the fender system shows the LS state, and hence it has more energy absorption than the building in the fender system.

On the other hand, for the building with a fender system, the energy absorptions by fenders are rapidly increased starting from the fender yield state up to its ultimate deformation state. The main building remains stable without any deformation, starting from the yield state due to the advantages of the fender system. The building energy can develop only during the fender elastic condition and after reaching the fender yield state, the building does not need to absorb the kinetic energy of moving debris. Additionally, the building energy in the fender system is lower than the building without the fender system at the same performance state as a consequence of hydrodynamic forces from the fender structure. It is also found that

the relationship between building energy and fender yield forces. The larger the fender yield forces; the more energy can be absorbed by the building.
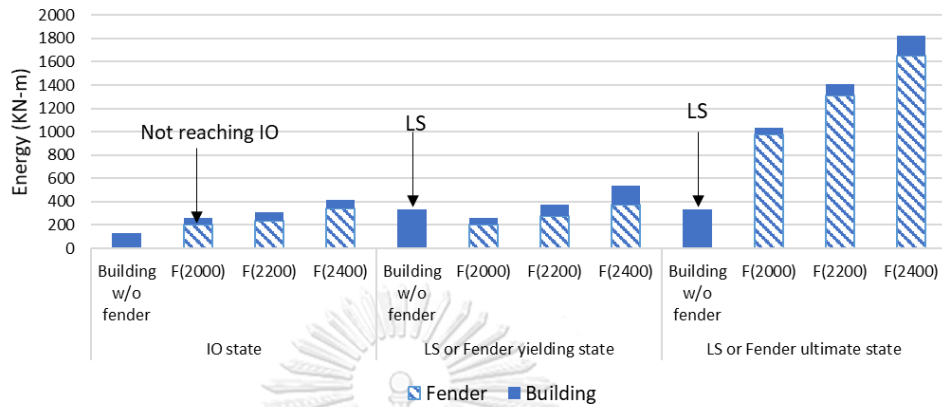

Figure 4.14 Energy of the building with and without fender system

As can be seen in Figure 4.15, the building with an $F_{(2400)}$ fender system is the largest energy absorption and the performance of the building show no extensive damages. According to the observations of the fender variation case, the fender yield force has influenced the performance of building connected with the fender system. As discussed earlier for the potential impact energy for the shipping container, the total energy of the building with fender $F_{(2200)}$ and $F_{(2400)}$ are larger than the kinetic energy of the maximum shipping container i.e. 1409 and 1823 kN-m > 1190 kN-m. Therefore, the building with a fender system can effectively absorb the impact energy.
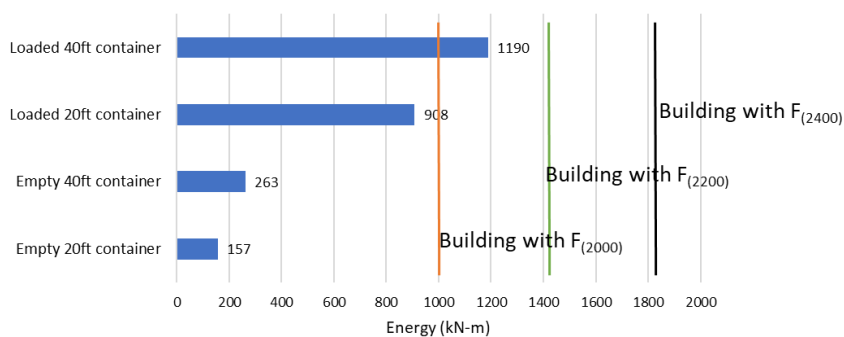

Figure 4.15 Energy performance of fender under shipping container impact

Table 4.2 shows the step-by-step percentage of energy absorption of the fender due to debris. Since the same hydrodynamic forces are applied to the building, all the

fenders utilize 5 percent of its energy due to hydrodynamic forces. When consideration the debris impact case, the energy absorbed by the fenders only is considered through the remaining capacity after the application of hydrodynamic forces. Therefore, the energy absorbed by the fender is evaluated starting from the remaining fender's capacity. As can be seen in Table 4.2, the larger the fender yield force is, the more energy can be absorbed by the fenders. After reaching the fender yield state, the energy absorbed by the fender is rapidly increased due to its inelastic deformation.

Table 4.2 Percentage of energy absorption of the fender based on fender's performance

Fender	$F_{(2000)}$	$F_{(2200)}$	$F_{(2400)}$
Performance state	Percentage of energy (debris after drag)		
B	1%	1%	1%
IO	12% (No IO)	11%	13%
F_y^f	12%	13%	14%
F_u^f	55%	59%	62%

Note-
F_y^f = fender yield state
F_u^f = fender ultimate deformation state

4.3 Design recommendations for the building with a fender structure
4.3.1 Approach for the building with a fender structure

A general approach for the selection of the fender structure is proposed here to account for the combined behavior of the fender and the building. The approach starts from a certain fender reaction, which can be effectively selected from the performance of the building. The kinetic energy of moving debris is at least equal to or lower than the energy absorbed by the structure. Using the energy concept, the energy balance is expressed as Equation (1), and the total energy of the building with a fender structure is shown in Equation (2).

$$KE \leq E^{Total} \qquad (1)$$

$$E^{Total} = E^F + E^b \qquad (2)$$

where KE denotes the kinetic energy of moving debris, E Total denotes the total energy of the building with a fender structure, EF denotes the energy absorbed by the fender, and Eb denotes the energy absorbed by the building.

The selected fender yield force for the building with a fender structure should be taken from the base shear force at the relevant performance state of the main building without inducing failure. The recommendation of the proposed design system is summarized in Fig. 23.
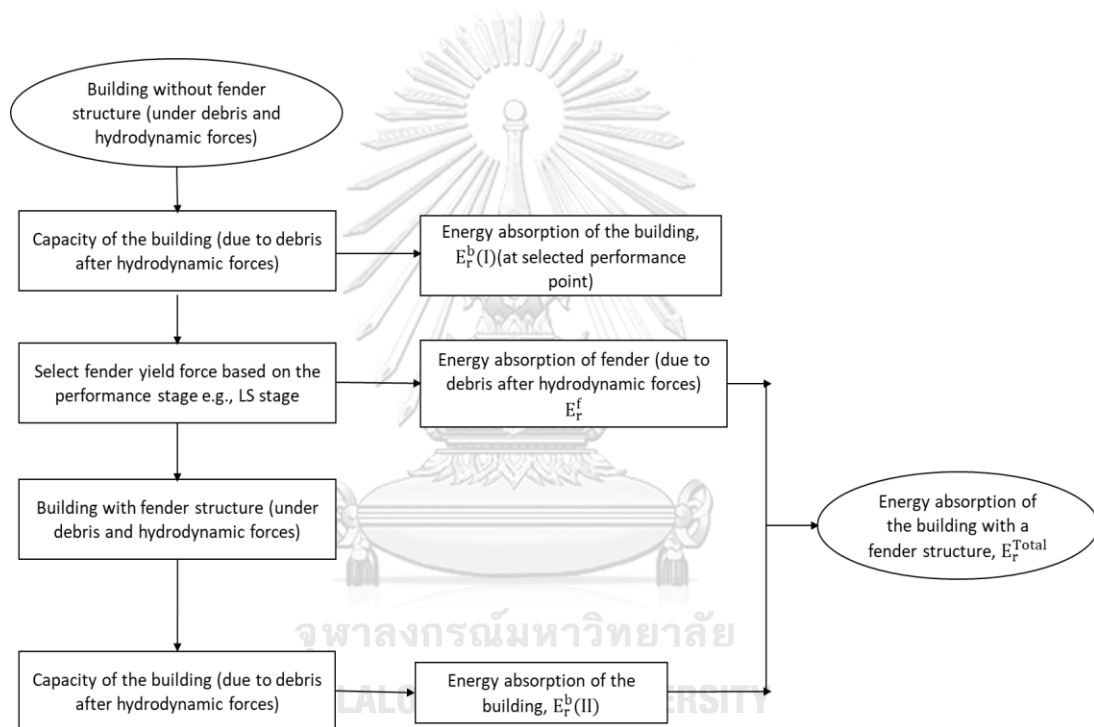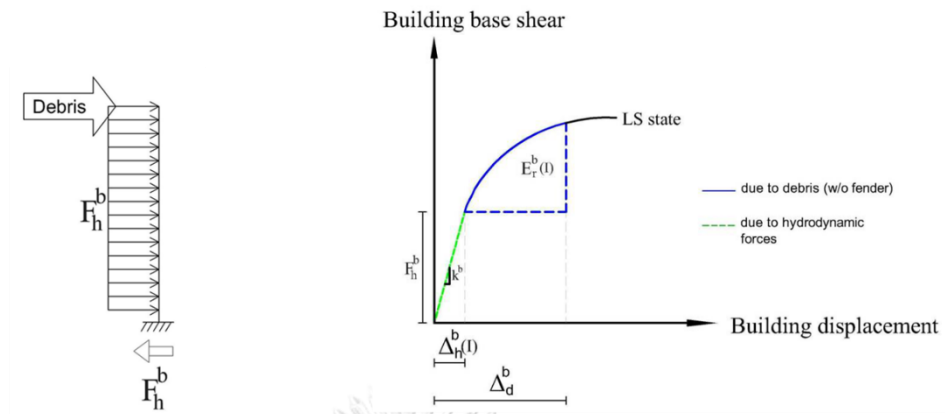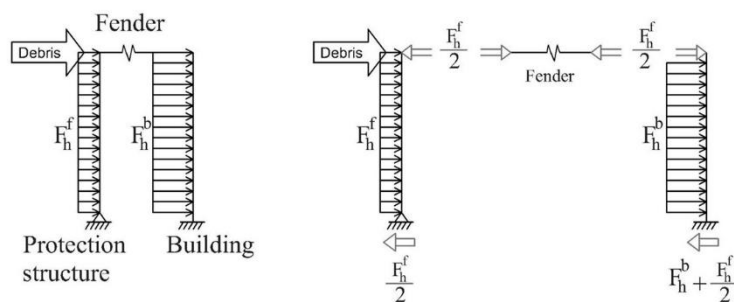
Figure 4.16 Flow chart of the proposed recommendation for the building with a fender structure
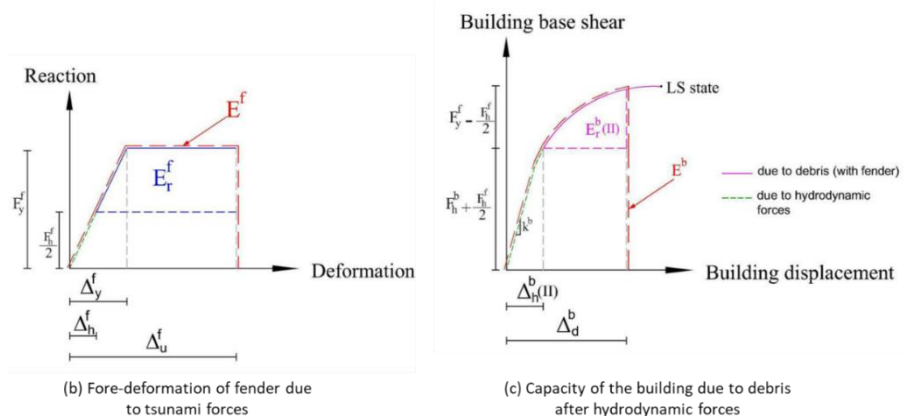
(a) Free body diagram of the building under tsunami forces

(b) Capacity of the building due to debris after hydrodynamic forces

Figure 4.17 Energy concept of the building without a fender structure (a) FBD of the building and (b) Capacity of the building

(a) Free body diagram of building with fender under tsunami forces

(b) Fore-deformation of fender due to tsunami forces

(c) Capacity of the building due to debris after hydrodynamic forces

Figure 4.18 Energy concept for the building with a fender structure (a) FBD of the building with a fender structure, (b) Force-deformation of the fender and (c) Capacity of the building

However, for the studied case in this paper, hydrodynamic forces are applied first, and then the debris is impacted to evaluate the remaining energy of the building. Therefore, the remaining energy of the building with a fender structure may be lower than the proposed Equation (2). The simplified models for the application of hydrodynamic forces and debris impact on the building with and without fender structures are respectively shown in Figs. 17 and 18. Therefore, for the case of debris impact after applying hydrodynamic forces, the total remaining energy absorption of the building with a fender structure is as follows:

$$E_r^{Total} = E_r^f + E_r^b(II) \tag{3}$$

The variables in Figs. 17 and 18 are defined as

$\Delta_h^b(I)$ = displacement of building due to hydrodynamic forces

$\Delta_h^b(II)$ = displacement of building with a fender structure due to hydrodynamic forces

Δ_d^b = displacement of building due to debris after applying hydrodynamic forces

Δ_h^f = displacement of the fender due to hydrodynamic forces

Δ_y^f = displacement of the fender at fender yielding state

Δ_u^f = displacement of the fender at fender ultimate state

F_h^f = hydrodynamic force in the fender structure

F_h^b = hydrodynamic force in the building

F_y^f = fender yielding force

E^b = energy absorption of the building

E^f = energy absorption of the fender

E_r^f = energy absorption of the fender due to debris after applying hydrodynamic forces

$E_r^b(I)$ = energy absorption of the building without a fender structure due to debris after applying hydrodynamic forces

$E_r^b(II)$ = energy absorption of the building with a fender structure due to debris after applying hydrodynamic forces

E_r^{Total} = total remaining energy absorption of the building with a fender structure due to debris after applying hydrodynamic forces

k^b = initial stiffness of the building.

The step-by-step equations to obtain the total remaining energy of the building with a fender structure in Equation (3) are as follows:

According to Fig. 18 (b), the remaining energy of the fender due to debris after applying hydrodynamic forces is

$$E_r^f = 0.5 \times (F_y^f - F_h^f)[(\Delta_u^f - \Delta_y^f) + (\Delta_u^f - \Delta_h^f)] \tag{4}$$

According to Fig. 25 (c), the displacement of building (with a fender structure) due to hydrodynamic forces is displaced more than that of the building (without fender structure) due to the hydrodynamic forces from the fender structure. Therefore, the displacement of building with a fender structure due to hydrodynamic forces is

$$\Delta_h^b(II) = \frac{(F_h^b + 0.5F_h^f)}{k^b} \tag{5}$$

Due to the displacement of the building from Equation (5), the remaining energy absorption of the building with a fender structure is lower than that of the building without fender structure. Therefore, the remaining energy absorption of the building with a fender structure due to debris after applying hydrodynamic forces ($E_r^b(II)$) is needed to reduce from the remaining energy absorption of the building without a fender structure due to debris after applying hydrodynamic forces ($E_r^b(I)$) because the hydrodynamic forces from the fender structure. According to Fig.18 (c), the remaining energy absorption of the building with a fender structure due to debris after applying hydrodynamic forces is

$$E_r^b(II) = E_r^b(I) - 0.25F_h^f(2\Delta_d^b - \Delta_h^b(I) - \Delta_h^b(II)) \tag{6}$$

4.3.2 Application of proposed method

The building is designed to resist the impact of a 40 ft loaded shipping container. The hydrodynamic force in the fender structure, F_h^f is 1519 kN. It should be noted that the fender absorbs half of the hydrodynamic force from the fender structure and then transfer to the main building. The evaluated energy for the shipping

container is 1190 kN-m according to the kinetic energy [35]. Using the energy concept, the total energy of the building with a fender structure to resist the impact of debris after hydrodynamic forces can be determined as follows:

Kinetic energy, K. E $\leq$ E_r^{Total}

According to Equation (8), $E_r^{Total} = E_r^f + E_r^b(II)$

Trial fender size is F_y^f = 2300 kN, L_f = 1.6 m, Δ_y^f = 0.53 m, and Δ_u^f = 1.15 m.

Using Equation (4), the remaining energy of fender due to debris after hydrodynamic forces is

$$E_r^f = 0.5 \times (F_y^f - F_h^f)[(\Delta_u^f - \Delta_y^f) + (\Delta_u^f - \Delta_h^f)] = 1229 kN$$

From the capacity curve of the building without fender structure (Fig. 4.19), the building properties based on the trial fender reaction are Δ_d^b = 0.185 m, $\Delta_h^b(I)$= 0.049m, k^b = 121347 kN/m, F_h^f = 1519 kN, F_h^b= 5946 kN, and E^b= 237 kN-m.

Using Equation (5), the displacement of building with a fender structure due to hydrodynamic forces is

$$\Delta_h^b(II) = \frac{(F_h^b + 0.5 F_h^f)}{k^b} = 0.055m$$

Using Equation (6), the remaining energy absorption of the building with a fender structure due to debris after applying hydrodynamic forces is

$$E_r^b(II) = E_r^b(I) - 0.25 F_h^f (2\Delta_d^b - \Delta_h^b(I) - \Delta_h^b(II)) = 136 kN - m$$

According to Equation (3), $E_r^{Total} = E_r^f + E_r^b(II)$ = 1229 + 136 = 1365 kN-m > K. E of shipping container (1190 kN-m).

Fig. 4.19 shows the target performance based on the trial fender reaction. This figure shows that the building target performance is between the IO and LS states if the fender force of 2300 kN and fender length of 1.6 m are used. The building with the proposed fender properties is used for the tsunami pushover analysis. The energy evaluated from the design recommendation is approximately the same with that from the nonlinear analysis and can be seen in Fig 4.21.
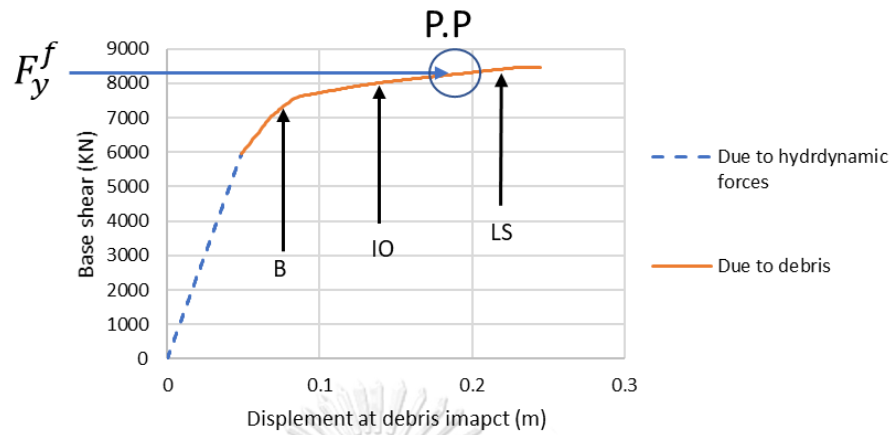
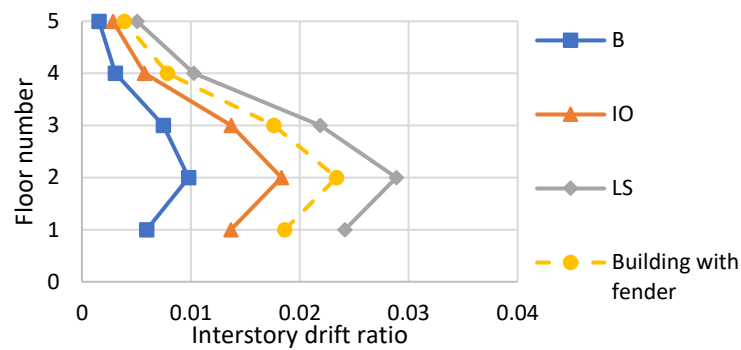Figure 4.19 Performance point based on selected fender yield force

Figure 4.20 Check the inter-story drift ratio for the proposed design system
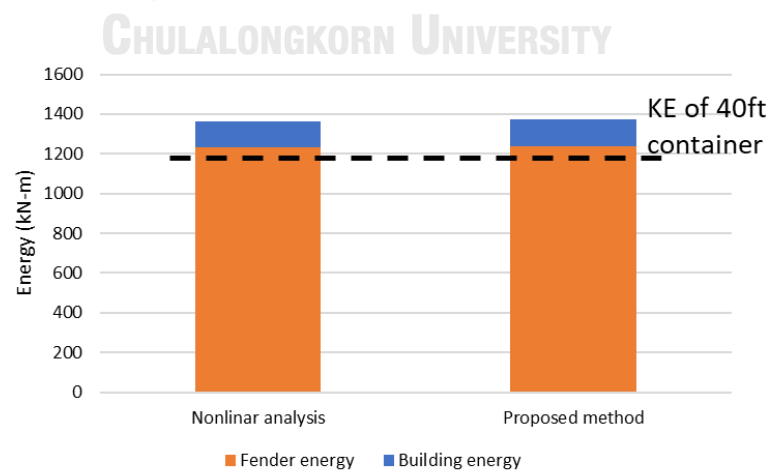

Figure 4.21 Validation of the proposed recommendation with tsunami pushover analysis

4.4 Building with a fender structure based on the efficiency of 2D frame results

4.4.1 Selection of the fenders

After understanding the concept of building with a fender system, a 3-dimensional analysis of building analysis is conducted in this study. The general concept of the building with the fender structure is the same as in section 4.2.2. For a 3-dimensional building, the fenders are installed only at the water level. The number of fenders required for this type of building is 6 units. Only one fender size is chosen to understand easily for the building system. The fender type is also the super cone fender. The selection of fender reaction is based on the base shear of the building without fender at the LS state. From the previous chapter, the lowest capacity has occurred at the debris impact location at C1. Therefore, the base shear is chosen from that impact location i.e. 33900 kN. The selected fender reaction is considered as 5000 kN per unit which is lower than the LS state of the building (30000 kN < 33900 kN) (see Figure4.15). The fender length is taken as 2.5 m according to the commercial catalog. The yield and ultimate fender deformation are considered as 33 % and 72 % of fender length to obtain 100 percent of the fender's energy. The idealized fender unit is shown in Figure 4.23. The impact locations of debris are the same as the building without the fender system and are shown in Figure 4.22.
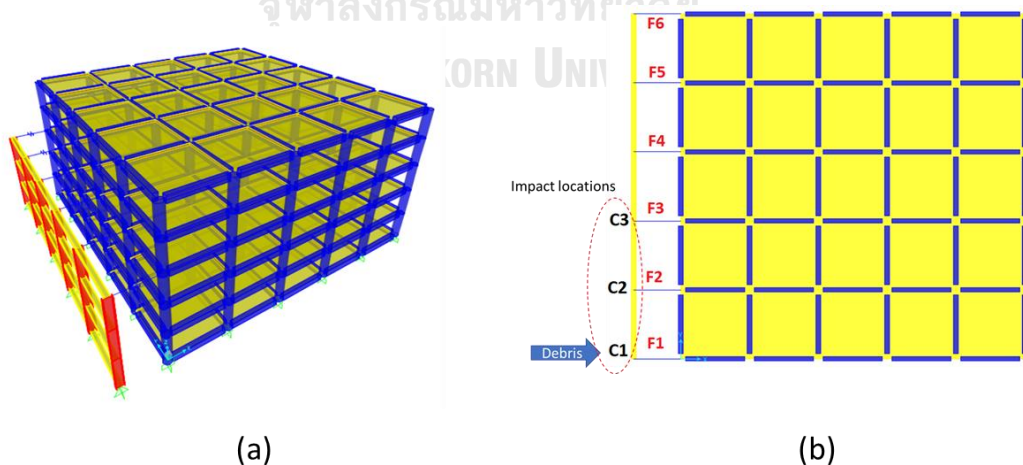

(a)   (b)

Figure 4.22 Building with fenders (a) 3-dimension view and (b) plan view
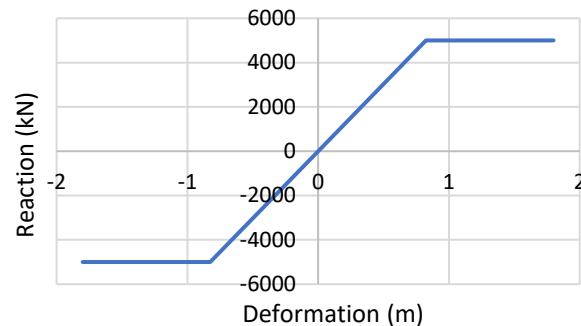
Figure 4.23 Idealized fenders for the building system

4.4.2 Response of the building with a fender structure (Case II (a) and Case II (b))

Figure 4.24 shows the capacity of the building with fenders under different impact locations. For all different impact locations, the displacement of the fender is needed to rest if one of the fender units reach ultimate fender deformation. As can be seen in Figure, the displacement of the fender for the building at impact location C1 is the largest deformation, among others. However, the maximum base shear is found at the building at debris impact, C3 case. Since the same hydrodynamic forces are applied in the building system for all impact locations, the force-deformation results due to actual hydrodynamic forces are the same.
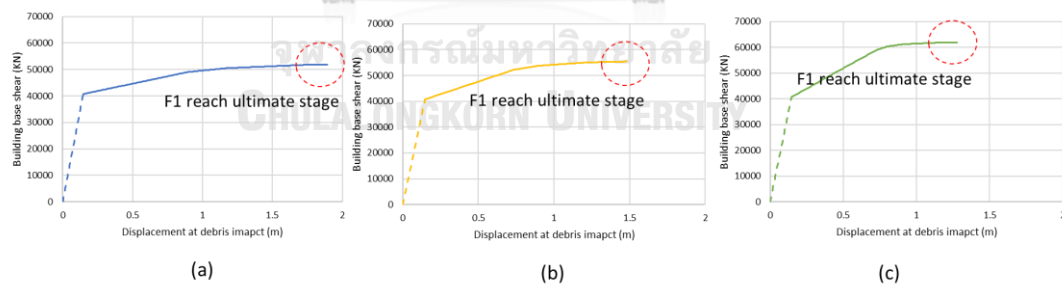

Figure 4.24 Capacity curve of the building with fenders at different impact location

(a) impact at C1, (b) impact at C2 and (c) impact at C3

Figure 4.25 to 4.27 show the step-by-step plastic hinge formation for different impact locations. There is no plastic hinge formation due to actual hydrodynamic forces. For the building at impact location C1, three fender units such as fender F1, F2, and F3 reach the fender yield state when one of the fenders i.e. F1 is found at ultimate fender deformation. Besides, the same behavior is found in the building at

impact location C2 (see Figure 4.26), but the plastic hinge formations are not the same. However, for the building at impact location C3, the fender units F1, F2, F3, and F4 are found at the fender yield state when one of the fenders i.e. F1 is found at ultimate fender deformation (See Figure 4.27).
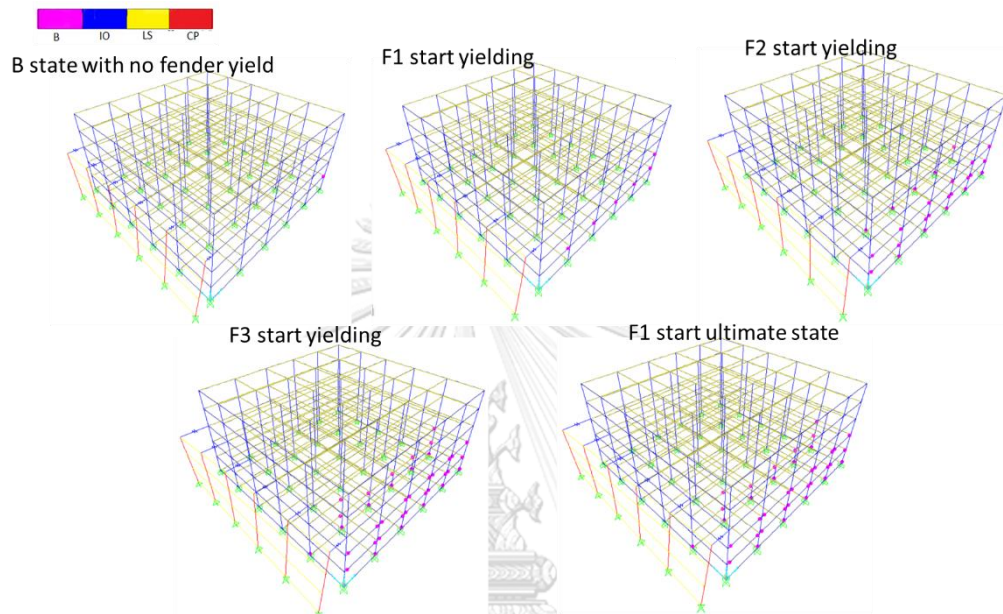

Figure 4.25 Step by step plastic hinge formation for the building at impact location, C1
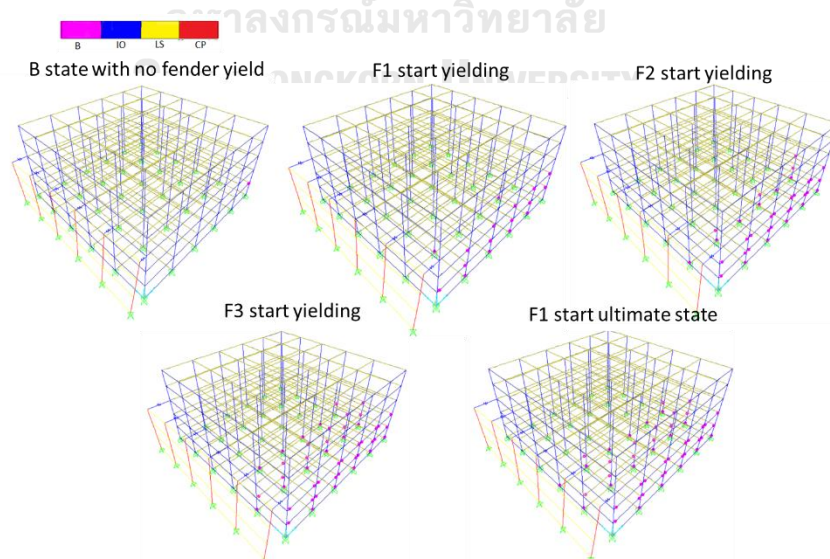

Figure 4.26 Step by step plastic hinge formation for the building at impact location, C2
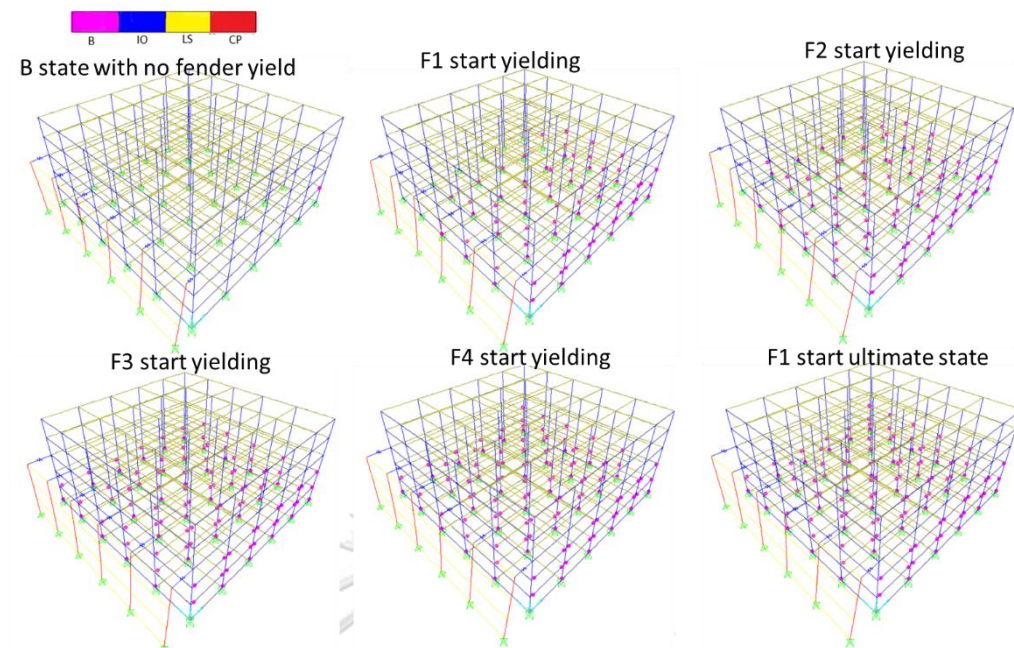
Figure 4.27 Step by step plastic hinge formation for the building at impact location, C3

Figure 4.28 shows the comparison of the capacity curve for the building with and without fenders. As can be seen, the performance of the building with fenders is lower than the LS state of the building specifically between the B and IO state. According to the 2D frame analysis, the base shear and deformation of the building with fenders are depending on the fender forces. Even though the fender yield forces were utilized about 30000 KN in the building system, the base shear that obtained is about over15000 kN in the building with fenders.
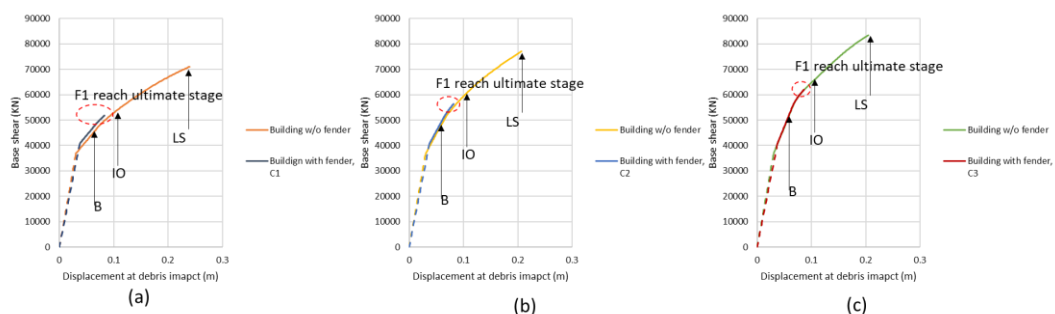

Figure 4.28 Comparison of the capacity curve for the building with and without fenders at different impact location (a) impact at C1, (b) impact at C2, and (c) impact at C3

As can be seen in Figure 4.29 and the results of plastic hinge formation, the performance state of the building with fenders is within the B and IO state of the building without fenders. This confirms that the advantage of using fenders.
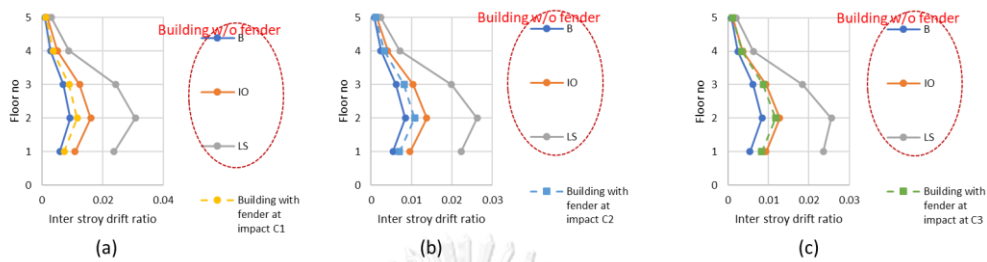

Figure 4.29 Comparison of inter-story drift ratio for the building with and without fenders at different impact location (a) impact at C1, (b) impact at C2, and (c) impact at C3

Figure 4.30 to 4.32 show the performance of each fender unit in the building with a fender system. As discussed in previous figures, for the building system at impact location C1 and C2, the fender unit F1, F2 and F3 have reached fender yield state (33 % of fender deformation) when one of the fenders obtain ultimate fender deformation (72 % of fender deformation) (See Figure 4.30 and 4.31). Also, the fender F1, F2, and F3 have more ability than the others because these fender units are closer to debris impact location C1 and C2. However, for the building system at impact location C3, the fender F1, F2, F3, and F4 have more performance than the others because the impact location is approximately in the middle of the frame and can be seen in Figure 4.32.
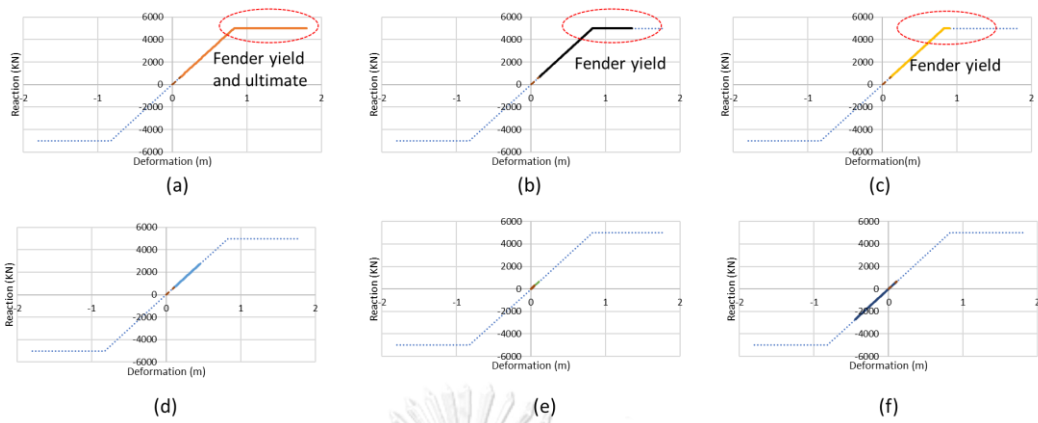
Figure 4.30 Performance of each fender for the building with fenders at impact location, C1 (a) Fender F1, (b) Fender F2, (c) Fender F3, (d) Fender F4, (e) Fender F5, and (f) Fender F6
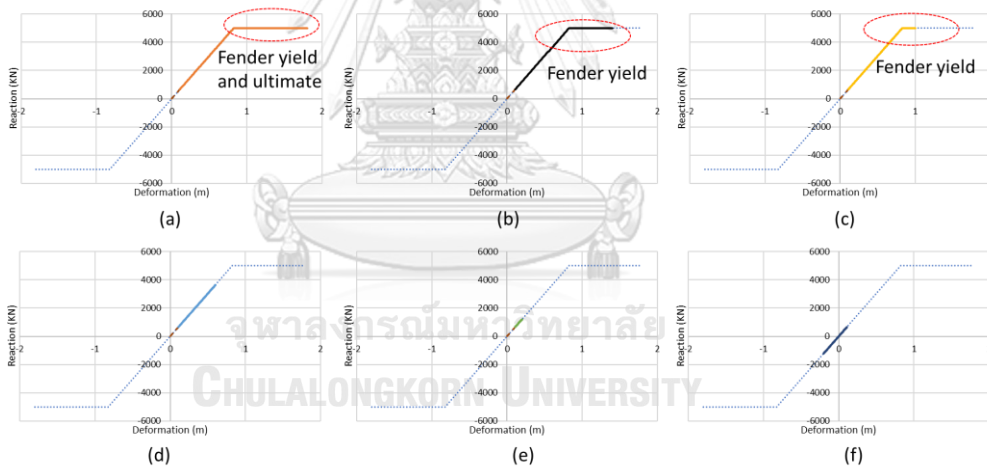

Figure 4.31 Performance of each fender for the building with fenders at impact location, C2 (a) Fender F1, (b) Fender F2, (c) Fender F3, (d) Fender F4, (e) Fender F5, and (f) Fender F6
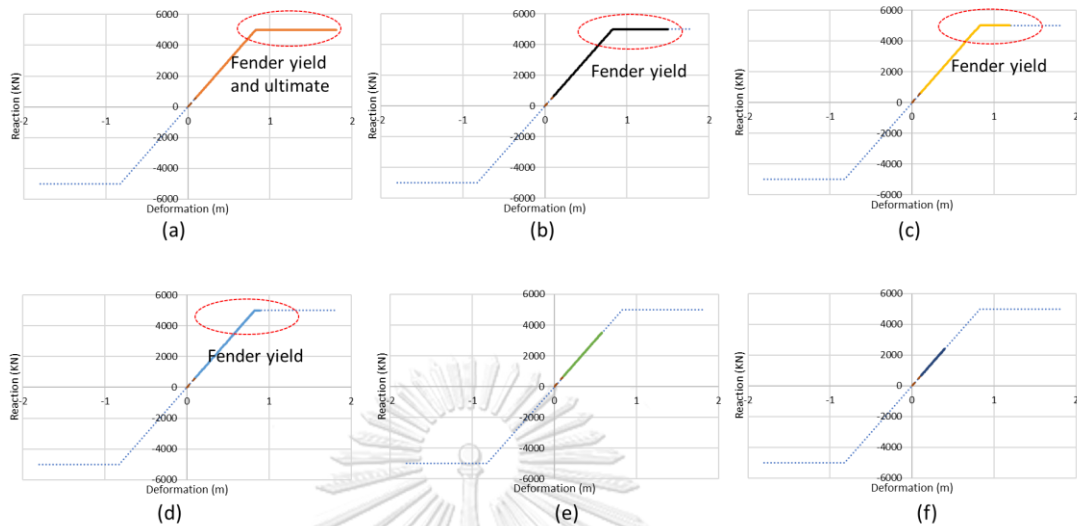
Figure 4.32 Performance of each fender for the building with fenders at impact location, C3 (a) Fender F1, (b) Fender F2, (c) Fender F3, (d) Fender F4, (e) Fender F5, and (f) Fender F6

As can be seen in Figure 4.33 to Figure 4.35 for different impact locations, as predicted in 2-dimensional analysis, the energy absorption of the building with fenders is larger than the building without a fender system. In the building without fender system, the building with the performance of IO state cannot resist the maximum impact of shipping container (40 ft loaded container). In contrast, the building with fender system with the performance of B state can effectively resist the impact of shipping container for all types. Therefore, the usage of the fenders is an effective way to reduce the impact of debris on the building system.
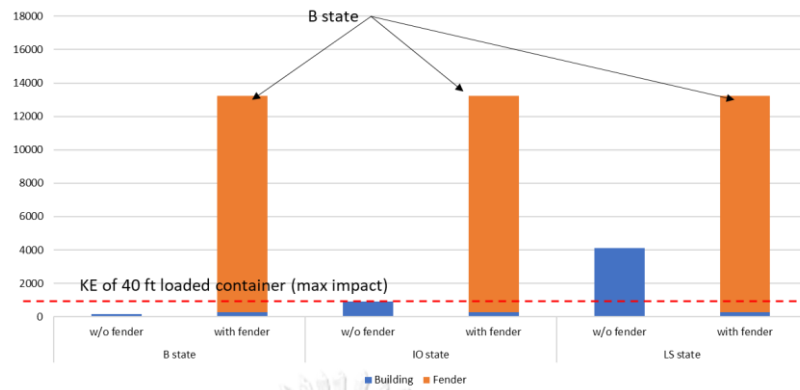
Figure 4.33 Energy absorption of the building with fender and without fenders at impact location C1
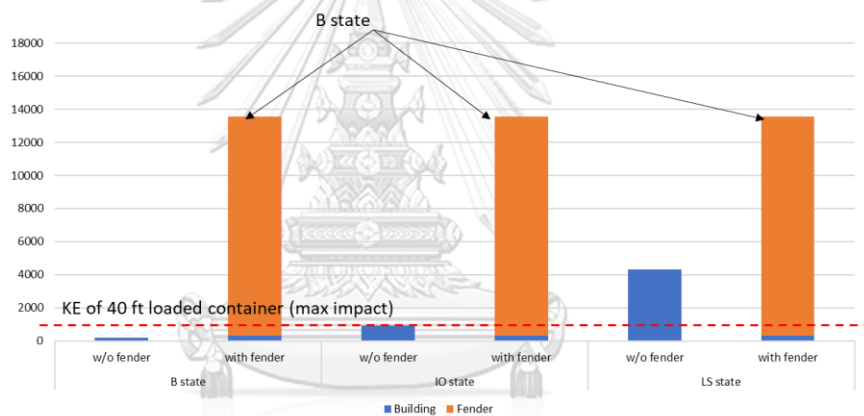

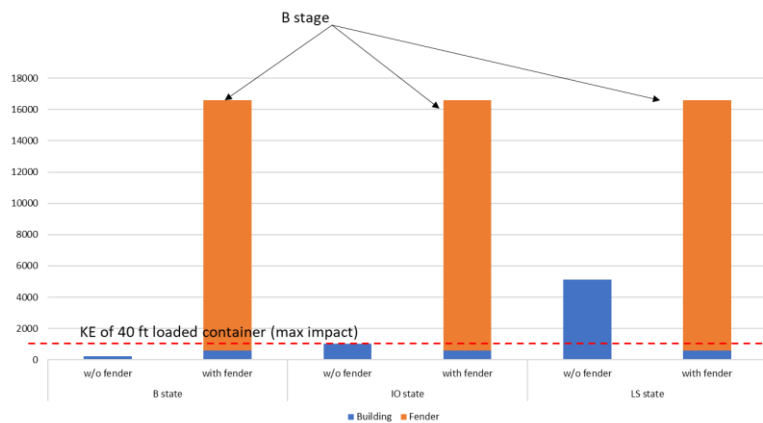Figure 4.34 Energy absorption of the building with fender and without fenders at impact location C2

Figure 4.35 Energy absorption of the building with fender and without fenders at impact location C3

CHAPTER (5)
CONCLUSIONS

5.1 Summary and conclusions

The building with a fender structure to resist the large debris and hydrodynamic forces has been established in this study. Actual hydrodynamic forces under constant inundation depth were considered in the building system using the force-controlled method. The response of the building due to debris after hydrodynamic forces were evaluated using the displacement-controlled method. This study has been introduced with the combination of tsunami forces including debris impacts.

Super cone fenders as connections are utilized in RC building with a fender structure. For the proposed methodology, the behavior of fender under varying force has been observed with the performance of the building. The capacity of the building was obtained through tsunami pushover methods. The resistance of the building was evaluated using the work-energy approach for the kinetic energy of the shipping container. The kinetic energy of the shipping container was evaluated using the work-energy approach to compare the resistance of the building with and without the fender structure. After investigating the building with a fender structure, the conclusions observed were divided into three parts in this study.

The first part is the comparison of energy absorption of the square and octagonal building. The conclusions are as follows:

1. In a comparison of the energy absorption of the square and octagonal building at different impact locations, energy absorption of square building is larger than the octagonal building at impact location C1, C2 and C3. The lowest energy absorptions are found in the corner column for both buildings. The largest energy absorption is found in the middle column for both buildings.

2. Furthermore, hydrodynamic forces applied to the building are larger in the octagonal building than in the square building because of the large number of columns. Therefore, inter story drift ratio in octagonal building are larger than that in square building.

3.   Due to the facts such as energy absorption, consideration of hydrodynamic forces, inter story drift ratio and simple profile for fender structure, the square building is selected for the analysis of building with a fender structure.

The second part is about the building with a fender structure using 2-dimensional analysis. The related conclusions are as follows:

1.   In the 2-dimensional analysis of the building without fender, the base shear forces at B, IO, and LS state are 1140, 2052, and 2488 kN respectively. The evaluated energy of the building with the LS performance state is 330 kN that cannot resist shipping container (loaded) impacts.

2.   For the building with a fender structure (2D analysis), the hydrodynamic forces applied in the building with a fender structure is about 6705.5 kN, which is larger than the hydrodynamic forces from the building without a fender structure, i.e 5946 kN because the building with fender structure absorbs hydrodynamic forces not only from its hydrodynamic loads but also from the fender structure.

3.   For the performance of the fender system, the fender absorbs half of the hydrodynamic forces from the fender structure and transfers to the main building i.e. 759.5 kN.

4.   For the building with a fender structure, the maximum base shear is depending on the fender yield force utilized in the system. For example, for the $F_{(2000)}$ fender, the maximum base shear is 1240.5 kN.

5.   In a comparison of the performance of building with and without fenders, the building with fenders did not show failure behavior while the building without fenders shows up the failure. This claim that the advantage of using fenders.

6.   As in the case of a building connected with a fender structure, continuous plastic hinge formation appeared in the building is found only before reaching the fender yield state, and after reaching the yield state, there is no plastic hinge formation. Simultaneously, the fender leads to the large inelastic

deformation from its yield to its ultimate state (72 % of its length). According to this observation, the fender which is lower than the maximum capacity of the building (LS state) can absorb the impact energy using its inelastic deformation without occurring damages to the main building starting from the fender yield state.

7. According to the results of the IDR ratio, the performance of building with and without fenders are the same, especially at the B state. However, as a result of the fender yield force of $F_{(2000)}$ is lower than the base shear of the building at IO state i.e. 2052 kN, consequently, the maximum IDR ratio is lower than that of the building without a fender system at that state. These behaviors are similar in the building with fender $F_{(2200)}$ and $F_{(2400)}$. From this observation, the performances of plastic hinge formation and the deformation of the building are related to the fender yield force values.

8. In the relationship of fender yield force and building's energy absorption, the larger the fender yield force; the more energy can be absorbed by the building.

9. In a comparison of fender's energy absorption, the larger the fender yield force, the more energy can be absorbed by the fender. It is investigated that fender, $F_{(2400)}$ which is the largest energy absorption, absorbs 62 % of its energy for the impact of debris after hydrodynamic forces.

10. For the resistance of the building, the buildings with fender $F_{(2200)}$ and $F_{(2400)}$ can successfully absorb the kinetic energy of all types of shipping container.

The final part of the conclusions is about the building with fenders under different impact locations in the 3-dimensional analysis. The related conclusions are as follows:

1. For the building with a fender structure, the displacement of the fender is needed to stop if one of the fenders reaches ultimate fender deformation. For three impact location cases, the fender F1 is firstly found ultimate fender deformation. However, the target displacement of the fender for each debris impact location is different. The displacement of the fender for the building at impact location C1 is the largest deformation, among others.

2. For the building with fenders at impact locations C1 and C2, three fender units are found with a 33 % fender deformation state (fender yield state) in the building system. For the building with fenders at impact location C3, four fender units are found with a 33 % deformation state in the building system.

3. It was found that the total fender yield forces were utilized about 30000 kN by installing 6 fender units in the building system, the base shear due to debris after hydrodynamic forces is about over15000 kN in the building with fenders.

4. In the case of each fender performance for the building system, the fender unit at the corner near the debris impact location utilize its energy completely while the others partially utilize its energy depending on the debris impact.

5. As predicted in the 2-dimensional analysis, the energy absorption of the building with fenders has more resistance than the building without fenders. Therefore, the usage of the fenders is an effective way to reduce the impact of debris on the building system.

5.2 Recommendations

According to the analysis of a building with a fender structure, there are some recommendations for the design of the building with a fender structure.

1. The building should design the tsunami forces including upcoming hydrodynamic forces from the fender structure and otherwise, the performance of the building with the fender structure is not the same as the initial main building.

2. For the installation of the fender in the building system, the distance between the building and the fender structure should allow for the deformation of the fender, otherwise, the main building can suffer several damages without utilizing the advantages of the fender structure.

REFERENCES

[1] FEMAP-646. Guidelines for design of structures for vertical evacuation from tsunamis. 2012.

[2] Yeh H. Design Tsunami force for onshore structure. Disaster Research. 2007;2.

[3] FEMAP-55. Coastal construction manual, principles and practices of planning, siting, designing, constructing, and maintaining residential buildings in coastal areas (fourth edition). 2011;II.

[4] CCH. City and country of Honolulu Building Code (CCH) 2000. 2000.

[5] Al-Faesly T, Palermo D, Nistor Ia, Cornett A. Experimental Modeling of Extreme Hydrodynamic Forces on Structural Models. Protective Structures. 2012;3.

[6] Robertson I, Chock G, Morla J. Structural Analysis of Selected Failures Caused by the 27 February 2010 Chile Tsunami. Earthquake Spectra. 2012;28.

[7] Palermo D, Nistor I, Nouri Y, Cornett A. Tsunami loading of near-shoreline structures: a primer. Canadian Journal of Civil Engineering. 2009.

[8] Nistor I, Palermo D, Nouri Y, Murty T, Saatcioglu M. Tsunami-Induced Forces on Structures. Handbook of Coastal and Ocean Engineering2009. p. 261-86.

[9] Nouri Y, Nistor I, Palermo D, Cornett A. Experimental investigation of tsunami impact on free standing structures. Coastal Engineering Journal. 2010.

[10] Árnason H. Interactions between an Incident Bore and free standing structure. 2005.

[11] Chinnarasri C, Thanasisathit N, Ruangrassamee A, Weesakul S, Lukkunaprasit P. The impact of tsunami-induced bores on buildings. Maritime Engineering. 2013.

[12] Wüthrich D, Pfister M, Nistor I, Schleiss AJ. Experimental study on the hydrodynamic impact of tsunami-like waves against impervious free-standing buildings. Coastal Engineering Journal. 2018.

[13] Naito C, Cercone C, Riggs HR, Cox D. Procedure for site assessment of the potential for tsunami debris impact. Journal of Waterway, Port, Coastal, and Ocean Engineering. 2014.

[14] ASCE7-16. Minimum design loads and associated criteria for buildings and other structures. 2016.

[15] Matsutomi H. A practical formula for estimating impulsive force due to driftwoods and variation features of the impulsive force. 1999;1999.

[16] Haehnel RB, Daly SF. Maximum Impact Force of Woody Debris on Floodplain Structures. 2002.

[17] Como A, Mahmoud H. Numerical evaluation of tsunami debris impact loading on wooden structural walls. Engineering Structures. 2013.

[18] Madurapperuma MAKM, Wijeyewickrema AC. Response of reinforced concrete columns impacted by tsunami dispersed 20′ and 40′ shipping containers. Engineering Structures. 2013.

[19] Piran Aghl P, Naito CJ, Riggs HR. Effect of nonstructural mass on debris impact demands: Experimental and simulation studies. Engineering Structures. 2015.

[20] Piran Aghl PP, Naito CJ, Riggs HR. Study of demands resulting from transverse impact of high mass, low velocity debris. Advances in Structural Engineering. 2016.

[21] Khowitar E, Riggs HR, M.ASCE, Kobayashi MH. Transverse Impact of a Horizontal beam on a vertical column. Engineering Mechanics. 2015.

[22] Cercone C, Naito C, Riggs HR, Schellberg R. Quantifying Structural Impact

Demands Due to Tsunami-Generated Debris. Structures congress. 2017.

[23] Lukkunaprasit P, Ruangrassamee A, Stitmannaithum B, Chintanapakdee C, Thanasisathit N. Calibration of Tsunami Loading on a Damaged Building. Journal of Earthquake and Tsunami. 2010.

[24] Shafiei S, Melville BW, Shamseldin AY. Experimental investigation of tsunami bore impact force and pressure on a square prism. Coastal Engineering. 2016.

[25] Wüthrich D, Pfister M, Nistor I, Schleiss AJ. Experimental study of tsunami-like waves generated with a vertical release technique on dry and wet beds. Journal of Waterway, Port, Coastal, and Ocean Engineering. 2018.

[26] Meyyappan P. Investigation on the effects of protective measures for coastal buildings against tsunami waves. 2016.

[27] Pimanmas A, Joyklad P, Warnitchai P. Structural design guideline for tsunami evacuation shelter. Journal of Earthquake and Tsunami. 2010.

[28] Lukkunaprasit P, Ruangrassamee A, Thanasisathit N. Tsunami loading on buildings with openings. Science of Tsunami Hazards. 2009;28:303.

[29] Triatmadja R, Nurhasanah ANY. Tsunami force on buildings with openings and protection. Journal of Earthquake and Tsunami. 2012.

[30] Robertson IN, Paczkowski K, Riggs HR, Mohamed A. Tsunami bore forces on walls. Volume 1: Offshore Technology; Polar and Arctic Sciences and Technology2011. p. 395-403.

[31] BS6349-4. Maritime structures. Code of practice for design of fendering and mooring systems. 1994.

[32] Hasumi K, Ito K, Oda Y, Honda T, Obi H. A study on fender piles installed around a tsunami evacuation building. International Ocean and Polar Engineering. 2015.

[33] Jariyaphan C. Mitigation Of Tsunami Debris Impact On Buildings. 2016.

[34] Magda W. Elastic fender-dolphin interaction for economic design of berthing dolphins. Journal of Waterway, Port, Coastal, and Ocean Engineering. 2019;145.

[35] PIANC. Guidelines for the design of fenders systems. 2002.

[36] Carbonari S, Antolloni G, Gara F, Lorenzoni C, Mancinelli A. A performance-based approach for the design of coupled dolphin-fender berthing structures. Marine Structures. 2019;64:78-91.

[37] Trelleborg. Fender systems.

[38] Macabuag J, Lloyd T, Rossetto T. Towards the development of a method for generating analytical tsunami fragility functions. Earthquake Engineering and Seismology. 2014.

[39] Petrone C, Rossetto T, Goda K. Fragility assessment of a RC structure under tsunami actions via nonlinear static and dynamic analyses. Engineering Structures. 2017;136:36-53.

[40] Rossetto T, De la Barra C, Petrone C, De la Llera JC, Vásquez J, Baiguera M. Comparative assessment of nonlinear static and dynamic methods for analysing building response under sequential earthquake and tsunami. Earthquake Engineering & Structural Dynamics. 2019;48:867-87.

[41] Park R, Paulay T. Reinforced Concrete Structures. 1975.

[42] Priestley MJN, Park R. Strength and Ductility of Concrete Bridge Columns Under Seismic Loading. ACI Structural Journal. 1987.

[43] Berry MP, Lehman DE, Lowes LN. Lumped-plasticity models for performance simulation of bridge columns. ACI Structural Journal. 2008.

[44] Bae S, Bayrak O. Plastic hinge length of reinforced concrete columns. ACI Structural Journal. 2008.

[45] Geng X, Zhou W. Plastic Hinge Capacity Prediction for Existing RC Rectangular Columns to Load Reversals. KSCE Journal of Civil Engineering. 2018;22:3883-93.

[46] Sezen H, Moehle JP. Shear strength model for lightly reinforced concrete columns. Journal of Structural Engineering. 2004;130:1692-703.

[47] Mander JB, Priestley MJN, Park R. Theoretical stress-strain model for confined concrete. Journal of Structural Engineering. 1988;114.

[48] ASCE/SEI-41-13. Seismic Evaluation and Retrofit of Existing Buildings. 2013.

[49] ASCE/SEI-41-17. Seismic evaluation and retrofit of existing buildings. 2017.

[50] H. Sezen aFA. Evaluation of FEMA 356 Models for Reinforced Concrete Columns and Beam-Column Joints. Structural Engineering Research Frontiers. 2007.

[51] ACI-318-14. Building code requirements for structural concrete. 2014.

[52] Crescenzo Petrone TR, Katsuichiro Goda Fragility assessment of a RC structure under tsunami actions via nonlinear static and dynamic analyses. Engineering Structures. 2017;136:36-53.

[53] Hanggara D, Wijeyewickrema AC. Vulnerability assessment of reinforced concrete buildings in indonesia subjected to tsunami inundation forces. International Journal of Disaster Resilience in the Built Environment. 2019;11:204-18.

จุฬาลงกรณ์มหาวิทยาลัย

CHULALONGKORN UNIVERSITY

APPENDIX

Equivalent force distribution using hand calculation

For square building
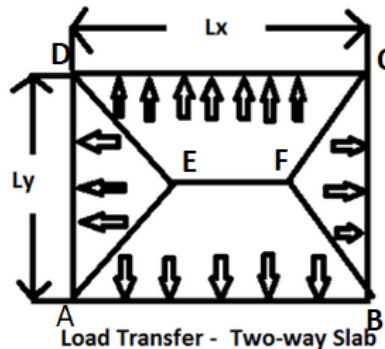
Figure A.1 Load transfer from slab to beam

For Super Dead Load

Changing super dead load from slab load to beam load,

According to Figure 1,

Lx= 5.83 m, Ly =5.83m

Check two-way slab, Lx/Ly = 5.83/5.83 = 1 ≤ 2 (Hence two ways slab)

Consider trapezoidal section "ABEF" of slab,

Area of ABEF = ½ (Lx Ly – 0.5 Lx^2) = 8.49 m^2

SDL load on slab = 1.5 KN/m2

SDL load acting on beam AB = 1.5 x 8.49 = 12.735 KN (For outer frames)

SDL load acting on beam AB = 1.5 x 8.49 x 2 = 25.47 KN (For inner frames)

Therefore,

The axial load on corner column, C1 = 12.735 KN

The axial load on inner column (3 beams connected), C2 = 6.37+ 6.37 + 12.735 = 25.47 KN

The axial load on inner column (4 beams connected), C3= 12.735+12.735+12.735+12.735 = 50.94 KN
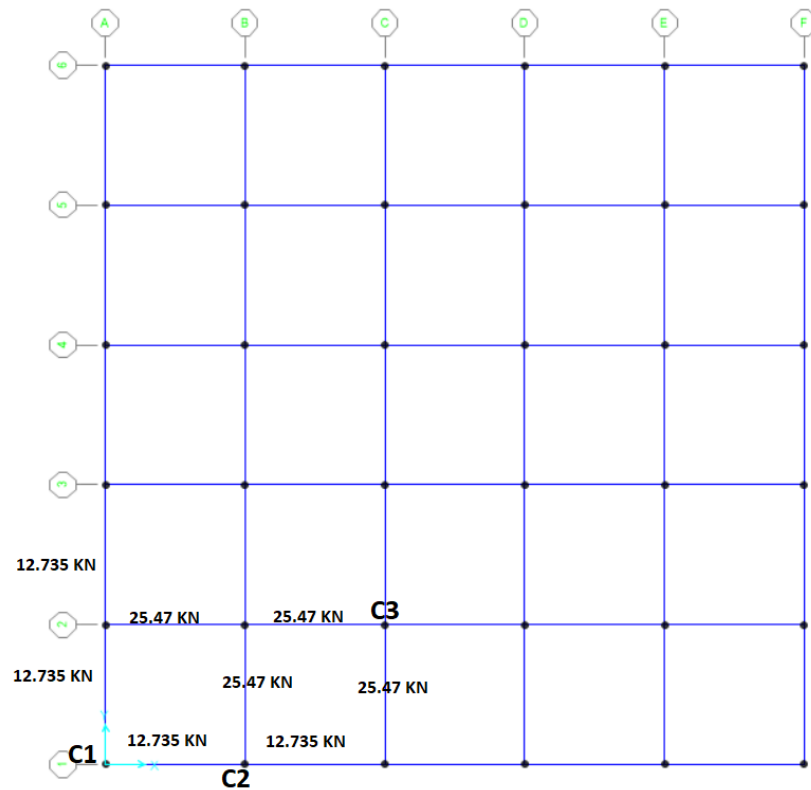
Figure A.2 Column arrangement of the building

Column Name	Axial load on column (Hand calculation) KN	Axial load on column (Sap 2000) KN
C1 (Corner column)	12.735	12.89
C2 (3 beams connected)	25.47	25.7
C3(4 beams connected)	50.94	50.32

Total number of columns, C1 = 4

Total number of columns, C2 = 16

Total number of columns, C3 = 16

Therefore,

Total axial load on all columns of the building = (4 x 12.735 + 16 x 25.47 + 16 x 50.94) x 5 = 6367.5 KN

Total axial load at base = (4 x 12.735 + 16 x 25.47 + 16 x 50.94) x 6 = 7641 KN

Total axial load at base (from Sap 2000) = 7647.502 KN **(OK)**

Figure A.3 Base reaction for super dead load from Sap 2000

For Live load

LL on slab (upper two floors) = 4.8 KN/m^2 (100 % full live load)

LL on slab (lower four floors) = 1.2 KN/m^2 (25 % of full live load)

The load distribution of slab to beam is the same procedure as SDL load.

For upper two floors,

LL load acting on beam AB = 4.8 x 8.49 = 40.75 KN (For outer frames)

LL load acting on beam AB = 4.8 x 8.49 x 2 = 81.5 KN (For inner frames)

For lower four floors,

LL load acting on beam AB = 1.2 x 8.49 = 10.19 KN (For outer frames)

LL load acting on beam AB = 1.2 x 8.49 x 2 = 20.38 KN (For inner frames)

Therefore,

For upper two floors,

The axial load on corner column, C1 = 40.75 KN

The axial load on inner column (3 beams connected), C2 = 20.375+ 20.375 + 40.75 = 81.5 KN

The axial load on inner column (4 beams connected), C3= 40.75+40.75+40.75+40.75= 163 KN

For lower four floors,

The axial load on corner column, C1 = 10.19 KN

The axial load on inner column (3 beams connected), C2 = 5.095+ 5.095+ 10.19 = 20.38 KN
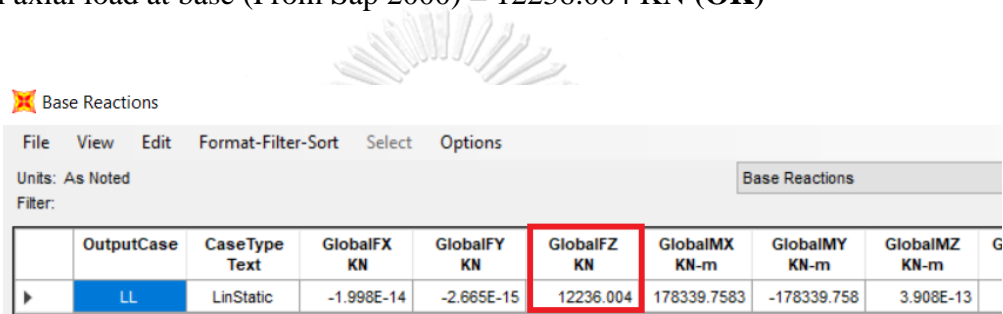
The axial load on inner column (4 beams connected), C3= 10.19+10.19+10.19+10.19= 40.76 KN

Column Name		Axial load on column (Hand calculation) KN	Axial load on column (Sap 2000) KN
Upper two floor	C1	40.75	40.81
	C2	81.5	81.66
	C3	163	163.07
Lower four floor	C1	10.19	10.8
	C2	20.38	20.86
	C3	40.76	40

Therefore,

Total axial load on all columns of the building = (4 x 40.75 + 16 x 81.5 + 16 x163) x 2 + (4 x 10.19 + 16 x 20.38 + 16 x40.76) x 4 = 12226 KN

Total axial load at base (From Sap 2000) = 12236.004 KN (**OK**)

Figure A.4 Base reaction for live load from Sap 2000

For buoyancy load,

The buoyancy load on slab = 2.21 KN/m^2

The load distribution of slab to beam is the same procedure as SDL load.

Buoyancy load acting on beam AB = 2.21 x 8.49 = 18.76 KN (For outer frames)

Buoyancy load acting on beam AB = 2.21 x 8.49 x 2 = 37.53 KN (For inner frames)

The axial load on corner column, C1 = 18.76 KN

The axial load on inner column (3 beams connected), C2 = 9.38 + 9.38 + 18.76 = 37.52 KN

The axial load on inner column (4 beams connected), C3 = 18.76 +18.76 +18.76 +18.76 = 75.04 KN

Column Name	Axial load on column (Hand calculation) KN	Axial load on column (Sap 2000) KN
C1	18.76	19.33
C2	37.52	37.99
C3	75.04	73.67

Total axial load on all columns of the building = (4 x 18.76 + 16 x 37.52 + 16 x 75.04) x 3 = 5628 KN

Total axial load at base (from Sap 2000) = 5633 KN **(OK)**

	OutputCase Text	CaseType Text	GlobalFX KN	GlobalFY KN	GlobalFZ KN	GlobalMX KN-m	GlobalMY KN-m	GlobalMZ KN-m
▶	Buoyancy	LinStatic	-1.332E-15	0	-5633.66	-82110.5971	82110.5971	1.421E-13

Figure A.5 Base reaction for buoyancy load from Sap 2000

For Hydrodynamic Load in x-direction

Figure A.6 Column arrangement of the frame

Column No	Lateral load applied (KN)
C1	80x3x3 = 720
C2	80x3x3 = 720
C3	80x3x3 = 720
C4	80x3x3 = 720
C5	80x3x3 = 720
C6	80x3x3 = 720
Total	4320
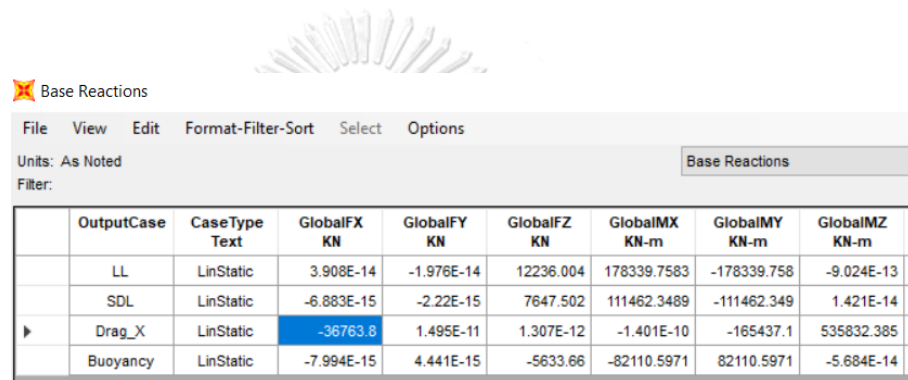
The building has six frames and hydrodynamic loading on all columns of the frame are the same. For six frame, Total lateral load applied on column = 4320 x 6 = 25920 KN

For the hydrodynamic load on beam, total beam length = 5.83 x 5 x 4 = 116.6 m

Hydrodynamic load on beam = 93 x116.6 = 10844 KN

Total base reaction of the building = 25920+116.6+10844 = 36880.6 KN

Total base reaction of the building, Fx (from Sap 2000) = 25920 + 10844 = 36764 KN **(OK)**

OutputCase	CaseType Text	GlobalFX KN	GlobalFY KN	GlobalFZ KN	GlobalMX KN-m	GlobalMY KN-m	GlobalMZ KN-m
LL	LinStatic	3.908E-14	-1.976E-14	12236.004	178339.7583	-178339.758	-9.024E-13
SDL	LinStatic	-6.883E-15	-2.22E-15	7647.502	111462.3489	-111462.349	1.421E-14
Drag_X	LinStatic	-36763.8	1.495E-11	1.307E-12	-1.401E-10	-165437.1	535832.385
Buoyancy	LinStatic	-7.994E-15	4.441E-15	-5633.66	-82110.5971	82110.5971	-5.684E-14

Figure A.7 Base reaction for hydrodynamic loads from Sap 2000

For Octagonal building

Check the results with the applied load using equilibrium condition.

For Super Dead Load

Changing super dead load from slab load to beam load,

According to Figure,

Lx = 5.5 m, Ly = 5.5 m

Check two-way slab, Lx/Ly = 5.5/ 5.5 = 1 ≤ 2 (Hence two ways slab)

Consider trapezoidal section "ABEF" of slab,

Area of ABEF = ½ (Lx Ly – 0.5 Ly^2) = 7.56 m^2

SDL load on slab = 1.5 KN/m2

Area of triangular shape = 0.5 x 5.5 x 5.5 = 15.125 m^2

SDL load on triangular shape = 15.125 x 1.5 = 22.69 KN

SDL load acting on beam AB = 1.5 x 7.56 = 11.34 KN (For outer frames)

SDL load acting on beam AB = 1.5 x 7.56 x 2 = 22.68 KN (For inner frames)

Therefore,

The axial load on corner column with Δ (3 beams connected), C1 = 22.68 /3 + 11.34 = 18.9KN

The axial load on outer column with Δ (4 beams connected), C2 = 2 x 22.69/3 + 11.34 = 26.47 KN

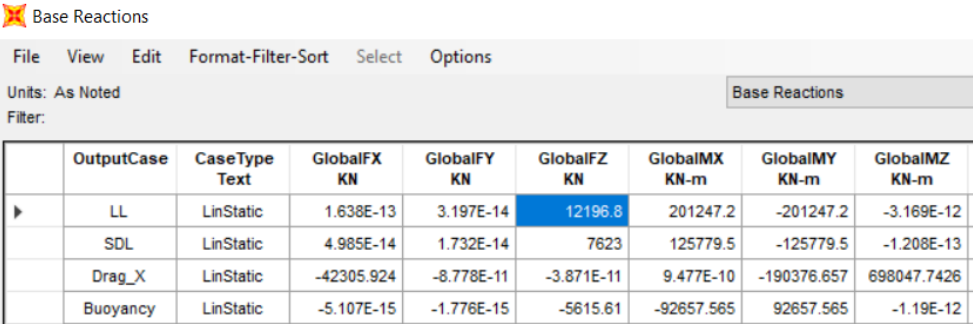The axial load on inner column with Δ (4 beams connected), C3= 22.68/3 + 11.34 + 22.68 = 41.58 KN

The axial load on inner column (4 beams connected), C4 = 22.68 + 22.69 = 45.37KN

The axial load on outer column (3 beams connected), C5 = 11.34 + 22.68/2 = 22. 68KN
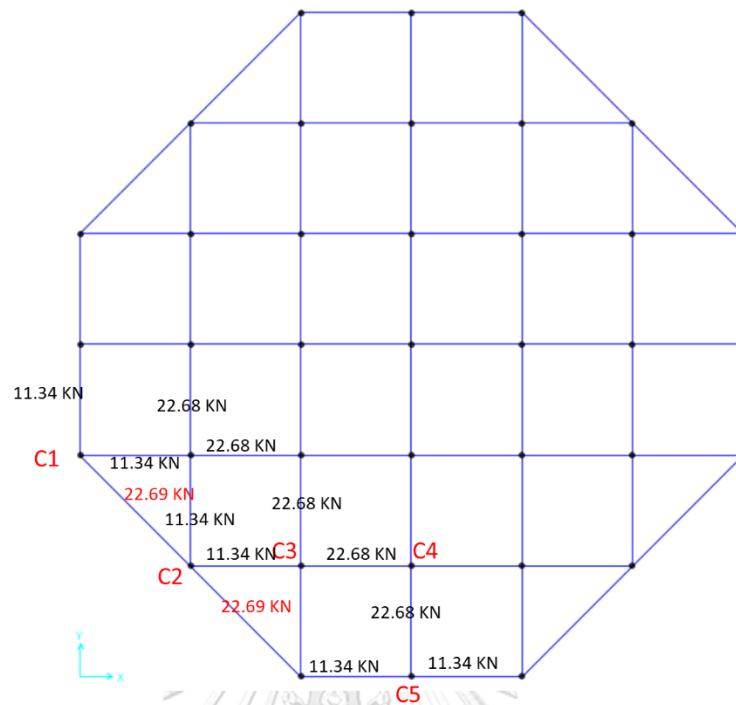
Figure A.8 Column arrangement of building

Total number of C1 = 8

Total number of C2 = 4

Total number of C3 = 8

Total number of C4 = 13

Total number of C5 = 4

Therefore,

Total axial load on all columns of the building = (8 x 18.9 + 4 x 26.47 + 8 x 41.58 + 13 x 45.37 + 4 x 22.67) x 5 = 6351 KN.

Total axial load at base = (8 x 18.9 + 4 x 26.47 + 8 x 41.58 + 13 x 45.37 + 4 x 22.67) x 6 = 7621 KN

Total axial load at base (from Sap 2000) = 7623 KN **(OK)**

Figure A.9 Base reaction for super dead load from Sap 2000

For Live load

LL on slab (upper two floors) = 4.8 KN/m^2 (100 % full live load)

LL on slab (lower four floors) = 1.2 KN/m^2 (25 % of full live load)

The load distribution of slab to beam is the same procedure as SDL load.

For upper two floors,

LL load on triangular shape = 4.8 x 15.125 = 72.6KN

LL load acting on beam AB = 4.8 x 7.56 = 36.29KN (For outer frames)

LL load acting on beam AB = 4.8 x 7.56 x 2 = 72.6KN (For inner frames)

For lower four floors,

LL load on triangular shape = 1.2 x 15.125 = 18.12KN

LL load acting on beam AB = 1.2 x 7.56 = 9.07KN (For outer frames)

LL load acting on beam AB = 1.2 x 7.56 x 2 = 8.14KN (For inner frames)

For upper two floors,

The axial load on corner column with Δ (3 beams connected), C1 = 72.6/3 + 36.29 =60.49 KN

The axial load on outer column with Δ (4 beams connected), C2 = 2 x 72.6 /3 + 36.29 =84.69 KN

The axial load on inner column with Δ (4 beams connected), C3= 72.6/3 + 36.29 + 72.6 = 133.09 KN

The axial load on inner column (4 beams connected), C4 = 72.6 + 72.6 = 145.2 KN

The axial load on outer column (3 beams connected), C5 = 36.29 + 72.6 /2 = 72.59 KN

For lower four floors,

The axial load on corner column with Δ (3 beams connected), C1 = 18.12/3 + 9.07 = 15.11 KN

The axial load on outer column with Δ (4 beams connected), C2 = 2 x 18.14 /3 + 9.07 = 21.16 KN

The axial load on inner column with Δ (4 beams connected), C3= 18.14/3 + 9.07 + 18.14 = 33.26 KN

The axial load on inner column (4 beams connected), C4 = 18.14 + 18.14 = 36.28 KN

The axial load on outer column (3 beams connected), C5 = 9.07 + 18.12 /2 = 18.13 KN

Therefore,

Total axial load on all columns of the building = (8 x 60.49 + 4 x 84.69 + 8 x 133.09 + 13 x 145.2 + 4 x 72.59) x 2 + (8 x 15.11 + 4 x 21.16 + 8 x 33.26 + 13 x 36.28 + 4 x 18.13) x 4 = 12194 KN

Total axial load at base (From Sap 2000) = 12196 KN **(OK)**

	OutputCase	CaseType Text	GlobalFX KN	GlobalFY KN	GlobalFZ KN	GlobalMX KN-m	GlobalMY KN-m	GlobalMZ KN-m
▶	LL	LinStatic	1.638E-13	3.197E-14	12196.8	201247.2	-201247.2	-3.169E-12
	SDL	LinStatic	4.985E-14	1.732E-14	7623	125779.5	-125779.5	-1.208E-13
	Drag_X	LinStatic	-42305.924	-8.778E-11	-3.871E-11	9.477E-10	-190376.657	698047.7426
	Buoyancy	LinStatic	-5.107E-15	-1.776E-15	-5615.61	-92657.565	92657.565	-1.19E-12

Figure A.10 Base reaction for live load from Sap 2000

For buoyancy load,

The buoyancy load on slab = 2.21 KN/m^2

The load distribution of slab to beam is the same procedure as SDL load.

Buoyancy load on triangular shape = 2.21 x 15.125 = 33.43KN

Buoyancy load acting on beam AB = 2.21 x 7.56 = 16.71 KN (For outer frames)

Buoyancy load acting on beam AB = 2.21 x 7.56 x 2 = 33.42 KN (For inner frames)

The axial load on corner column with Δ (3 beams connected), C1 = 33.43/3 + 16.71 = 27.85 KN

The axial load on outer column with Δ (4 beams connected), C2 = 2 x 33.43 /3 + 16.71 = 39 KN

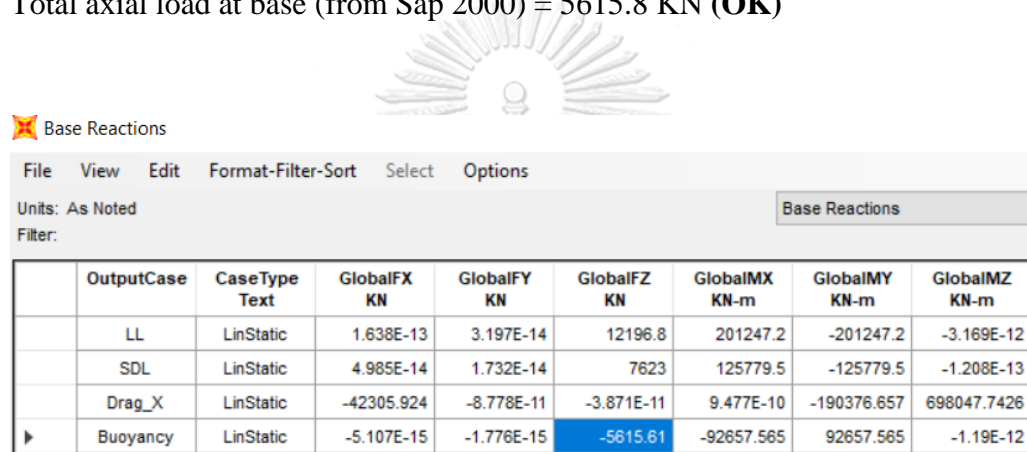The axial load on inner column with Δ (4 beams connected), C3= 33.43/3 + 16.71 + 33.43 = 61.28KN

The axial load on inner column (4 beams connected), C4 = 33.43 + 33.43 = 66.86KN

The axial load on outer column (3 beams connected), C5 = 16.71 + 33.43 /2 = 33.43KN

Total axial load on all columns of the building = (8 x 27.85 + 4 x 39 + 8 x 61.28 + 13 x 66.86 + 4 x33.43) x 3 = 5615.82 KN

Total axial load at base (from Sap 2000) = 5615.8 KN **(OK)**

Base Reactions

File   View   Edit   Format-Filter-Sort   Select   Options

Units: As Noted   Base Reactions
Filter:

OutputCase	CaseType Text	GlobalFX KN	GlobalFY KN	GlobalFZ KN	GlobalMX KN-m	GlobalMY KN-m	GlobalMZ KN-m
LL	LinStatic	1.638E-13	3.197E-14	12196.8	201247.2	-201247.2	-3.169E-12
SDL	LinStatic	4.985E-14	1.732E-14	7623	125779.5	-125779.5	-1.208E-13
Drag_X	LinStatic	-42305.924	-8.778E-11	-3.871E-11	9.477E-10	-190376.657	698047.7426
Buoyancy	LinStatic	-5.107E-15	-1.776E-15	-5615.61	-92657.565	92657.565	-1.19E-12

Figure A.11 Base reaction for buoyancy load from Sap 2000

For Hydrodynamic Load in x-direction

Column	Lateral load applied (KN)
C	80x3x3 = 720

The building has 37 columns and hydrodynamic loading on all columns of the frame are the same.

For six frame, Total lateral load applied to building = 720 x 37 = 26640 KN

For hydrodynamic load on beam, = (93 KN/m x 15.56 m x 2 two sided + 93 KN/m x 11 m) 4 =15668.64 KN

Total base reaction of the building, Fx (from Sap 2000) = 26640 + 15668.64 = 42308.64 KN **(OK)**

Figure A.12 Base reaction for hydrodynamic load from Sap 2000

Check capacity for the beam (40 x 60 cm)

To check the design the beam for the building, the following procedures are considered.

1.Choose a beam from key plan from Sap 2000 plan

2. Choose max moment and shear from Sap 2000 analysis.

3. Check moment capacity.

4. Check shear capacity
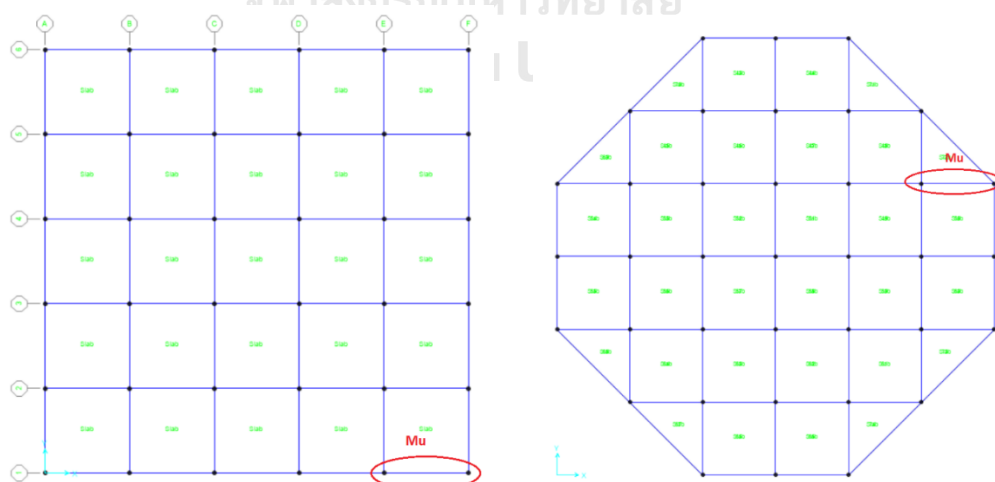
1.Choose a beam from key plan from Sap 2000 plan

Figure A.13 Beam key plan for square and octagonal building

2. From Sap 2000 analysis,

For S building, M_{max} = 316 KN-m, V_{max} = 137 KN

For O building, M_{max} = 370 KN-m, V_{max} = 231 KN

Check beam design for B 600 x 400 mm size
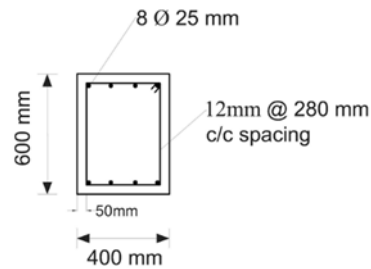
Figure A.14 Detailed properties of beam

DB=25 mm, RB= 12 mm, Cover=50mm, fc' = 35MPa, fy = 500 MPa

$d = h - 0.5d_b - r_b - \mathrm{cov}\,er$

$d = 0.6 - 0.5 \times 0.025 - 0.012 - 0.05 = 0.53m$

A_s= A_s'=1.96x10^{-3} m^2,

f_y =500MPa,

E_s = 1.99 x 10^8, E_c = 2.57 x 10^7,

ε_0 = 0.002

3. Check moment capacity, use the equivalent stress block method.

Stress in Compressive reinforcement.

$\varepsilon_s{}' = \frac{c-d}{c}\varepsilon cu = \frac{c-0.005}{c} \times 0.003$

From ACI code, 28MPa<f'$_c$ = 25MPa<56MPa

$\beta_1 = 0.85 - 0.05\frac{f'c - 28MPa}{7MPa} = 0.8$

Compression in steel,

$\varepsilon_s{}' = \frac{c-d}{c}\varepsilon cu = \frac{c-0.05}{c} \times 0.003$

$C_s = A_s{}'E_s \varepsilon_s$ = 1.96 x 10^{-3} x 1.99 x 10^8 x $\frac{c-0.05}{c}$ x 0.003

$= 1.76 \times \frac{c-0.05}{c}$

Compression in concrete,

$C_c = 0.85f'_c \, b\beta_1 c$ = 0.85 x 35 x 10^3 x 0.4 x 0.8c

$= 9520c$

Tension in steel

$T = A_s f_y = 1.96 \times 10^{-3} \times 500 \times 10^3$

$\qquad = 980$

From equilibrium condition,

$C_s + C_c - T = 0$

$1176(\frac{c-0.05}{c}) + 9520c - 980 = 0$

$1176c - 58.8 + 9520c^2 - 980c = 0$

$9520c^2 + 196c - 58.8 = 0$

$c = 0.07mm$

$a = \beta_1 c = 0.8 \times 0.07 = 0.056$

From Equilibrium

$M_n = C_c\,(d-\frac{a}{2}) + C_s(d-d^,)$

$\qquad = 666.4(0.54-\frac{0.056}{2}) + 326\,(0.54-0.05)$

$\qquad = 505.83\ KN\text{-}m > M_{max}$ (applied)

4. Check beam shear capacity

$\varphi\,V_n\,max = \varphi\,V_c + \varphi\,V_s$

$\phi Vc = \phi \times 0.17 \times \sqrt{f'_c} \times bd$

$\phi Vc = 0.75 \times 0.17 \times \sqrt{35} \times 0.4 \times 0.53 = 160 KN$

$\phi V_s = \phi \dfrac{A_v f_{yt} d}{s}$

$\varphi\,Vs = 125\ KN$

$\varphi\,V_n\,max = \varphi\,V_c + \varphi\,V_s$

$\varphi\,V_n\,max = 160 + 200 = 360\ KN > V_{max}$

$\therefore$ Ok for the beam design section.

Check column shear failure or flexural failure

According to the equation of Sezen and Moehle (2004)

$$V_n = V_s + V_c = k \frac{A_v f_y d}{s} + k \left(\frac{0.5 \sqrt{f_c'}}{a/d} \sqrt{1 + \frac{P}{0.5 \sqrt{f_c'} A_g}} \right) 0.8 A_g \text{ (MPa)}$$

Table A. 1 Prediction of column failure

Column Size(mm)	700	750	800	800	850
fc' (MPa)	30	30	30	35	35
Ag	0.38	0.44	0.5	0.5	0.56
Stirrup size (mm)	12	12	12	16	16
Avs (m²)	1.13x10-4	1.13x10-4	1.13x10-4	2.10x10-4	2.10x10-4
Eff depth, d	0.61	0.66	0.72	0.7	0.73
Axial, Pu (KN)	1728	1744	1764	1764	1788
Mu (KN-m)	1312	1454	1606	1606	1779
Vu (KN)	875	915	954	954	997
My (KN-m)	2288	2821	3202	3387	3215
Mu/Vud	2.46	2.37	2.33	2.4	2.44
Vs (KN)	1292	1399	1550	2638	2751
Vc (KN)	626	736	800	851	916
Vcol (KN)	1918	2135	2350	3489	3667
Vye(KN)	1525.333	1880.667	2134.667	2258	2143
Vye/ Vcol	0.795	0.884	0.908	0.647	0.58
Failure mode	Shear	Shear	Shear	Shear	Flexural

Note -columns with Vp /Vo ≥ 1.0, fail in shear (ASCE 41/17)

-columns with Vp /Vo ≤ 0.6,   fail in flexure

-columns with 0.6 <Vp /Vo < 1.0, flexure-shear failure

For Nonlinear modeling of the structural elements

Table A. 2 Nonlinear modeling parameters

Nonlinear modeling parameters		
	Column	Beam
Size	850 mm dia	400 x 600 mm
Longitudinal steel	28 - Db 28 mm	8 - DB 25mm
Transverse steel	16 mm dia @ 100 mm spacing	12 mm dia @ 280 mm spacing
fc' (expected)	53 Mpa	53 Mpa
fy (expected)	625 Mpa	625 Mpa
Transverse reinforcement ratio, pt = Av/bs	= 3 x 2.01x10^-4 / (0.85 x 0.1) = 0.007	= 2 x 1.13 x10^-4/ (0.4 x0.28) = 0.002
Axial load, Pu	1788 KN	0 KN
Mu	1779 KN-m	316 KN-m
Vu	997 KN	137 KN
From M-phi analysis, My	3210 KN-m	607 KN-m
Vy = 2 My/L	2140 KN	208 KN
Curvature, phi	0.009 1/m	0.012 1/m
Plastic length, Lp	0.32 m	0.36 m
θy	0.0029 rad	0.0043 rad

Table A. 3 Nonlinear modeling parameters (ASCE 41/17)

Plastic hinge modeling parameters (ASCE41/17)	Column (rad)	Beam (rad)
a	0.048	0.025
b	0.1	0.05
c	0.22	0.2
IO	0.005	0.01
LS	0.045	0.025
CP	0.063	0.05

Validation of tsunami pushover analysis

1.Single cantilever column

Without consider meaterial nonlinearity (wihout plastic hinge on the column)

Section Properties

A= 400x400 mm2

I = 0.002133 mm4

Height of column = 3 m

 Material Properties

E = 24855578 KN/m2

Actual hydrodynamic forces = 50 KN/m
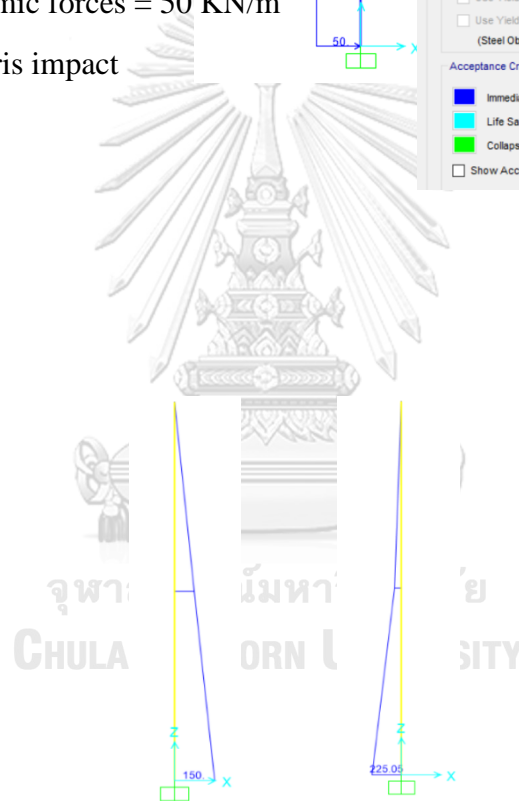
Push at top = Debris impact

Using Sap 2000
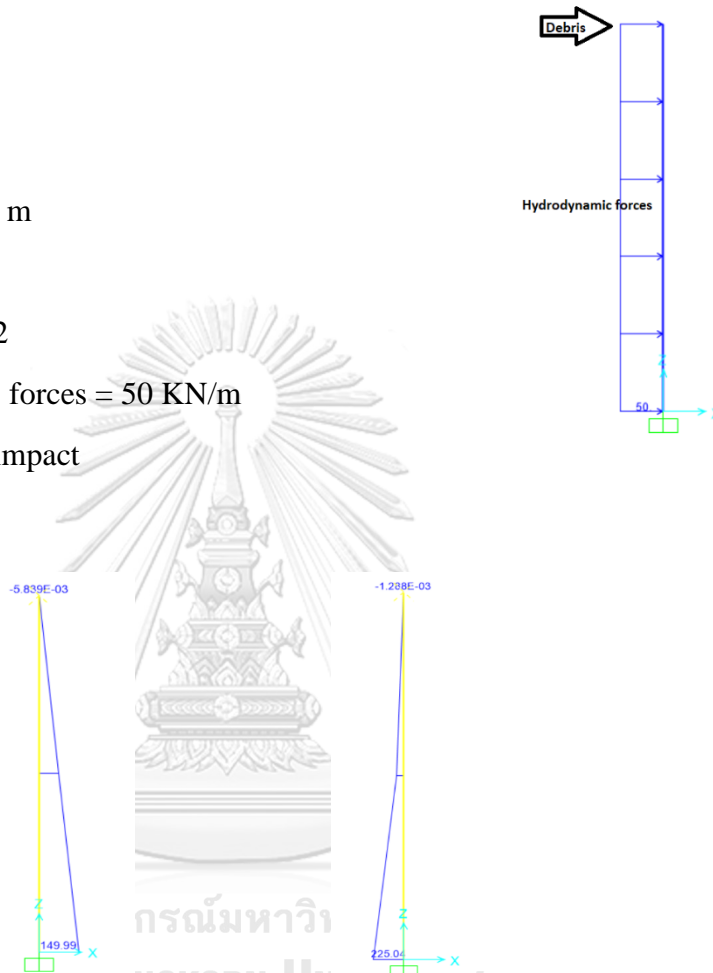
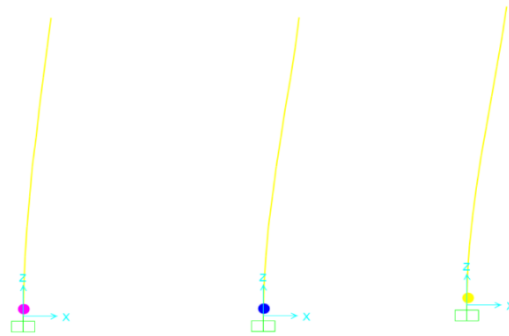Figure A.15 Shear force and bending moment diagram due to actual hydrodynamic forces
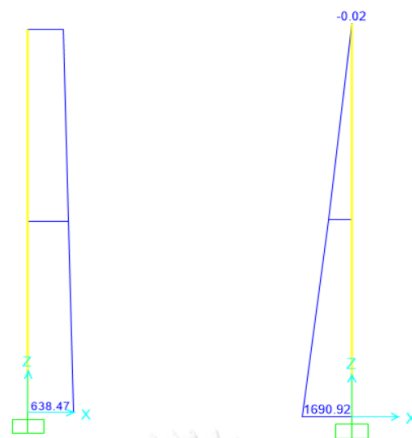
Figure A.16 Max shear force and bending moment diagram due to debris imapct
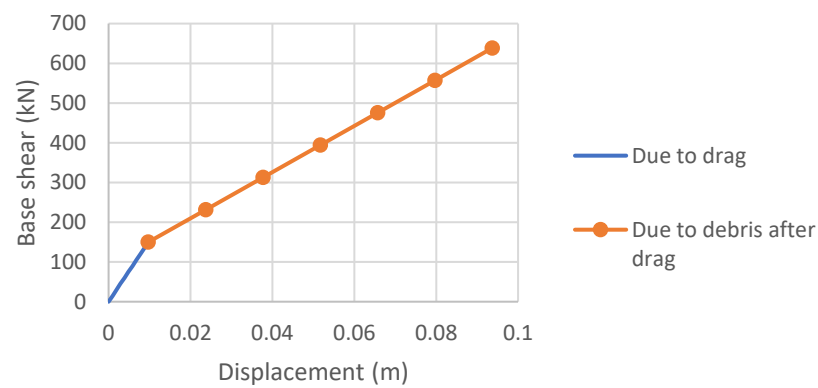
Figure A.17 Capacity of the column due to debris after hydrodynamic forces

Validation with hand calculation
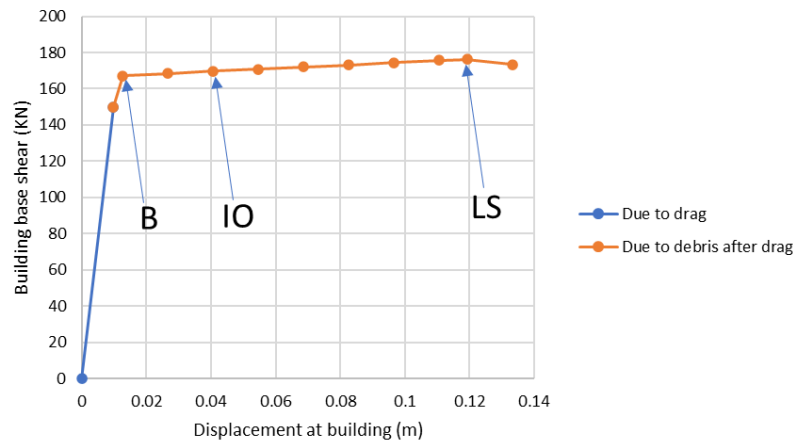
For the hydrodynamic forces on column (uniformly distributed load on column)

Hydrodynamic forces, P_h= 150 KN

Deformation of column, $= P_h L^3 / 8\ EI = 0.0095$ m

For the debris impact at top of the column (point load on column)

Deformation of column $= P_d L^3 / 3EI$

P_d (KN) due to debris after drag	$\Delta = P_d L^3 / 3EI$ (m)
100	0.0169
300	0.0509
500	0.0849

	Total base shear (start from initial) KN	Displacement, Δ (m)
	0	0
Due to drag	150	0.0095
Due to debris	250	0.0264
Due to debris	450	0.0604
Due to debris	650	0.0944
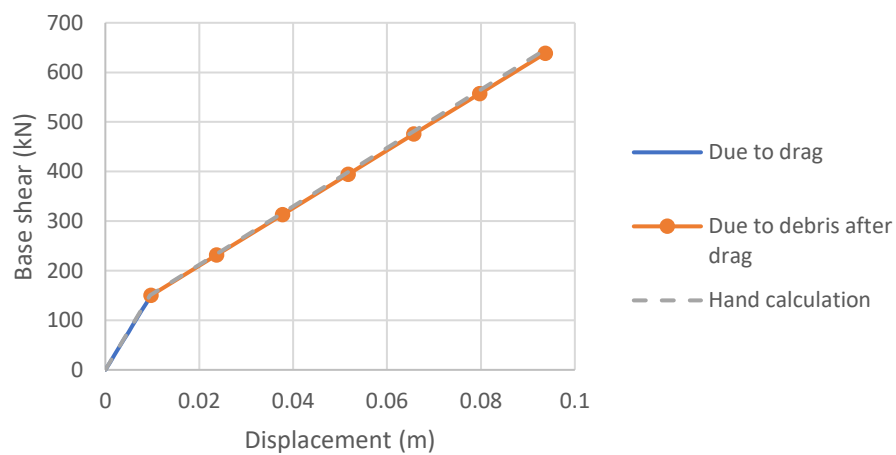
Figure A.18 Comparison of capacity of the column due to debris after hydrodynamic forces

2.Single cantilever column

Consider meaterial nonlinear (plastic hinge on the column)

Section Properties

A= 400x400 mm2

I = 0.002133 mm4

Height of column = 3 m

Material Properties

E = 24855578 KN/m2

Actual hydrodynamic forces = 50 KN/m

Push at top = Debris impact
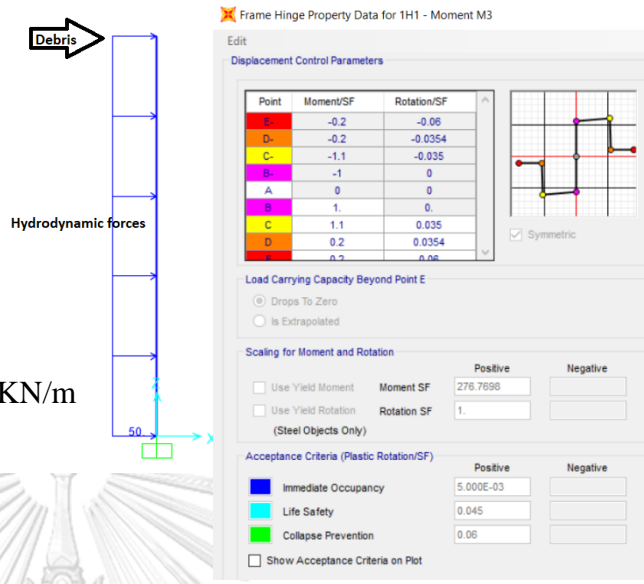
<u>Using Sap 2000</u>

Figure A.19 Shear force and bending moment diagram due to actual hydrodynamic forces

Figure A.20 Step by step plastic hinge formation due to debris after hydrodynamic forces
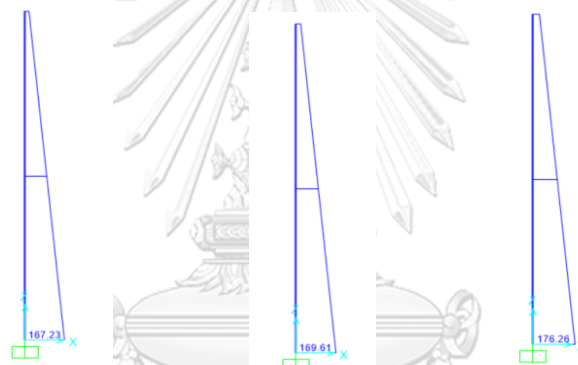
Figure A.21 Step by step shear force diagram due to debris after hydrodynamic forces
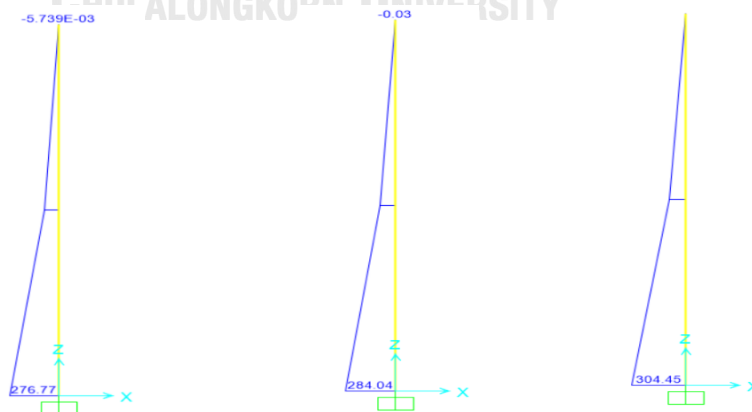
Figure A.22 Step by step bending moment diagram due to debris after hydrodynamic forces

Figure A.23 Capacity curve due to debris after hydrodynamic forces

Validation with hand calculation

For actual hydrodynamic forces on column (uniformly distributed load on column)

Hydrodynamic forces, $P_h = 150$ KN

Displacement of column, $\Delta = P_h L^3 / 8\ EI = 0.0095$ m

For the debris impact at top of the column (point load on column)

Bending moment due to hydrodynamic forces $= 150 \times 1.5 = 225$ KN-m

At column yield, remaining moment for the debris, M(remain) $= 276.77 - 225 = 51.77$ KN-m

At column yield, remaining shear, P_d (remain) $= 51.77 / 3 = 17.26$ KN

Displacement of column, $\Delta = P_d L^3 / 3EI = 0.00293$ m

At column ultimate condition, due to debris after drag,

Remaining moment, M(remain) $= 304.45 - 225 = 79.45$ KN-m

Remaining shear, P_d (remain) $= 79.45 / 3 = 26.48$ KN

$\Delta = P_d L^3 / 3EI +$ rotation x length

$= 0.0045 + 0.035 \times 3 = 0.109$ m

	Total base shear (Start from initial) KN	Displacement, Δ (m)
	0	0
Due to drag	150	0.0095
At yield, due to debris	167.26	0.01243
At ultimate, due to debris	176.48	0.1185
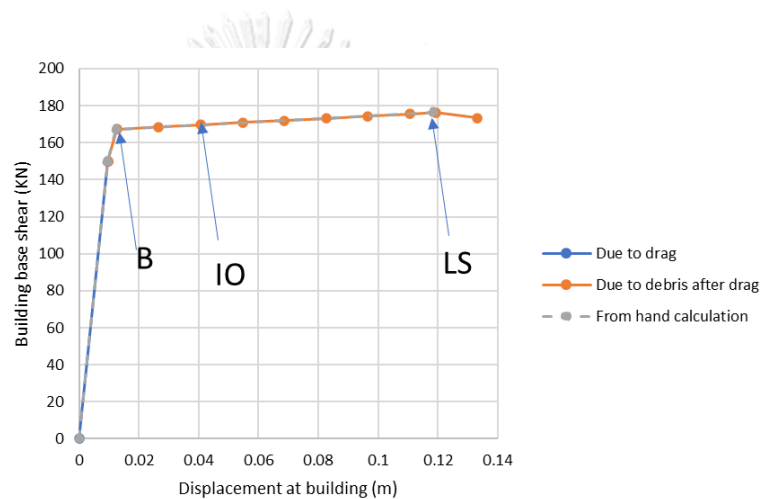
Figure A.24 Comparison of capacity of the column due to debris after hydrodynamic forces

3.Simple frame with fender

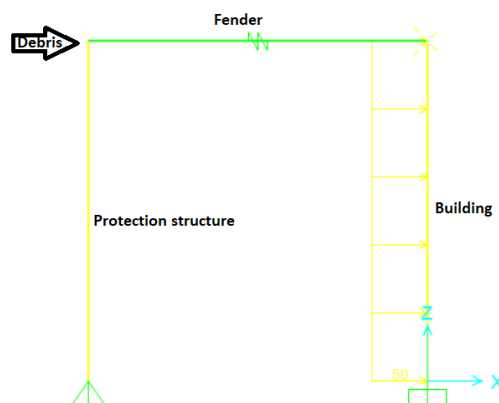Wihout consider meaterial nonlinear (wihout plastic hinge on the column)
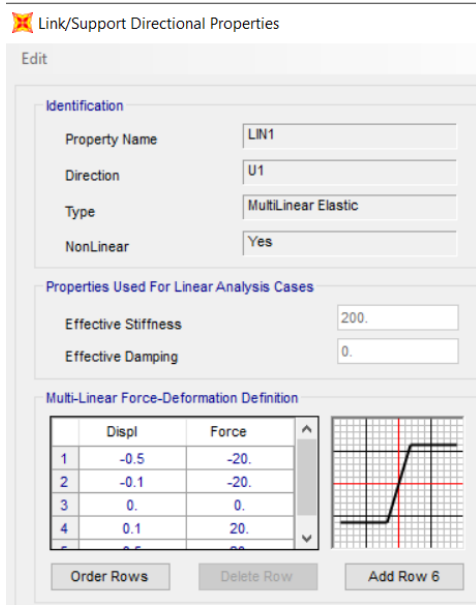
Section properties

A= 400x400 mm

I = 0.002133 mm4

Material properties

E = 24855578 KN/m2

Fender model

Using Sap 2000
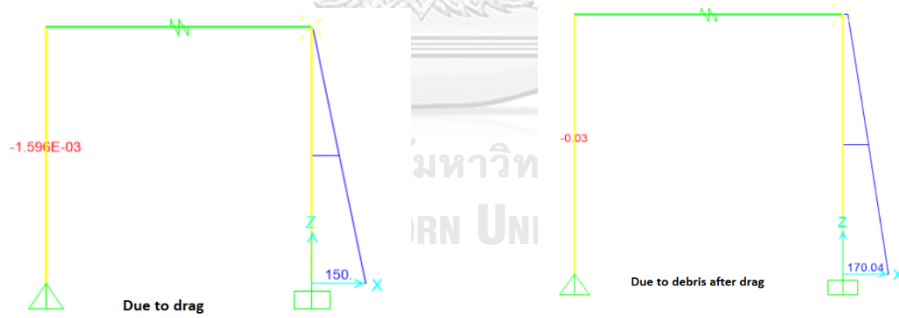
Figure A.25 Shear force diagram due to drag and debris after drag
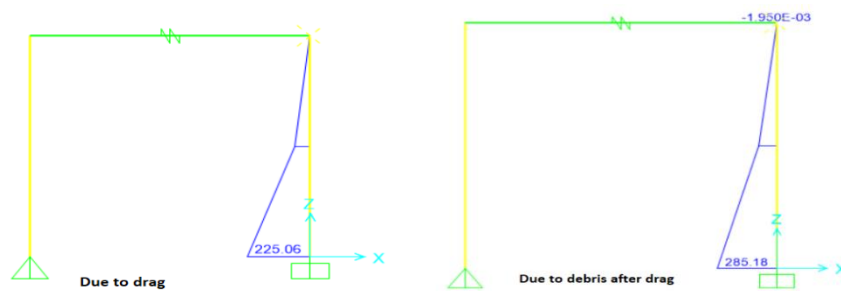
Figure A.26 Bending moment diagram due to drag and debris after drag
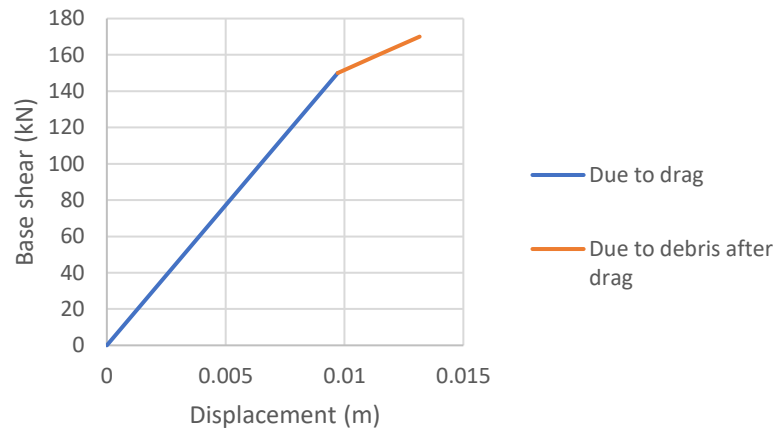
Figure A.27 Capacity of the column at building displacement

Validation with hand calculation

For the hydrodynamic forces on column (uniformly distributed load on column)

Hydrodynamic forces, $P_h = 150$ KN

Displacement of column, $\Delta = P_h L^3 / 8 EI = 0.0095$ m

For the debris impact at top of the column (point load on column)

Displacement of column, $\Delta = P_d L^3 / 3EI$

จุฬาลงกรณ์มหาวิทยาลัย
CHULALONGKORN UNIVERSITY

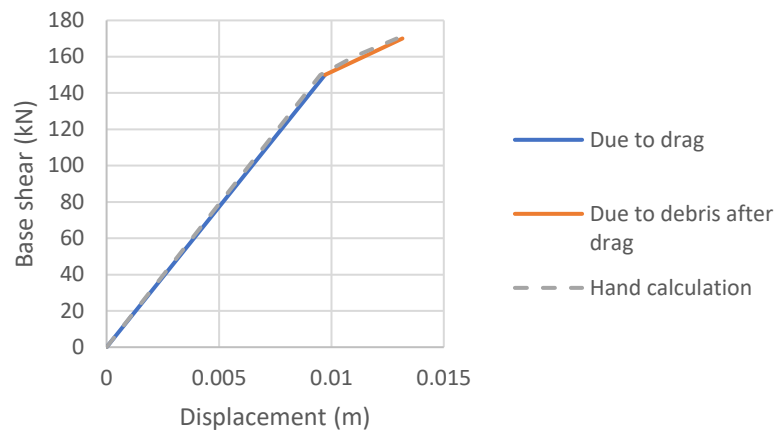|	Total base shear (Start from initial) KN	Displacement, Δ (m)
	0	0
Due to drag	150	0.0095
For debris (depend on fender force)	160	0.011
For debris (depend on fender force)	170	0.0129

Figure A.28 Comparison of capacity of the column with hand calculation

4.Simple frame with fender

Consider meaterial nonlinear (plastic hinge on the column)
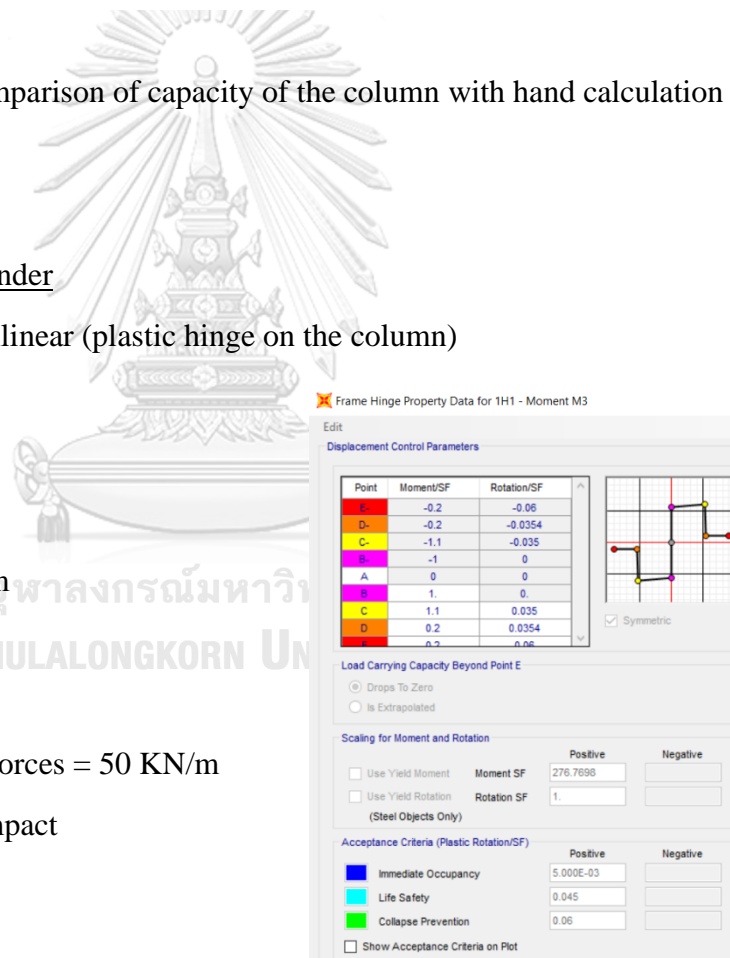
Section Properties

A= 400x400 mm2

I = 0.002133 mm4

Height of column = 3 m

 Material Properties

E = 24855578 KN/m2

Actual hydrodynamic forces = 50 KN/m
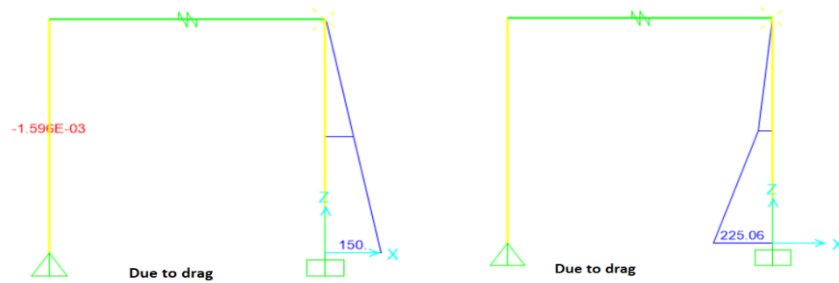
Push at top = Debris impact

Using Sap 2000

-1.596E-03

150.

Due to drag

225.06

Due to drag

Figure A.29 Shear force and bending moment diagram due to actual hydrodynamic forces

B state   IO state   Fender yield state
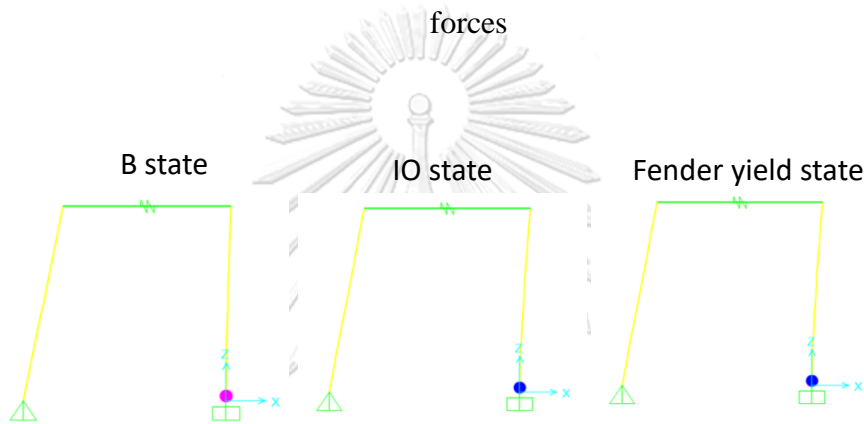
Figure A.30 Step by step plastic hinge formation due to debris after actual drag

B state   IO state   Fender yield state

-0.02

167.23

-0.02

169.61

-0.04

169.99
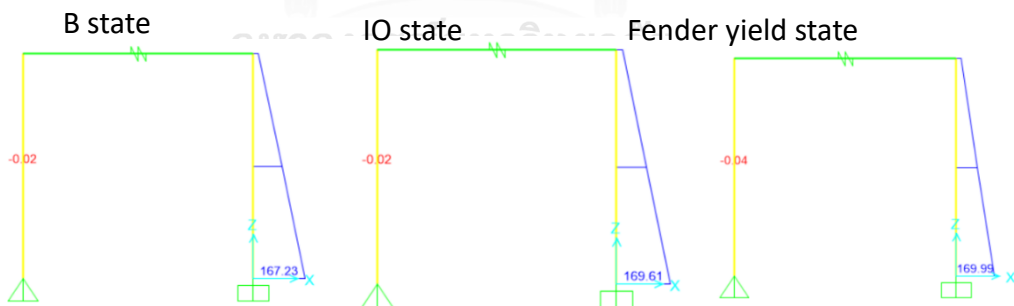
Figure A.31 Step by step shear force diagram due to debris after actual drag

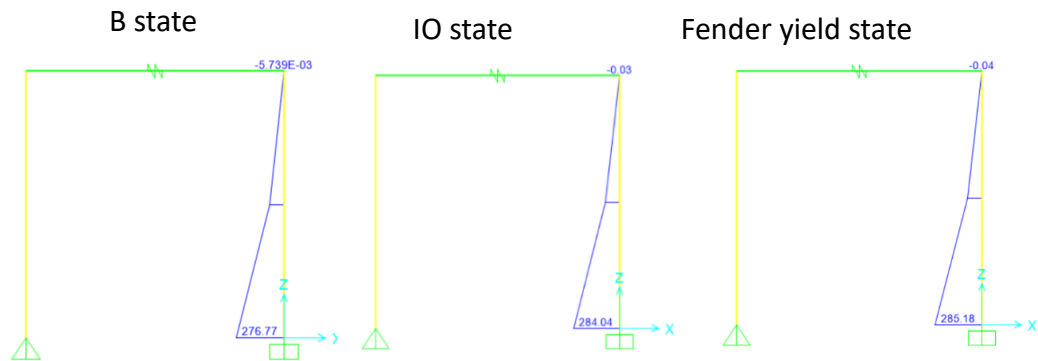| B state	IO state	Fender yield state

Figure A.32 Step by step bending moment diagram due to debris after actual drag
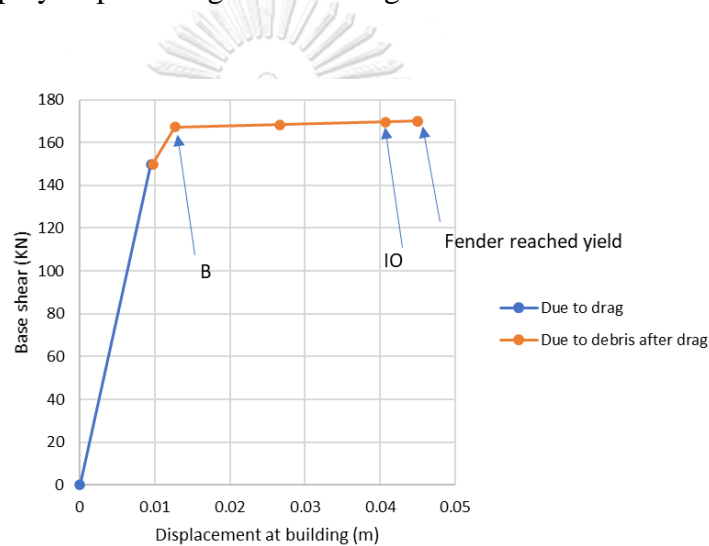
Figure A.33 Capacity of the column due to debris after

Validation with hand calculation

For the hydrodynamic forces on column (uniformly distributed load on column)

During elastic condition,

Hydrodynamic forces, P_h = 150 KN

Displacement of column, $\Delta = P_h L^3 / 8 EI = 0.0095$ m

For the debris impact at top of the column (point load on column)

Bending moment due to hydrodynamic forces = 150 x 1.5 = 225 KN-m

At column yield, remaining moment for the debris, M(remain) = 276.77 – 225 = 51.77 KN-m

At column yield, remaining shear, shear force due to debris after drag, P_d (remain) = 51.77 /3 = 17.26 KN

Displacement of column, $\Delta = P_d L^3/ 3EI = 0.00293$ m

For the fender forces Fy = 20 KN, remaining shear = 20 – 17.26 = 2.74 KN

From plastic moment hinge, rotation at shear 20 KN (276.66 + 2.74 x 3 = 284.99 KN-m), rotation = 0.0103 rad

At fender yield forces, shear force due to debris after drag, P_d(remain) = 20 KN

Displacement of column, $\Delta = P_d L^3/ 3EI$ + rotation x length

= 0.0034 + 0.0103 x3 = 0.0343 m

	Total base shear (Start from initial) KN	Displacement, Δ (m)
	0	0
Due to drag	150	0.0095
At yield, due to debris	167.26	0.01243
For debris (depend on fender force)	170	0.0438
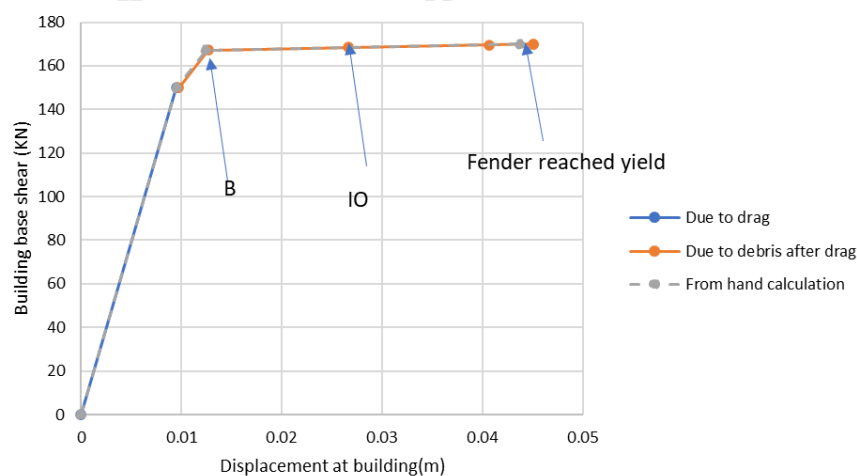
Figure A.34 Comparison of capacity of the column due to debris after hydrodynamic forces

VITA

NAME	Miss Zin Zin Tun
DATE OF BIRTH	17 July 1990
PLACE OF BIRTH	Mandalay
INSTITUTIONS ATTENDED	Mandalay Technological University
HOME ADDRESS	Ta Ta 18/18, Pyi Gyi Tagon Township, Mandalay, Myanmar.